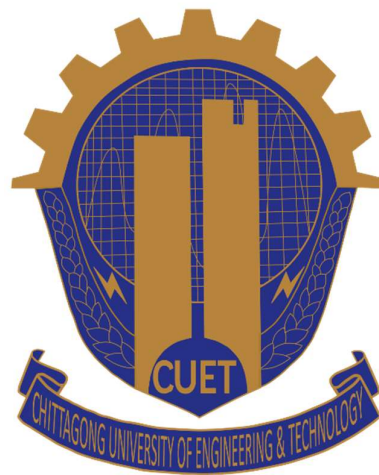


Master Thesis

A PARAMETRIC EVALUATION OF BURIED PIPELINE SUBJECTED TO SEISMIC EXCITATIONS

SANJOY DAS

13MCE033P



Department of Civil Engineering

Chittagong University of Engineering & Technology (CUET)

Chattogram-4349

Bangladesh

2023

A Parametric Evaluation of Buried Pipeline Subjected to Seismic Excitations

A Thesis

Submitted to the Department of Civil Engineering,
CHITTAGONG UNIVERSITY OF ENGINEERING AND TECHNOLOGY,
Chattogram-4349, Bangladesh
in partial fulfillment of the requirements for the degree of

MASTER OF SCIENCE IN CIVIL ENGINEERING

By

SANJOY DAS
13MCE033P



CHITTAGONG UNIVERSITY OF ENGINEERING AND TECHNOLOGY

Chattogram-4349, Bangladesh

2023

DEDICATION

To my amazing **Parents**

and

To my beloved **Wife**

APPROVAL STATEMENT

The thesis titled **A parametric evaluation of buried pipeline subjected to seismic excitations** Submitted by **Sanjoy Das**, Roll No: **13MCE033P**, Session: **2013-2014** has been accepted as satisfactory in partial fulfilment of the requirements for the degree of **MASTER OF SCIENCE IN CIVIL ENGINEERING** on **25 May 2023**.

BOARD OF EXAMINATION

- | | | |
|----|---|-----------------------|
| 1. | <hr/> Mr. Sultan Mohammad Farooq
Associate Professor
Department of Civil Engineering, CUET | Chairman (Supervisor) |
| 2. | <hr/> Professor Dr. Asiful Hoque Head
Department of Civil Engineering, CUET | Member (Ex-Officio) |
| 3. | <hr/> Dr. Md. Shajib Ullah
Associate Professor
Department of Civil Engineering, CUET | Member (Internal) |
| 4. | <hr/> Professor Dr. Mehedi Ahmed Ansary
Dept. of Civil Engg., BUET | Member (External) |

DECLARATION STATEMENT

I hereby declare that the work contained in this Thesis has not been previously submitted to meet requirements for an award at this or any other higher education institution. To the best of my knowledge and belief, the Thesis contains no material previously published or written by another person except where due reference is cited. Furthermore, the Thesis complies with PLAGIARISM and ACADEMIC INTEGRITY regulation of CUET.



Sanjoy Das

13MCE033P

Department of Civil Engineering
Chittagong University of Engineering &
Technology (CUET)

Date: 25-05-2023

Copyright © Sanjoy Das, 2023.

This work may not be copied without permission of the author or Chittagong University of Engineering & Technology.

DECLARATION BY THE SUPERVISOR(S)

This is to certify that **Sanjoy Das** has carried out this research work under our supervision, and that he has fulfilled the relevant Academic Ordinance of the Chittagong University of Engineering and Technology, so that he is qualified to submit the following Thesis in the application for the degree of MASTER of SCIENCE in Civil Engineering. Furthermore, the Thesis complies with the PLAGIARISM and ACADEMIC INTEGRITY regulation of CUET.

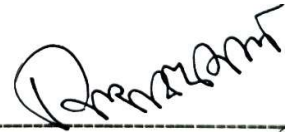


Mr. Sultan Mohammad Farooq (Principal Supervisor)

Associate Professor

Department of Civil Engineering

Chittagong University of Engineering & Technology



Dr. Md. Aftabur Rahman (Co-Supervisor)

Professor

Department of Civil Engineering

Chittagong University of Engineering & Technology

ACKNOWLEDGMENT

First and foremost, the author conveys her profound gratitude to the almighty Creator.

The author would first want to use this opportunity to recognize the contributions of the associated individuals which helped to bring this research successfully to a conclusion.

The author would like to express sincere and heartfelt gratitude to **Mr. Sultan Mohammad Farooq**, Associate Professor, Department of Civil Engineering, Chittagong University of Engineering and Technology (CUET) for his proper guidance, sincere supervision, and co-operation throughout this dissertation.

The author would like to thank **Dr. Md. Aftabur Rahman**, Professor, Department of Civil Engineering, (CUET) for suggesting this topic to me and giving me the opportunity to work on such an interesting topic. Furthermore, his continuous support, knowledge and valuable critical discussions and reviews related to the research work helped the author through the thesis work.

The author would like to express special gratitude to **Dr. Mehedi Ahmed Ansary**, Professor, Department of Civil Engineering, BUET and **Dr. Md. Shajib Ullah**, Associate Professor, Department of Civil Engineering, CUET for their valuable suggestions to improve the quality of this research work.

The author would also like to thank **Dr. Asiful Hoque**, Professor & Head, Department of Civil Engineering, CUET for his help and encouragement in completing this work.

A special thanks goes out to **Dr. Mohammad Arif Mohiuddin**, Project Geotechnical Engineer at Tetra Tech Coffey, Perth, Australia, who provided valuable input throughout the entire thesis.

Finally, the author expresses a deep sense of gratitude and indebtedness to his parents, teachers, colleagues, spouse and friends for their endless devotion, encouragement, and mental support throughout the tenure of the research work.

====

ABSTRACT

Buried pipelines, usually carrying essential facilities, are generally known as lifeline facilities and are considered one of the most susceptible structures under seismic action. Considerable research has been conducted addressing the response of buried pipes under fault rupture and permanent ground deformation. However, research on the response of buried pipes under seismic action is seldom found in technical writings. A three-dimensional numerical analysis has been performed in this research using a FEM based software, Abaqus 6.14 to focus on the insight response of buried pipe considering potential parameters under real seismic excitation. Shell element has been used to define the pipe model, while soils have been modeled by solid elements. The interface between soil and pipeline has been modeled by penalty friction to ascertain a realistic soil-pipe interaction. The vertical time history of the 1940 El Centro Earthquake has been used for this study, and the model has been validated with an experimental study in a static case, and a similar response has been observed that implicitly justifies the accuracy of the model. The seismic response of buried ductile iron pipe under seismic excitation portrays higher displacement, and significant stress has been observed. The maximum pipe response due to seismic excitations was noticed at the mid-span along the crest line of the pipe. Accounting for the finite model, the response of pipes under different boundary conditions has been studied to clutch the overall response of pipelines under different constraints.

Furthermore, a parametric study has been carried out to comprehensively examine the sensitivity of different parameters such as burial depth, and aspect ratio (D/t); embedment ratio (h/D), Soil-pipe interface friction co-efficient, pipe end-restraint conditions, soil characteristics (Dry density, Modulus of elasticity, Friction angle, Poisson's ratio), Traffic load, operational water pressure, Unidirectional Seismic excitation on the seismic response of straight buried pipes. The observed maximum vertical spatial displacement, deformation, von Mises stress, plastic strain, etc., are graphically depicted to analyze the seismic behavior of the buried pipeline. Significant response has been noticed at shallow burial depths in the parametric analysis, and both the burial depth and boundary conditions have been found as critical parameters in the response of pipes under seismic action. The increase in embedment ratio (h/D) from 1 to 5 by up to 5 times, decreases pipe displacement, stress and strain by 28.7 %, 1.3 % and 23.2 % respectively. The maximum displacement and stress magnitude generated in the

pipe increases by up to 2.87 % and 34.9 % respectively for hinge support; also, it increases by up to 2.83 % and 34.9 % respectively for fixed support with respect to roller support. The observed plastic strain in the pipe was 90.1% lower (roller); 53.1 % higher (hinge); 45.9 % higher (fixed) than the minimum elongation (10%) of DI pipe. In addition, soil properties and induced traffic load contribute substantially to the deformation of buried pipes. The maximum displacement, stress and strain developed in the pipe decreased by up to 59.2%, 84% and 100% respectively, due to an increase in soil density (from 1700 to 2160 kg/m³ by 1.27 times), the modulus of elasticity (from 19 to 96 MPa by ~5 times) of soil, the Poisson's ratio (from 0.2 to 0.45 by 2.25 times) of soil and the friction angle (from 30° to 45° by 1.5 times) of the soil. The greatest displacement and stress values occurred in the pipe considering the traffic load (1100 kPa) on the soil significantly increased by 135.7% and dramatically increased by (1326 %) respectively compared to the no traffic load case. The observed plastic strain in the pipe due to traffic load was 90 % lower than the minimum elongation (10%) of DI pipe. Overall, numerical results demonstrate that these influencing factors can impact the seismic behaviors of the buried pipeline to different degrees and cannot be neglected in the seismic analysis. In a nutshell, this research can be used as a direction for further research to provide a comprehensive guideline for the design, safety evaluation, and protection of buried pipelines crossing seismic areas.

Keywords: *Seismic excitations; 3D Finite Element Analysis; Buried Pipe; Parametric study.*

বিমূর্ত

ভূগর্ভস্থ পাইপলাইনসমূহ, সচরাচর প্রয়োজনীয় সুবিধাসমূহ বহন করে বলে এদেরকে লাইফলাইন বলা হয় এবং এ সমস্ত পাইপলাইনসমূহ ভূমিকম্পের সময় সবচেয়ে সংবেদনশীল কাঠামোগুলির মধ্যে একটি হিসাবে বিবেচিত হয়। ‘ফল্ট’ নড়াচড়া এবং স্থায়ী ভূমি বিকৃতি দ্বারা প্রভাবিত ভূগর্ভস্থ পাইপের প্রতিক্রিয়ার উপর যথেষ্ট গবেষণা পরিচালিত হয়েছে। তবে, ভূকম্পন ক্রিয়ার মাধ্যমে ভূগর্ভস্থ পাইপের প্রতিক্রিয়া নিয়ে গবেষণা প্রযুক্তিগত লেখাগুলিতে খুব কমই পাওয়া যায়। প্রকৃত ভূমিকম্পনজনিত আলোড়নের অধীনে, এই গবেষণায় একটি ফাইনাইট এলিমেন্ট মডেল ভিত্তিক সফটওয়্যার, এবাকাস ৬.১৪ ব্যবহার করে এবং গুরুত্বপূর্ণ প্যারামিটারসমূহ বিবেচনাপূর্বক ভূগর্ভস্থ পাইপের আভ্যন্তরীণ প্রতিক্রিয়ার উপর ফোকাস করতে একটি ত্রিমাত্রিক সংখ্যাগত বিশ্লেষণ করা হয়েছে। পাইপ মডেল সংজ্ঞায়িত করতে ব্যবহার করা হয়েছে শেল এলিমেন্ট, যখন মাটিকে মডেল করা হয়েছে সলিড এলিমেন্ট দ্বারা। মাটি এবং পাইপলাইন এর ইন্টারফেসকে পেনালটি ঘর্ষণ দ্বারা মডেল করা হয়েছে যেটি একটি বাস্তবধর্মী পাইপলাইন এর সাথে মাটির মিথস্ক্রিয়া নিশ্চিত করে। এই গবেষণার জন্য ১৯৪০ সালের এল সেট্রো ভূমিকম্পের উল্লম্ব ত্বরণ সময় ইতিহাস ব্যবহার করা হয়েছে এবং ব্যবহৃত মডেলটিকে স্ট্যাটিক বলের সাপেক্ষে পরীক্ষাগারে সম্পাদিত একটি পরীক্ষামূলক গবেষণার সাথে তুলনা করা হয়েছে, এবং একটি অনুরূপ প্রতিক্রিয়া পরিলক্ষিত হয়েছে যা পরোক্ষভাবে মডেলটির যথার্থতাকে সমর্থন করে। ভূমিকম্পের উত্তেজনার অধীনে ভূগর্ভস্থ নমনীয় লোহার পাইপের সিসমিক প্রতিক্রিয়া অধিক স্থানচ্যুতি ঘটিয়েছে, এবং উল্লেখযোগ্য চাপ পরিলক্ষিত হয়েছে। ভূমিকম্পের উত্তেজনার কারণে পাইপের সর্বোচ্চ প্রতিক্রিয়া ক্রেস্ট লাইন বরাবর মধ্য-স্প্যান লক্ষ্য করা গেছে। ফাইনাইট এলিমেন্ট মডেলের মাধ্যমে, পাইপের বিভিন্ন বাউন্ডারী কন্ডিশনের অধীনে পাইপলাইন এর প্রতিক্রিয়া বিশ্লেষণ করা হয়েছে যাতে করে বিভিন্ন বাউন্ডারী কন্ডিশনে পাইপলাইন এর সামগ্রিক প্রতিক্রিয়া জানা যায়।

উপরন্তু, ভূমিকম্পনজনিত আলোড়নের কারণে ভূমধ্যস্থ সোজা পাইপ লাইনের ভূকম্পনে প্রতিক্রিয়ার উপর বিভিন্ন প্যারামিটার এর যেমন পাইপের গভীরতা, পাইপের ব্যাস ও পুরুত্বের অনুপাত; পাইপের গভীরতা ও ব্যাস এর অনুপাত, মাটি ও পাইপের আন্তঃতলীয় ঘর্ষণ সহগ, পাইপের সাপোর্ট কন্ডিশন, মাটির বৈশিষ্ট্য (শুষ্ক ঘনত্ব, স্থিতিস্থাপক গুণাঙ্ক, ঘর্ষণ কোণ, পয়সনের অনুপাত), ট্রাফিক লোড, অপারেশনাল পানির চাপ, একমুখী ভূকম্পন সংবেদনশীলতা ব্যাপকভাবে পরীক্ষা করার জন্য একটি প্যারামেট্রিক বিশ্লেষণ করা হয়েছে। ভূগর্ভস্থ পাইপলাইনের ভূকম্পনে প্রতিক্রিয়া বিশ্লেষণ করার জন্য পর্যবেক্ষিত সর্বোচ্চ উল্লম্ব স্থানচ্যুতি, বিকৃতি, ভন মিসেস স্ট্রেস, প্লাস্টিক স্ট্রেস ইত্যাদি গ্রাফিকভাবে চিত্রিত করা হয়েছে। প্যারামেট্রিক বিশ্লেষণে অগভীর পাইপের গভীরতায় তাৎপর্যপূর্ণ প্রতিক্রিয়া লক্ষ্য করা গেছে; সিসমিক অ্যাকশনের অধীনে পাইপের প্রতিক্রিয়া বিশ্লেষণে পাইপের গভীরতা এবং বাউন্ডারী কন্ডিশন উভয়ই গুরুত্বপূর্ণ প্যারামিটার হিসাবে পাওয়া গেছে। পাইপের গভীরতা ও ব্যাস এর অনুপাত ১ থেকে ৫ পর্যন্ত ৫ গুণ পর্যন্ত বৃদ্ধি, পাইপ

স্থানচ্যুতি, চাপ এবং স্ট্রেন যথাক্রমে ২৮.৭ %, ১.৩ % এবং ২৩.২ % হ্রাস করে। রোলার সাপোর্টের সাপেক্ষে, হিঞ্জ সাপোর্টের জন্য পাইপে উৎপন্ন সর্বোচ্চ স্থানচ্যুতি এবং চাপের মাত্রা যথাক্রমে ২.৮৭ % এবং ৩৪.৯ % পর্যন্ত বৃদ্ধি পায়; এছাড়াও ফিক্সড সাপোর্টের জন্য যথাক্রমে ২.৮৩ % এবং ৩৪.৯ % পর্যন্ত বৃদ্ধি পায়। নমনীয় লোহার পাইপের ন্যূনতম প্রসারণের (১০ %) চেয়ে, পাইপে পর্যবেক্ষণ করা প্লাস্টিক স্ট্রেন ছিল ৯০.১ % কম (রোলার); ৫৩.১ % বেশি (হিঞ্জ); ৪৫.৯ % বেশি (ফিক্সড)। উপরন্তু, মাটির বৈশিষ্ট্য এবং আরোপিত ট্র্যাফিক লোড ভূগর্ভস্থ পাইপের বিকৃতিতে যথেষ্ট অবদান রাখে। পাইপে উৎপন্ন সর্বাধিক স্থানচ্যুতি, চাপ এবং স্ট্রেন যথাক্রমে ৫৯.২ %, ৮৪ % এবং ১০০ % পর্যন্ত হ্রাস পেয়েছে, মাটির ঘনত্ব বৃদ্ধির কারণে (১৭০০ থেকে ২১৬০ কেজি/মিটার^৩ পর্যন্ত ১.২৭ গুণ) মাটির স্থিতিস্থাপক গুণাঙ্ক (১৯ থেকে ৯৬ এম পি এ পর্যন্ত ~ ৫ গুণ), মাটির পয়সনের অনুপাত (০.২ থেকে ০.৪৫ পর্যন্ত ২.২৫ গুণ) এবং মাটির ঘর্ষণ কোণ (৩০° থেকে ৪৫° থেকে ১.৫ গুণ)। মাটিতে নো ট্র্যাফিক লোড কেসের তুলনায়, ট্র্যাফিক লোড (১১০০ কে পি এ) উল্লেখযোগ্যভাবে ১৩৫.৭ % এবং নাটকীয়ভাবে (১৩২৬ %) বৃদ্ধির বিবেচনায় পাইপে সবচেয়ে বড় স্থানচ্যুতি এবং চাপের মানগুলি ঘটেছে। ট্র্যাফিক লোডের কারণে পাইপে পর্যবেক্ষণ করা প্লাস্টিক স্ট্রেন ডিআই পাইপের ন্যূনতম প্রসারণের (১০ %) চেয়ে ৯০ % কম ছিল। সামগ্রিকভাবে, বিশ্লেষণ থেকে প্রাপ্ত ফলাফলগুলি দেখায় যে এই প্রভাবক কারণগুলি ভূগর্ভস্থ পাইপলাইনের ভূকম্পনজনিত আচরণকে বিভিন্ন মাত্রায় প্রভাবিত করতে পারে যার কারণে এই প্যারামিটার গুলোকে পাইপের ভূমিকম্পজনিত প্রতিক্রিয়া বিশ্লেষণে উপেক্ষা করা যাবে না। সংক্ষেপে, এই গবেষণাটি আরও বিশদ গবেষণার জন্য একটি ব্যাপক নির্দেশিকা হিসাবে ব্যবহার করা যেতে পারে বিশেষ করে যে সমস্ত পাইপলাইন সিসমিক এলাকা অতিক্রম করছে তাদের ডিজাইন, নিরাপত্তা মূল্যায়ন, এবং ভূগর্ভস্থ পাইপের সুরক্ষার জন্য।

কীওয়ার্ডঃ ভূকম্পনজনিত আলোড়ন, ত্রিমাত্রিক ফাইনাইট এলিমেন্ট বিশ্লেষণ, ভূগর্ভস্থ পাইপ, প্যারামেট্রিক বিশ্লেষণ।

Table of Contents

CHAPTER 1. INTRODUCTION	1
1.1 General Overview.....	1
1.2 Background Study	3
1.3 Problem Statement.....	5
1.4 Significance of the Study.....	7
1.5 Objectives of the Study	8
1.6 Outlines of the Thesis	8
CHAPTER 2. LITERATURE REVIEW	10
2.1 General Overview.....	10
2.2 Fundamentals of Buried Pipeline	10
2.3 Factors Affecting Dynamic Response of Buried Pipelines	11
2.3.1 Soil–Pipe Interaction	11
2.3.2 Permanent Ground Deformation.....	11
2.3.3 Seismic Wave Propagation.....	11
2.3.4 Miscellaneous Factors	12
2.4 Failure Modes of Buried Continuous Pipelines.....	12
2.4.1 Local or Shell Mode Buckling.....	13
2.4.2 Beam Mode Buckling.....	13
2.4.3 Flexural Failure.....	14
2.4.4 Tensile Failure	14
2.4.5 Cross-Section Ovalization	14
2.5 Failure Mechanism in the segmented pipeline	15
2.6 Previous Research on Buried Pipe	15
2.6.1 Experimental Study	16
2.6.2 Analytical Study	16
2.6.3 Numerical Study	16
2.7 Scope of the Current Research	19
2.8 Insights from Literature Review.....	20
CHAPTER 3. NUMERICAL PROCEDURE.....	22
3.1 General Overview.....	22
3.2 Background of Numerical Procedure	22
3.2.1 Finite Element Method	23
3.2.2 Non-linear FEM.....	24
3.2.3 3-Dimensional FEM	24
3.3 Numerical Modelling of Soil-Pipe System.....	25

3.3.1 Constitutive Relation for Soil	27
3.3.2 Constitutive Relation for Pipe	31
3.3.3 Mechanical Properties of Pipe and Soil.....	31
3.3.4 Soil-Pipe Interaction	32
3.3.5 Incremental Loading and time steps	35
3.3.6 Loads on Pipeline and Soil	36
3.3.7 Boundary Conditions	40
3.3.8 The Type and Shape of Element.....	42
3.3.9 Mesh Accuracy	43
3.3.10 The size of element.....	44
3.4 FE Model Performance.....	46
3.5 Summary.....	49
CHAPTER 4. RESULTS AND DISCUSSIONS.....	50
4.1 General Overview.....	50
4.2 Static and Seismic Response of Pipe.....	51
4.2.1 Response under Static and Seismic Load	51
4.2.2 Effect of Boundary Conditions	54
4.3 Parametric Study	60
4.3.1 Effect of Buried Depth of Pipe (Embedment Ratio, h/D)	60
4.3.2 Effect of D/t Ratio of Pipe	65
4.3.3 Effect of the Operational Water Pressure	70
4.3.4 Effect of Traffic load	77
4.3.5 Effect of Soil Density	82
4.3.6 Effect of the Angle of Internal Friction of Soil	87
4.3.7 Effect of Soil Stiffness.....	90
4.3.8 Effect of the Poisson's Ratio of Soil.....	93
4.3.9 Effect of Interface Friction Co-efficient	96
4.4 Summary.....	100
CHAPTER 5. CONCLUSION AND RECOMMENDATION.....	102
5.1 General Overview.....	102
5.2 Conclusions	102
5.3 Mitigation Measures Against Seismic Actions	104
5.4 Limitations of the Current Study	105
5.5 Scope for Further Research	105
REFERENCES.....	107
APPENDIX A: MODAL ANALYSIS	117

List of Figures

Figure 1-1: Examples of some earthquake induced buried pipeline failures due to: i) bending shell buckling of steel pipeline (1999 Kocaeli earthquake); ii) liquefaction-induced lateral spreading (1995 Kobe earthquake); iii) pullout of mechanical joints (2011 Tohoku earthquake); iv) Joint failure of concrete pipeline (1985 Mexico City earthquake); v) axial pullout of Asbestos Cement pipe (1999 Izmit earthquake); vi) axial shell buckling of steel pipeline (1971 San Fernando earthquake) [Gautam et al, 2018]	2
Figure 2-1: a) Local buckling of a spiral welded pipe, $D/t = 119$, subjected to longitudinal bending because of severe pipe wall compression (Vasilikis et al., 2014); b) Locally buckled steel gas pipeline in the compression zone at north slope of Terminal Hill in 1994 Northridge Earthquake (EERI, 1995)13	
Figure 2-2: Beam buckling of buried pipeline due to excessive axial loading (after Karamanos et al., 2014)	14
Figure 2-3: Most common failure mechanisms in buried and continuous steel pipelines: (a) shell-mode buckling due to uniform axial compression (top) and pure bending (bottom); (b) beam-mode buckling; (c) tensile rupture and (d) cross- section ovalization (O'Rourke & Liu,1999).....	15
Figure 3-1: Grid based methods (Finite Element Method (FEM))	23
Figure 3-2: Schematic 3D diagram of a) soil and b) pipeline model.....	25
Figure 3-3: 3D FE models: (a) soil as deformable solid (b) pipeline as deformable shell, in the complete ABAQUS environment.	27
Figure 3-4: Elastic-perfectly plastic assumption of Mohr-Coulomb Model. (After Smith & Griffith, 1982).....	28
Figure 3-5: Mohr-Coulomb failure model	29
Figure 3-6: Mohr-Coulomb yield surface in meridional and deviatoric planes.....	30
Figure 3-7: Typical stress-strain curve for ductile metals (Collected from-Ductile Iron Society)	31
Figure 3-8: Surface-to-surface contact model (Penalty) in between pipe and soil.	33
Figure 3-9: Schematic diagram of the penalty method	34
Figure 3-10: A general friction curve with penalty friction formulation.....	35
Figure 3-11: Schematic diagram of the distribution of steps and increments, according to (Bower, 2010).	36

Figure 3-12: Water pressure inside the pipe under full flow, half flow.....	37
Figure 3-13: 8-Wheel HB Truck Loading with a wheel load on contact area of 0.102 m ²	38
Figure 3-14: A uniform surface load of 1100 kPa on soil.	38
Figure 3-15: The accelerogram [Acceleration time history] (Vert. Comp.) of El Centro Earthquake of 18th May 1940 (https://strongmotioncenter.org).	39
Figure 3-16: Fourier spectrum of Vert comp. (Predominant frequency, 8.43 Hz) for the recording of El Centro Valley Irrigation District Station during the Imperial Valley Earthquake (1940).....	40
Figure 3-17: Boundary Conditions for soil continuum.....	41
Figure 3-18: Boundary Conditions for pipe end.....	42
Figure 3-19: Effect of the element size on the Displacement of pipe.....	44
Figure 3-20: Meshing of soil box around pipe.....	45
Figure 3-21: Cross section of FE Model.....	48
Figure 3-22: a) Front view of Experimental Model, b) PVC Pipe (Pires & Palmeira, 2021)	48
Figure 3-23: Comparison between numerical result and experimental result (Pires & Palmeira, 2021)	49
Figure 4-1: The location of monitoring lines.....	50
Figure 4-2: Displacement response of pipe.....	51
Figure 4-3: Stress response of pipe	52
Figure 4-4: Strain response of pipe	53
Figure 4-5: Effect of pipe end support on vertical displacement of buried pipeline (along crest line): (a) total displacement, (b) net deformation.....	55
Figure 4-6: Displacement contour of DI pipe for a) roller, b) hinge, and c) fixed support at the pipe end	56
Figure 4-7: Effect of pipe end support on stress of buried pipeline (along crest line)...	57
Figure 4-8: Stress contour of DI pipe for a) roller, b) hinge, and c) fixed support at the pipe end.....	58
Figure 4-9: Effect of pipe end support on strain of buried pipeline (along crest line)...	59
Figure 4-10: Effect of embedment ratio (h/D) on seismic response of pipe: (a) total displacement, (b) net deformation	61
Figure 4-11: Displacement contour of DI pipe for h/D=1~5	62
Figure 4-12: Effect of embedment ratio (h/D) on seismic response (stress) of pipe	63
Figure 4-13: Stress contour of DI pipe for h/D=1~5	64

Figure 4-14: Effect of embedment ratio (h/D) on seismic response (strain) of pipe	65
Figure 4-15: Effect of diameter-to-thickness ratio of pipe on seismic response of pipe (a) total displacement (b) net deformation.....	66
Figure 4-16: Displacement contour of DI pipe for various D/t (64.8 to 73.8).....	67
Figure 4-17: Effect of diameter-to-thickness ratio of pipe on seismic response (stress) of pipe	68
Figure 4-18: Stress contour of DI pipe for various D/t (64.8 to 73.8)	69
Figure 4-19: Effect of diameter to thickness ratio of pipe on seismic response (strain) of pipe.....	70
Figure 4-20: Effect of inside water pressure on seismic response of pipe: (a) displacement with deformation; (b) enlarged view of total displacement; (c) enlarged view of net deformation	72
Figure 4-21: Displacement contour of the ductile iron pipe for different flow conditions (full, half and no flow)	73
Figure 4-22: Effect of inside water pressure on seismic response (stress) of pipe	74
Figure 4-23: Stress contour of the ductile iron pipe for different flow conditions (full, half and no flow).....	75
Figure 4-24: Effect of inside water pressure on seismic response (strain) of pipe	76
Figure 4-25: Effect of traffic load on seismic response of pipe (a) displacement with deformation, (b) net deformation.....	78
Figure 4-26: Displacement contour of the ductile iron pipe with a traffic load of 1100 kPa and without traffic load.....	79
Figure 4-27: Effect of the traffic load on seismic response (stress) of pipe	80
Figure 4-28: Stress contour of the ductile iron pipe with a traffic load of 1100 kPa and without traffic load.....	81
Figure 4-29: Effect of the traffic load on seismic response (strain) of pipe	82
Figure 4-30: Effect of soil density on seismic response of pipe: (a) total displacement, (b) net deformation	83
Figure 4-31: Displacement contour of DI pipe due to variation in dry densities (1700 kg/m^3 to 2160 kg/m^3) of soil	84
Figure 4-32: Effect of soil density on seismic response (stress) of pipe.....	85
Figure 4-33: Stress contour of DI pipe due to variation in dry densities (1700 kg/m^3 to 2160 kg/m^3) of soil.....	86
Figure 4-34: Effect of soil density on seismic response (strain) of pipe.....	87

Figure 4-35: Effect of friction angle of soil on seismic response of pipe (a) total displacement (b) net deformation	88
Figure 4-36: Effect of friction angle of soil on seismic response (stress) of pipe	89
Figure 4-37: Effect of friction angle of soil on the seismic response (strain) of pipe ...	89
Figure 4-38: Effect of modulus of elasticity of soil on seismic response of pipe (a) total displacement (b) net deformation	91
Figure 4-39: Effect of modulus of elasticity of soil on seismic response (stress) of pipe	92
Figure 4-40: Effect of modulus of elasticity of soil on seismic response (strain) of pipe	92
Figure 4-41: Effect of Poisson's Ratio of soil on seismic response of pipe (a) total displacement, (b) net deformation	94
Figure 4-42: Effect of Poisson's Ratio of soil on seismic response (stress) of pipe	94
Figure 4-43: Effect of Poisson's Ratio of soil on seismic response (strain) of pipe	95
Figure 4-44: Effect of interface friction co-efficient (μ) on the seismic response of pipe: (a) total displacement (b) net deformation	96
Figure 4-45: Displacement contour of the ductile iron pipe for different interface friction co-efficient ($\mu = 0.5$ to 0.9)	97
Figure 4-46: Effect of interface friction co-efficient (μ) on the seismic response (stress) of pipe	98
Figure 4-47: Stress contour of the ductile iron pipe for different interface friction co-efficient ($\mu = 0.5$ to 0.9)	99
Figure 4-48: Effect of interface friction co-efficient (μ) on the seismic response (strain) of pipe	100
Figure A-1: Variation of damping ratio with natural frequency of a system. (Chowdhury & Dasgupta, 2003)	118

List of Tables

Table 3-1: Mechanical properties of Kubota Ductile Iron pipe (ISO 2531/ BS EN 545 and 598)	32
Table 3-2: Material properties of Sandy soil (Liu et al., 2010; Seed & Duncan, 1985; Nixon & Child, 1989)	32
Table 3-3: Static and seismic loads (BSI., 2006, BSI., 2010, and https://strongmotioncenter.org).....	36
Table 3-4: Displacement (U), Rotational (UR) and Acceleration (A) constraints.....	40
Table 3-5: Selected type and shape of element for 3D-FE soil-pipe model	43
Table 3-6: Element sizes for soil and pipe	46
Table 3-7: Parameters used for both the experimental and numerical models	47
Table A-1: Chart of α and β for soil and pipe	119

NOMENCLATURE

<u>Symbol</u>	<u>Unit</u>	<u>Definition</u>
D _o or D	[m]	Outer diameter of pipe
D _i	[m]	Inner diameter of pipe
DN	[mm]	Nominal diameter of pipe
DI		Ductile Iron
t	[mm]	Wall thickness of pipe
H	[m]	Depth of soil continuum
L	[m]	Length of soil continuum/pipe
h	[m]	Buried depth of pipe from soil top surface to the crest of the pipe
W	[m]	Width of the soil continuum
U	[cm]	Spatial displacement of pipe
UR	[rad.]	Rotation
A	[m/s ²]	Acceleration
S. Mises	[MPa]	Von Mises stress of pipe
μ	---	Soil-pipe interface Friction coefficient/ratio
E _P	[MPa]	Modulus of elasticity of pipe
E _S	[MPa]	Modulus of elasticity of soil
FEM		Finite Element Method
FE, FEA		Finite Element, Finite Element Analysis
R _r	---	Rigidity ratio (E _P / E _S)
$\rho_{d \text{ pipe}}$	[kg/m ³]	Dry density of pipe
$\rho_{d \text{ soil}}$	[kg/m ³]	Dry density of soil
Dr		Density Ratio ($\rho_{d \text{ pipe}} / \rho_{d \text{ soil}}$)
ϕ	[°]	Friction angle of soil
ψ	[°]	Dilation angle of Soil
ε	[mm/mm]	Strain
ε_p or PE	[mm/mm]	Plastic strain
ν	---	Poisson's ratio
ρ_d (γ_d)	[kg/m ³]	Dry mass density (Dry unit weight of soil)
ΔD	[mm]	Change in pipe diameter or vertical deflection of pipe due to soil
f=($\Delta D/D$)	---	Flattening parameter or deflection (or ovality) due to soil

C3D8R		3D 1 st order brick elements with reduced integration or eight-node reduced-integration solid elements
S4R		Four-node reduced-integration shell elements
D/t	---	Pipe diameter to thickness ratio
h/D	---	Embedment ratio
X	[m]	Distance along width
Y	[m]	Distance along depth
Z	[m]	Distance along length
g	[m/s ²]	Acceleration of gravity
ζ		Damping ratio
α		Coefficients for mass proportional damping
β		Coefficients for stiffness proportional damping
ω		Natural frequency of a system
NLGEOM		Non-linear geometry
PGD		Permanent Ground Deformation
TGD		Transient Ground Deformation
ALA		American Lifelines Alliance
V _s	[m/s]	Shear wave velocity or theoretical velocity of S waves
ASCE		American Society of Civil Engineers
[C]		Damping matrix of the physical system
[M]		Mass matrix of the physical system
[K]		Stiffness matrix of the physical system
MC		Mohr-Coulomb
CAE		Complete Abaqus Environment or Computer-Aided Engineering
HB load	[kN]	Highest Body loading
PGA	[g]	Peak Ground Acceleration
λ	[m]	Wavelength of the input wave
f _{max}	[Hz]	Highest frequency (pre-dominant frequency) of the input motion
Δl	[m]	Maximum or minimum element size

LIST OF PUBLICATIONS

Peer-Reviewed Proceedings:

[1] **S. Das**, M. A. Rahman, & S. M. Farooq; “Buried Pipeline Under Seismic Excitations: A Review”; *5th International Conference on Civil Engineering for Sustainable Development (ICCESD)*; KUET, Khulna, Bangladesh; 7~9 February 2020; ID:4212, pp. 1-9.

[2] **S. Das**, M. A. Rahman, & S. M. Farooq; “Response analysis of buried pipeline under seismic action: A numerical study”; *3rd International Conference on Planning, Architecture & Civil Engineering (ICPACE)*; RUET, Rajshahi, Bangladesh; 09 - 11 September 2021; ID: CE_001, pp. 1-6.

Chapter 1. INTRODUCTION

1.1 General Overview

Due to higher population growth, rapid urbanization and industrialization, construction of various buried structures e.g., pipelines etc., are commonly seen in big cities to fulfill the demand of the increasing populations and infrastructures as well. These buried pipelines, as utility service provider like water, sewage, oil, and gas etc., have been constructed due to their relatively low-cost, environmental efficiency, high-reliability, low maintenance cost, public safety etc. (Ariman & Muleski, 1981)

Underground installations placed in earthquake zones eventually endures both seismic and static loads. Earthquake is one of the natural hazards most damaging to various urban and non-urban life-line utilities. With the rapid increase of the urbanization, possible disruption due to earthquakes has been accelerated, and rehabilitation attempts must therefore be initiated to restore some of the essential resources including lifeline services by recognizing the most vulnerable areas that reduce structural, human, and earthquake-related effects. The seismic behavior of buried structures is different compared to surface structures due to fully soil or rock enclosures and substantial length. During a medium to strong earthquake, both life and property encounter short term and long-term threats if the operational pipelines collapse or lose their capacity during the emergency operations. Generally, geotechnical loads are applied on the buried pipe by relative displacement between the pipe and its surrounding soil. It increases the stress and strain levels in the pipe, which may distract the function and mechanical integrity of the pipeline. Buried pipelines interact with the surrounding soil and neighboring structures both statically and dynamically. Hence, the pipeline resistance against seismic threats should be given higher importance otherwise it may lead to breakdown and leakage of pipes which can disturb normal civil life, environment, the flora and fauna of the area etc. Figure 1-1 depicts examples of some earthquake induced buried pipeline failure.



Figure 1-1: Examples of some earthquake induced buried pipeline failures due to: i) bending shell buckling of steel pipeline (1999 Kocaeli earthquake); ii) liquefaction-induced lateral spreading (1995 Kobe earthquake); iii) pullout of mechanical joints (2011 Tohoku earthquake); iv) Joint failure of concrete pipeline (1985 Mexico City earthquake); v) axial pullout of Asbestos Cement pipe (1999 Izmit earthquake); vi) axial shell buckling of steel pipeline (1971 San Fernando earthquake) [Gautam et al, 2018]

To prevent these seismic hazards and secure lifeline system in urbanized areas, further investigation of buried pipelines subjected to earthquakes is necessary. Till date, numerous researches have concentrated on permanent ground deformation (PGD) due to fault movement, liquefaction, differential soil movement, landslides, etc. But few researches are available on transient ground deformation (TGD) due to seismic excitations. Also, considering the limitations of analytical formulation and experimental facilities, numerical analysis can be a good option. Moreover, in the water supply industry, ductile iron pipe is used due to its good flexibility, ductility, efficiency, and cost-effectiveness as an alternative to PVC, AC, GI, CI, and MS pipe in most of the country, as well as in Bangladesh. Ductile Iron has ductility and toughness superior to all other Cast Irons, and equal to many Cast and Forged steels. The advantages of Ductile Iron are versatility, and higher performance at lower cost. This versatility is especially evident in mechanical properties where Ductile Iron offers the designer the option of choosing high ductility, with grades guaranteeing more than 18% elongation, or high strength, with tensile strengths exceeding 120 ksi

(825 MPa). The use of the most common grades of Ductile Iron "as-cast" eliminates heat treatment costs, offering a further advantage. To shed light on these issues, this study is concerned with a parametric evaluation of a seismically excited, relatively large diameter, ductile iron buried pipeline.

1.2 Background Study

The buried pipelines are subjected to earthquake hazards for their considerable length and wide geographical coverage. Breakdown or collapse of straight pipe, elbows; distortion, pull-out or leakages of joints and fittings; failure of asbestos-cement or concrete pipe bodies; failure of cast iron pipes etc. were some common modes of failure observed during the 1964 Niigata earthquake, around the Niigata City (Ariman & Muleski, 1981). It is also observed that earthquake damage has generally been significant and common in pipelines carrying water and low-pressure natural gas or oil (Narita, 1976). When a pipe travels from hard to soft soil having different dynamic properties, seismic damages are caused by axial deformations of the pipe due to the relative displacement of these two horizontally neighboring soil layers (Kubo, 1974). The displacement of buried pipelines followed by surrounding soil in both transverse and longitudinal directions due to seismic excitations was reported by (Leon & Wang, 1978).

Extensive study was conducted on severe damages caused by various high intensity earthquakes to lifeline utilities especially the gas and water supply pipelines such as 1971 San Francisco (O'Rourke & McCaffrey, 1984), 1989 Loma Prieta (O'Rourke et al, 1991), 1994 Northridge (O'Rourke & Palmer, 1996), 1995 Hyogoken-Nanbu (Oka, 1996), 1995 Kobe (Shinozuka et al., 1995), 1999 Kocaeli (Hashash et al., 2001), 1999 Chi-Chi (EERI, 1999) and Izmit (JSCE, 1999) and 2010 Chile (EERI, 2010) earthquakes.

In fact, there are sufficient evidence to demonstrate that the buried structures were weak to seismic ground motion. In southern California, in the northern San Fernando Valley, the Northridge earthquake deformed 76 meters of the underground pipeline, which had a diameter of 2.4 meters (Bardet & Davis, 1997). The San Francisco earthquakes of magnitude of 7.8 and 6.6 caused huge damage to underground tanks and buried pipelines in 1906 and 1971 (O'Rourke & Liu, 1999). In 1999, almost

8000 kilometers of water supply pipelines were destroyed during the Chi-Chi earthquake of magnitude 7.7 and 200 failures were recorded in the gas pipeline (Chi et al., 2001). The Kobe earthquake of magnitude of 6.9 in 1995 caused huge damages in buried pipelines; leaking gas from municipal gas pipeline contributed to explosions and fires and hindered water supply to million people due to failure of water pipelines. In Hachinohe city, the water supply pipelines suffered severe damages like as leakages due to pull-out of mechanical joints of these pipes during the 1968 Tokachi-Oki earthquake at northern part of Japan (Miyajima et al, 1976). These failures indicate that failure characteristics of strong earthquake-induced buried structures need to be studied for the protection of lifelines from the earthquake.

The main factors that affect the seismic damage include: i) the size, shape and buried depth of structure; ii) the characteristics of the surrounding soil; iii) the characteristics of the buried structure; and iv) the severity of the seismic excitation (Dowding & Rozen, 1978; St. John & Zahrah, 1987). The structural integrity and serviceability of the pipeline get significantly affected because of the relative displacement between the soil and buried pipelines. Relative displacement of pipe-soil happens under geotechnically troublesome conditions due to earthquakes, fault ruptures, landslides, aquifer over-pumping, mining and tunneling disturbances and frost or thaw induced ground deformations ‘(Wang et al, 2011; Ni et al, 2018; Trickey et al, 2016)’and more. In most cases, the internal pressure and the external loads such as seismic loads, installation mechanisms, soil and pipe properties, and degradation of materials are responsible for causing pipe failures (Davies et al, 2001; Saadeldin et al, 2015). In general, the dynamic responses of buried pipelines are influenced by frequency and types of seismic waves, pipe material and dimension, surrounding soil condition, joint types, internal pressure etc. (Datta, 1999).

Generally, there are two types of seismic hazards for buried pipeline: 1) transient ground deformations due to seismic wave propagation, 2) permanent ground deformations due to seismic faults, landslide, land subsidence, and liquefaction induced lateral spreading. In the past earthquakes, buried pipelines suffered considerable damages, as stated by (O’Rourke, 2003). These damages are due to both transient and permanent deformations on the ground (Liang & Sun, 2000).

1.3 Problem Statement

The pipelines that are buried form an essential structural category called lifelines (Hassani & Basirat, 2019). The buried pipeline network, which forms part of lifeline engineering, is engaged in long-distance water supply and drainage, oil, and gas transport etc. If the lifeline is damaged by geological disasters, particularly by a strong earthquake, the structural integrity of the lifeline would suffer a significant hazard. For dynamic analysis of seismic behavior of buried structures, the effects of soil stratification, soil-structure interaction, multi directional seismic excitations, ground water table fluctuation, material non-homogeneity, and intrinsic soil strata properties should be considered. Seismic damages of buried pipelines are mostly due to relative ground displacement, seismic waves travelling, liquefaction in sandy soil, fault ruptures or differential stiffness in between two horizontally adjoining soil layers etc. (Kubo, 1974). To determine the pipeline response subjected to strong ground shaking, these critical factors for geo-hazard analysis of buried pipe play a prominent role.

Bangladesh is also a Seismically active country. In the past 200 years, Bangladesh has been subjected to numerous destructive as well as mild earthquakes. Since gaining independence in 1971, Bangladesh has seen more than 250 earthquakes, some of which had a magnitude larger than 6.0, however the threats cannot be ignored. During these events, numerous structural damages of buildings, bridges, factories, schools, medicals, and buried pipelines were occurred. In the case of 8 July 1918 Srimangal Earthquake ($M = 7.6$) scenarios in Sylhet, Damage to potable water pipes were addressed as Total number of damaged points 204 (total affected length 118.53 km) and Damage to natural gas supply pipes were observed as Total number of damaged points 981 (total affected length 436 km) (Sarker et al., 2010). Despite the fact that numerous building damages were observed during the earthquakes in Bangladesh, some utility lines (buried water and gas pipelines) were also affected and damaged, which were not well addressed in any technical writings. For this reason, buried pipelines need more attention during an earthquake event. So, there is an enough scope for any structural damage specially buried pipeline damages due to

such kind of devastating earthquakes. These examples indicate that failure characteristics of strong earthquake-induced buried structures need to be studied for the protection of lifelines from the earthquake.

Permanent ground deformation (PGD) is a kind of large-scale ground deformation caused because of fault rupture or movement, settlement, subsidence/uplift, liquefaction induced lateral spreading or landslides deformations, etc. There has been a lot of study taking into consideration the occurrence of soil liquefaction (O'Rourke et al. 1991, Sumer et al. 2006) and fault movement (Karamitros et al. 2007, O'Rourke et al. 2016). For pipelines that have been running across active faults, seismic reaction mainly depends on several aspects, such as the type of fault movement (strike-slip, normal & reverse fault), soil conditions, dip angle, fault displacement etc. A simplified analytical model to analyze the influence of substantial fault movements on underground pipelines was first devised in (Newmark & Hall, 1975). A revised analytical method for estimating the elongation of pipelines which span either strike-slip or reverse strike-slip faults utilizing a large deflection theory was introduced by (Wang & Yeh, 1985). Kennedy et al. (1977) presented an approximate estimate of the pipe displacement for pipelines buried in liquefied soil. Chaudhari et al. (2013) showed that compression failure of buried pipeline is greatly influenced by pipe wall thickness and geometrical behavior is more significant than material behavior, when exposed to PGD because there is a thrust fault movement. Hongjing et al. (2008) discovered that the peak stress in buried pipe increases with increasing D/t ratio due to fault rupture caused by PGD, and that the seismic response of buried pipe increases with increasing soil displacement, crossing angle, and with lower buried depth.

In line with the analysis of the buried pipe under PGD, only a few studies have been conducted on the buried pipe subjected to seismic excitations causing Transient Ground Deformation (TGD). Newmark initiated research on the buried pipeline under the earthquake in 1967, whose theory is based on the concept of the inertial-free interaction of the soil-pipeline. In China, Yaoxian Ye (Ye, 1982) first conducted research about the soil-pipe interaction problem through a vibratory experiment in the various filling conditions including straight and bent pipe triggered by explosion. Afterwards, (Wenshui & ZhongHang, 1988) investigated the seismic response of 3-D

buried pipeline using finite element approach under traveling seismic waves. However, in the previous investigations, the soil around the pipeline was always simplified as a spring, so how to choose a spring's stiffness coefficient in the actual soil would be a challenge. However, significant research on the seismic response of the buried pipe was discovered using a 2D plain strain model, modeling the soil as a spring, a 3D model with harmonic loading, and so on. But very few works were found in the literature review regarding the 3D FE analysis of the buried pipe under real seismic excitations. The separate effect and failure mode of the buried pipe is studied in this paper based on a prescribed seismic wave. Also due to comparatively less research on the seismic response of ductile iron as pipeline material under uni-directional seismic excitations was investigated in this paper.

1.4 Significance of the Study

Pipelines are frequently referred to as "lifelines" due to their significance in distributing life-dependent utilities such as water, oil, gas, etc. For this reason, the seismic related problems on the underground utility systems have drawn attention to the recent researchers (Chaudhuri & Choudhury, 2019).

Moreover, there has been more attention given to the use of finite element approaches that include the linear and nonlinear soil-pipe interaction in 3D numerical analysis but less attention given to the seismic analysis. Due to the complex dynamic pipe-soil interaction, the behavior of the burial pipeline under seismic excitations is still not well known. In the analysis process it is also essential to take into consideration the variation of field conditions and soil nonlinearity. This will lead us to take scope of the future works on pipeline and soil (Chaudhuri & Choudhury, 2019).

In this context, all potential parameters that would adversely affect the structural integrity and reduce the life of a pipeline, must be taken into consideration. All potential parameters are required to investigate their prominent role in the seismic response of buried pipelines under a prescribed earthquake loading to provide some recommendations and probable modifications to rehabilitate the buried

pipe performance. Therefore, buried pipes under seismic events become safe if the critical parameters are addressed properly.

1.5 Objectives of the Study

To have a precise idea of parametric evaluation of buried pipeline subjected to earthquake excitations, numerical modelling of soil-buried pipe was conducted keeping following objectives in mind.

- To numerically investigate the dynamic response of the soil-buried pipe system by FEM analysis.
- To examine the sensitivity of different parameters (burial depth, and aspect ratio (D/t); embedment ratio (H/D) on the pipe's deformations and induced strains, type of buried pipeline, end-restraint conditions, soil characteristics, earthquake input ground motion etc.) on dynamic response of the soil-buried pipe system.

1.6 Outlines of the Thesis

This thesis comprises five chapters. A brief outline of each chapter is given below:

Chapter 1 provides the background and significance of the present study and key objectives of the study.

Chapter 2 gives a review of current literature on buried pipes for evaluating the response of buried pipeline subjected to seismic excitations. It also provides a brief overview of different study and their potential ability to evaluate the pipeline performance under seismic excitations. It also summarizes the factors affecting seismic response of buried pipe and failure mechanism of buried pipe.

Chapter 3 gives details of the 3-dimensional (3-D) finite element analysis used for the research. It also discusses the development of the FE models used in the response analysis of buried water-carrying pipes, and includes the geometry of the model, the material model, boundary conditions, and the model meshing as well.

Chapter 4 presents the results of a parametric study on buried DI pipe in seismic environment. Several influential parameters are explored including the D/t and h/D

ratio, pipeline's burial depth, diameter and thickness of pipe, soil density, modulus of elasticity of soil, friction angle of soil, interface friction co-efficient between pipe and surrounding soil, boundary conditions at both pipe ends, unidirectional seismic excitations, water flow condition etc.

Finally, **Chapter 5** summarizes the key findings from the work and outlines for further research and challenges in this area. The limitations associated with this current work are also stated.

Chapter 2. LITERATURE REVIEW

2.1 General Overview

A comprehensive overview of the literature on the response analysis of buried pipe under seismic excitations is provided before continuing to the original contribution of current research. The fundamentals of the buried pipe subjected to medium to strong earthquake is focused. The governing factors affecting the seismic response of buried pipeline is diagnosed elaborately. The failure mechanism of buried pipe under seismic event are also presented. A brief synopsis on experimental, analytical and numerical study on response analysis of buried pipe are discussed here. In this chapter, numerical investigation has been elaborately presented to bring a succinct review of the relevant knowledge and understandings, and then to present the research gaps.

2.2 Fundamentals of Buried Pipeline

Structural efficiency of buried pipelines in geo-hazardous areas is becoming more and more important now a days. In fact, the pipeline operators' primary aim is to reduce seismic damage to the pipeline in the event of an earthquake, while at the same time protecting the unimpeded flow of fluid supplies. Buried pipelines are deformed seriously much beyond its elastic limit due to severe seismic excitations. To preserve the structural integrity and avoid leakages, the structural damage of the buried pipeline should be kept to a minimum for this reason. Since buried pipelines normally travel long geographical distances, several failures may be experienced during seismic events, because of permanent ground displacement (PGD) and/or seismic wave propagation. Because of permanent ground deformations, the damages usually happen in extreme ground failure associated with higher rate of damage, whereas damages due to transient ground deformations occur over a larger area, associated with lower rate of damages (O'Rourke, 2003). The effects of transient ground deformations caused by on continuous buried pipelines are discussed in this context.

2.3 Factors Affecting Dynamic Response of Buried Pipelines

2.3.1 Soil–Pipe Interaction

The behavior of buried pipe exposed to seismic excitation is significantly influenced by the soil-pipe interaction (Corrado et al., 2009). When the stiffness of soil is comparable to the stiffness of pipeline, at that situation soil-structure interaction would be essential. Differential displacement can develop during seismic excitation because of differences in the dynamic properties of buried pipelines and the surrounding soil medium, resulting in differential strain and stress. Eventually, pipeline failure may occur due to induced axial and bending stresses by crushing or buckling. Mavridis and Pitilakis (1996) and Dwivedi et al. (2010) demonstrated analytically that dynamic soil-pipe interaction (SSI) effects play a significant role in case of axial response of pipeline rather than lateral response. They also suggested that stronger pipe material, thicker pipe wall, flexible joints etc. may improve the seismic response of continuous segmented pipeline. A penalty friction algorithm was used for soil-pipe interface interaction in this study to consider the friction between the interface between soil and pipe with finite sliding.

2.3.2 Permanent Ground Deformation

Large-scale soil deformation resulting from soil liquefaction, differential soil movement, landslide or fault movement is regarded as permanent ground deformation (PGD). The geometrical behavior of buried pipe, when exposed to PGD under thrust fault movement, becomes more significant than that of the material behavior of pipe or its failure (Chaudhari et al., 2013). For example, Hongjing et al. (2008) observed that the seismic response (peak stress) of buried pipeline subjected to PGD, was reasonably increased as the D/t , soil displacement, and crossing angle were increased, and decreased as the buried depth increased.

2.3.3 Seismic Wave Propagation

There are two main forms of seismic waves: (i) Body waves e.g., compressional and shear waves, and (ii) surface waves e.g., Love and Rayleigh waves. In general, high ground strain is produced due to the low propagation velocity of surface waves. The reverse is true for body waves. As a matter of fact, surface waves can cause more damages to buried pipelines than body waves. The effect of seismic wave propagation on dynamic response of buried pipeline was investigated by Boorboor & Hosseini

(2015) who found that the effect of transient action of seismic wave in the form of stress, rotation, or damage along the straight portion of pipeline is less significant than at the intersection or joints or at the bends of pipeline. Shaalan et al. (2014) observed that stiffer soils permit faster seismic wave propagation by amplifying it whereas softer soils allow slower seismic wave propagation by dampening it. In the design of underground structures (Wood, 2015), it has been established that earthquake-ovaling or racking deformations can be produced in a buried structure when seismic waves propagate along the perpendicular direction (with respect to the longitudinal axis) of the structure.

2.3.4 Miscellaneous Factors

Various other factors e.g., pipe diameter, wall thickness, buried depth, soil characteristics, fluid density & velocity inside pipe, longitudinal slope etc. can influence the dynamic behavior of soil-buried pipe system (Mukherjee et al., 2013; Sahoo et al., 2013; Hosseiny et al., 2014). Mukherjee et al. (2013) reported that the axial strain in pipe increases as the diameter increases which results in an increased pipeline slippage. Whereas increase in buried depth reduces pipeline slippage since the confining pressure increases with depth. It was also observed that bending moment in pipe increases exponentially in the vicinity of the support and away from the support, increases linearly. Sahoo et al. (2013) found that displacement and stress variation in pipe is not significant if the burial depth is equal or greater than twice the pipe diameter. Hosseiny et al. (2014) observed that due to the increase in seismic acceleration, applied tension and shear on the pipe rises due to the increase in increase in period of earthquake. It was also reported that density of fluid inside the pipe influences the pipe deformation.

2.4 Failure Modes of Buried Continuous Pipelines

The dominant modes of failure for continuous non-corroded and welded steel pipelines are wall rupture due to axial tension and local buckling due to axial compression and flexural failure. The beam mode buckling due to excessive compression can also be seen where the burial depth is shallow in case of continuous pipelines. The failure modes of the continuous pipeline are summarized below based on the information found in O'Rourke & Liu (1999) and Psyrras & Sextos (2018).

2.4.1 Local or Shell Mode Buckling

This bulking due to compressive load or pure bending is usually found in large diameter pipe buried in deeper depth shown in Fig. 2-1 and Fig. 2-3 (a). Local buckling (or wrinkling) creates local structural instability at the pipeline wall. Since local shell wrinkling initiates, the more geometric distortion is concentrated in the wrinkle or buckle, as significant compressive strains are induced by ground deformation and seismic wave propagation. Due to big curvatures in the pipeline wall, circumferential cracking in the pipe wall and leakage are observed. Also, repeated loading (e.g. minor internal pressure or temperature variations) can lead to the development of fatigue cracks, which seriously threaten the pipeline's structural integrity (Dama et al., 2007). This type of failure to a buried water pipeline in Mexico City was occurred due to seismic wave propagation in the 1985 Michoacán event. (Gresnigt & Karamanos, 2009) proposed that the buckling or Compressive strain limit generally depends on diameter-to-thickness ratio (D/t), internal or external pressure on pipe, yield stress of pipe material, Initial imperfections, and residual stresses.

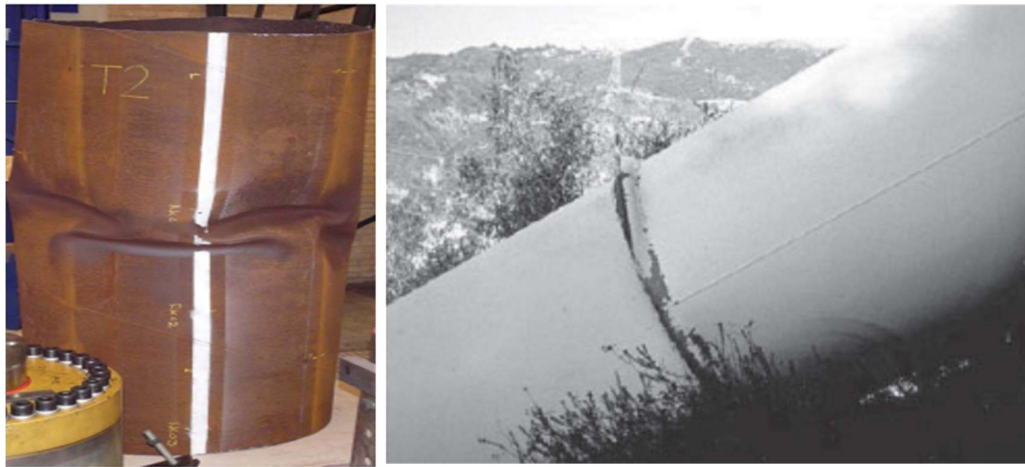


Figure 2-1: a) Local buckling of a spiral welded pipe, $D/t = 119$, subjected to longitudinal bending because of severe pipe wall compression (Vasilikis et al., 2014); b) Locally buckled steel gas pipeline in the compression zone at north slope of Terminal Hill in 1994 Northridge Earthquake (EERI, 1995)

2.4.2 Beam Mode Buckling

The pipeline as a slender member may buckle as a beam due to excessive quasi-uniform compression presented in Fig. 2-2. Under this bulking, pipe is subjected to compression causing upward bending which resisted by overlying soil displayed in Fig.2-3 (b). This

kind of failure exists in shallowly buried pipes with smaller diameter (about 3 feet or less). Beam buckling is resisted by the lateral resistance applied by the surrounding soil. Shallow trenches and/or backfills with loose materials generally promotes this failure. Usually, beam bulking is influenced by buried depth, stiffness of backfill material, bending stiffness of pipe etc. (O'Rourke, 2003) suggested that the critical cover depth of a buried pipeline by setting the minimum beam buckling stress equal to local buckling stress so that beam buckling governs before local buckling.

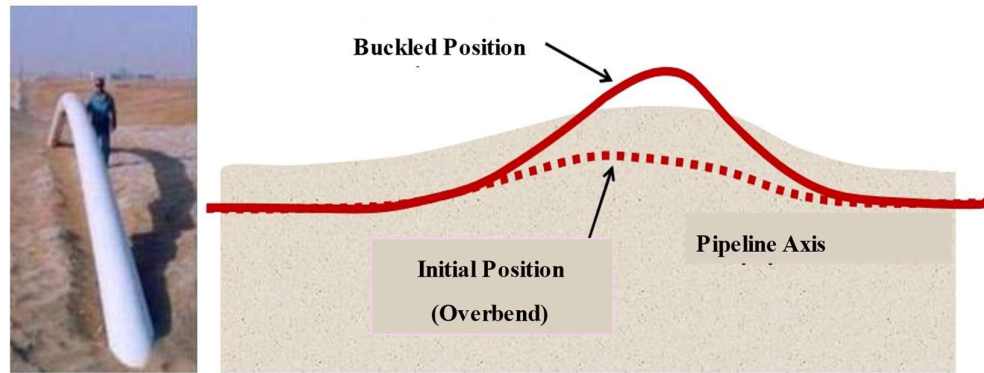


Figure 2-2: Beam buckling of buried pipeline due to excessive axial loading (after Karamanos et al., 2014)

2.4.3 Flexural Failure

This type of failure is due to excessive bending strains in the pipe section. In addition, significant bending deformations, depending on the R/t ratio of pipe, may lead to the moment-curvature equilibrium to an ovalization or an instability limit.

2.4.4 Tensile Failure

Seismic-related threats like faulting, landslide, liquefaction, seismic excitation, and differential ground movement causing tensile strain in the joints (i.e., arc welded butt joints) of pipeline are responsible for this failure, displayed in Fig. 2-3 (c). Ductility controlled pipelines are less susceptible to this kind of failure as like as Ductile Iron pipe. (Karamanos et al., 2014) proposed that the ultimate tensile strain should be from 2% to 5% for butt-welded-water pipelines.

2.4.5 Cross-Section Ovalization

This type of failure due to bending stress changes the original diameter of the pipe and changes the shape of pipe section from circular to oval, demonstrated in Fig. 2-3 (d). The cross-sectional distortion may be defined with a non-dimensional “flattening

parameter" f , in terms of change in pipe diameter to original diameter i.e., $f = \Delta D/D$. According to Gresnigt (1986), when ' f ' turns to 0.15, a cross-sectional flattening limit condition is achieved.

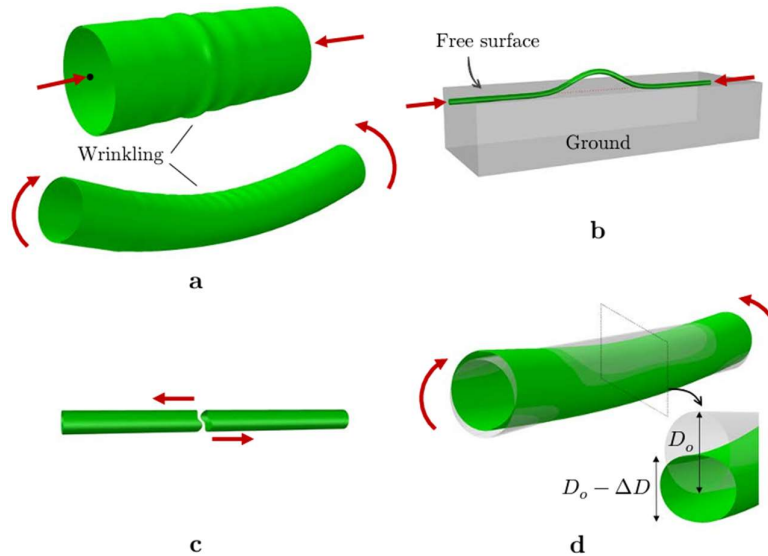


Figure 2-3: Most common failure mechanisms in buried and continuous steel pipelines: (a) shell-mode buckling due to uniform axial compression (top) and pure bending (bottom); (b) beam-mode buckling; (c) tensile rupture and (d) cross- section ovalization (O'Rourke & Liu,1999)

2.5 Failure Mechanism in the segmented pipeline

Axial pull out failure occurs due to tensile strain at the joints of segmented pipeline when the joint caulking material's shear strength is much lower than the strength of pipe. Crushing of bell and spigot joints failure occurs due to compressive strain at such joints. Flanged joint failure occurs at such joint due to the collapse of the flange connection by tensile strain. Circumferential flexural failure and joint rotation occur due to lateral permanent ground displacement or seismic excitations by a combination of joint rotation and flexure in pipe segments.

2.6 Previous Research on Buried Pipe

The impact of seismic excitations on buried pipelines and soil-pipe interaction has been extensively studied previously. This has led to the development of numerous analytical, experimental and numerical solutions to assess pipeline responses due to seismic excitations. Some of these studies are discussed in the following section.

2.6.1 Experimental Study

Ye (1982) first conducted research about the soil-pipe interaction problem through a vibratory experiment in the various filling conditions including straight and bent pipe triggered by explosion. Hosseini & Tafreshi (2002) developed a physical model under seismic vertical excitation for flexible pipes. (Argyrou et al., 2019) investigated the efficiency of a flexible ductile iron pipe strengthened by linings against the seismically induced fault rupture using laboratory large scale experiments and 2D finite element analysis. The dynamics response of the underground pipeline was studied initially by Sakurai & Takanashi, 1969; and found that axial deformations in the pipe fit the ground movement for low intensity earthquake during the Matsushiro earthquake, employing field tests. It may also be pointed out from the test findings derived from O'Rourke et al. (2008) 's large-scale split box test and centrifuge test that high-density Polyethylene (HDPE) pipes can be utilized to handle substantial deformation due to earthquakes, for their high ductility behavior.

2.6.2 Analytical Study

Newmark initiated research on buried pipeline under the action of earthquake in 1967, whose theory was based on the concept of inertial-free interaction of soil-pipeline. For a buried pressurized pipeline in a homogeneous elastic soil medium, Lee et al., (1984) employed an elasto-plastic cylindrical shell formulation based on a basic flow plasticity theory and to verify the stability of a pipe shell's dynamic equilibrium used a variational formulation for equations of motion. Their results indicated that, under static and dynamic conditions, the pipeline's axisymmetric bulking stress and strain are basically the same. Yun & Kyriakides, (1990) analyzed a buried pipeline under compressive load and used large-deflection beam kinematics and Sander's nonlinear thin shell theory to formulate the problems analytically. Kouretzis et al. (2006) developed the elastic shell equations to evaluate axial and hoop strain distribution in a long cylindrical pipe because of out-of-phase vibration produced by travelling harmonic S-waves.

2.6.3 Numerical Study

Mesh-based numerical methods such as the Finite element method (FEM) and the Finite-difference method (FDM) have been considered as the standard numerical methods for solving geotechnical problems. Various methods of analysis have so far

been proposed by researchers for the computation of seismic response of buried pipelines, based on different types of models and the response quantities of concern.

Newmark (1967) suggested that if no soil-pipe interaction is considered, the straight pipeline portion would follow the deformation of soil. Sakurai & Takahashi (1969) and O'Rourke & Hmadi (1988) proposed a quasi-static analysis incorporating beam elements to consider the soil pipe interaction. Lee et al. (2009) conducted a numerical simulation on buried pipes under earthquake ground motions.

As the beam model cannot assess the large deformation developed in the pipe cross section, researchers have suggested the FEM shell model to overcome this problem (Takada et al., 1995; Datta, 1999; Kouretzis et al., 2006). Few Studies on straight rigid and flexible buried pipes, also conducted by Wang et al. (1906), O'Rourke et al. (2004), and Shi et al. (2008). In all the above research, the soil-pipe interaction was simulated with the Winkler principle and usually expressed by soil spring elements in the axial, transverse horizontal and transverse vertical directions.

Lanzano et al. (2014) investigated the seismic behavior of a buried steel pipe by means of 2D finite element analysis. By 3D finite-element analysis, Sahoo et al. (2014a) analyzed the seismic responses of single steel pipe and two interacted steel pipes, which were buried in sandy soil. Liu et al. (2017) investigated the seismic response of segmented cast iron pipes by means of finite element analysis. Using 3D finite element analysis, Somboonyanon & Halmen, (2018) analyzed the seismic response of the buried steel pipeline. Lee (2010) also used FEM to investigate the response of steel pipelines due to dead loads, traffic loads and seismic loads. The mechanical behavior of underground pipelines under multi directional seismic excitations was analyzed by (Yang & Zhang, 2011) using 3D FEM analysis. Datta (1999) investigated response analysis methods, seismic performance of buried pipelines with various parametric variations, seismic damages in pipe and seismic risk assessment of buried pipelines. For an extreme earthquake, Ogawa & Koike (2001), suggested a simpler FEM approach for assessing plastic deformation of the buried pipeline using a popular FE Software, ABAQUS.

2.6.3.1 Finite Element Method (FEM)

The finite element method (FEM) is the most popular numerical tool for addressing issues in diverse fields of engineering and mathematical models. Structural analysis, geo-hazard analysis, fluid flow, heat transfer, mass transportation, and electromagnetic potentials are some common areas of FEM. FEM applications in geotechnical engineering include a study of buried pipeline analysis, slope stability analysis, seismic wave propagation, dynamic soil structural interactions, analysis of dams and tunnels, seepage analysis in soil and rock, etc. The Finite Element Method (FEM) in computational geomechanics has been recognized as the standard grid-based numerical solution for small and large-scale deformation problems. In the field of geotechnical earthquake engineering, it is often troublesome to carry out field tests. As such, numerous geotechnical problems such as retaining wall, pile foundation, embankment, dam, buried pipe, etc. under seismic loads, have been investigated using several numerical methods. In these problems, the dynamic finite element analysis (DFEA) is considered as one of the efficient and powerful numerical tools to investigate the stress, displacement, and strain responses of the soil-structure systems. In addition, FEA needs a suitable soil constitutive model, a proper characterization of soil by field and laboratory tests and a clearly defined seismic records as input.

FEM is useful for rigorous analysis of static and dynamic responses of underground pipelines (Datta, 1999). Though there are limitations for exact analysis of such problems, FEM is still capable of solving linear and non-linear problems, like the forecasting of relative displacement, deformation, stress, strain, etc. between soil and buried pipelines.

2.6.3.2 Time History Analysis (THA)

THA is a nonlinear dynamic analysis where a chosen seismic ground motion is applied at the base of the structure. Instantaneous stresses in the structure are assessed at small intervals for the entire period of the earthquake. THA provides precise results compared to pushover analysis since it imparts real seismic data as an input file, although owing to its greater computational time, the time history analysis is less commonly used. A selection of earthquake records, then a digitalization of the database, is the key steps for THA. The digitalized record is applied to the base of the model and analysis is executed after creating the mathematical model for the structure. After that the maximum

response of the structure in the form of displacement, stress, strain etc. can be achieved. Taking the advantages of this method of analysis with the El Centro seismic record, it was successfully employed in this study.

2.7 Scope of the Current Research

Many complex engineering problems related with geo-hazardous events may now be resolved by numerical method utilizing computer codes in all disciplines of engineering and the physical sciences. Now a days, due to less computational time and accuracy, numerical simulation has superseded conventional analytical and experimental work and getting popular. It is observed that in the literature, there is a little scope in analytical approach to deal all important features of buried pipe. Sometimes analytical solutions are excessively complicated, and many assumptions must be made for exact solution. For experimental work, it needs more time to conduct the experimental procedure efficiently. Also, the experimental installation must be adequately equipped, otherwise it is impossible to correctly carry out measurements and observations. But in numerical method these limitations are properly addressed. Additionally, numerical simulations may be used as a tool to validate analytical solutions and experimental findings, respectively.

For dynamic analysis of seismic behavior of buried structures, the effects of soil stratification, soil-structure interaction, multi directional seismic excitations, ground water table fluctuation, material non-homogeneity, and intrinsic soil strata properties should be considered. If fluid carrying pipelines are placed in seismic prone areas, they are subjected to seismic loads during operation. Since this issue is being investigated sufficiently, there is not enough evidence on the study of Ductile Iron pipes using seismic loads in the available literature. The assessment method for evaluating stresses due to seismic loads contained in the ALA Guideline is limited to manual calculations and its application in the FEM analysis is not adequately addressed. Due to insufficient guidelines in the available codes, designers often fail to analyze the pipe properly which lead to under design or overdesign of it.

Buried pipeline is the most efficient, cost-effective, and safe way of carrying fluid to consumers and communities through long distance and is very concerned with structural safety and durability. Flexible pipes must be able to deform considerably under

maximum load as like as thin-walled pipes. Many hundreds of kilometers of pipeline as flexible pipeline are used for fluid supply in urban areas. In addition, the size of pipelines that provide utility services to the metropolitan region has been increasing day by day with the high demand of fluid. For this reason, many cities are replacing old, corroded, narrow pipelines with a large diameter pipeline to meet the rising demand. There is no doubt that larger pipelines are more vulnerable to various forces like traffic loads and seismic loads, etc. To determine the actual damage to the pipeline considering different parameters, an analysis of large diameter pipeline under seismic loads is therefore necessary.

The expected outcome of the proposed research is to analyze the seismic performance of buried pipelines. The interaction between soil and buried pipe will also be analyzed. In addition, the effect of various parameters on response of buried pipeline will be checked quantitatively. Based on the parametric study, it is expected to find the sensitive parameters accountable for the buried pipe analysis. Then, some recommendation and probable modifications can be suggested to rehabilitate the buried pipe performance. Based on this research work, the future scope of work on this topic will be outlined.

2.8 Insights from Literature Review

The single response spectrum is generally not practical for a lengthy buried pipeline. Keeping this fact in mind, displacement or acceleration time history of a prescribed (real) earthquake is useful for seismic response assessment with a seismic wave propagation velocity and a certain direction in the underground pipeline. For this reason, in this research, time history analysis was employed to investigate the seismic response of pipe.

Another important aspect of this study is- adaption of ductile iron (DI) pipe as buried pipeline. DI pipes can be a key component in maintaining contemporary living, providing enough ways to transfer drinking water, sewage, and storm water etc. Evidence from past investigations has shown that seismic excitation damages underground structures, including pipelines. Very few investigations into the response and design of underground pipes under seismic shaking have been discovered in the literature. To shed some lights on that aspect, this study was aimed at investigating the seismic response of underground pipes when subjected to seismic excitations. A

3D finite element model has been created in a popular FE Software, ABAQUS to study the combined effects of the seismic excitations, traffic load, water pressure and pipe diameter and thickness, burial depth, and the pipe end constraints etc.

Chapter 3. NUMERICAL PROCEDURE

3.1 General Overview

A limited number of researches have been carried out on the seismic assessment and seismic behavior of the underground pipelines. Moreover, very few studies focus on the 3D numerical modeling of buried pipes, the non-linear interaction between pipeline and soil, and the seismic responses of pipelines caused by earthquakes. Since a 3D dynamic analysis of the interaction between the pipeline and soil during multipoint seismic excitation is taken into account, assessing the seismic response of underground pipelines is quite complicated (Wang & Raymond, 1979). So, a detailed seismic analysis should be required. To solve this problem, Finite Element Analysis (FEA) plays a vital role considering the non-linear behavior of soil as well as buried pipeline. In this chapter, a detailed numerical procedure using Abaqus (6.14) software for the seismic analysis of buried pipe installed in the 3D soil continuum under prescribed seismic excitations is presented.

3.2 Background of Numerical Procedure

Using computer codes, it is now possible to solve plenty of complex problems relating to real-world events in all engineering and physical science disciplines. Numerical simulation has replaced conventional theoretical approaches and experimental methods because of its less computational time, higher accuracy and enables us to estimate solutions to problems that can be very difficult to solve precisely by other techniques. Obtaining a useful solution from an analytical approach frequently requires the construction of a number of assumptions, which makes the approach too complicated. Measurements and observations are challenging to perform accurately without a properly equipped experimental setup. In addition to aiding in the explanation and creation of new affairs, computational simulation serves as a tool for validating theoretical hypotheses and experimental results. Through numerical simulation, a bridge can be made between theoretical approaches and experimental models. Numerical

simulations are generally carried out using two methods: grid-based or mesh-based methods and mesh free methods. For the current thesis, Finite Element method as a mesh-based methods were used to reproduce the soil and pipeline for a realistic simulation using a FEM tool, Abaqus Program (version 6.14) and the nonlinear time history analysis of the buried pipeline was performed.

3.2.1 Finite Element Method

In this method, the computational frame includes grid or mesh. It consists of grid nodes which estimate the problem domain geometry. The grid nodes are the positions where the field variables are analyzed, and their relationships are characterized by nodal connectivity. Following the connectivity, grid nodes are linked to create a mesh. The precision of the numerical extrapolation is directly correlated to the cell size and patterns of any mesh. Mesh-based numerical methods such as the Finite element method (FEM) and the Finite-difference method (FDM) have been considered as the standard numerical methods for solving geotechnical problems. The finite element method (FEM) is by far the most commonly known tool to solve engineering problems and mathematical models. Common fields of FEM involve structural analysis, fluid flow, heat transfer, mass transport, and electromagnetic potential. In geotechnical engineering, FEM applications include stress analysis, propagation of stress waves, dynamic soil-structure interactions, analysis of dams, tunnels, boreholes, buried pipes, seepage of fluids in soils and rocks, slope stability analysis, and so on. In computational geomechanics, the finite element method (FEM) has been regarded as the standard grid-based numerical solution and is effective for large-scale problems. Figure 3-1 shows the meshing concept of FEM.

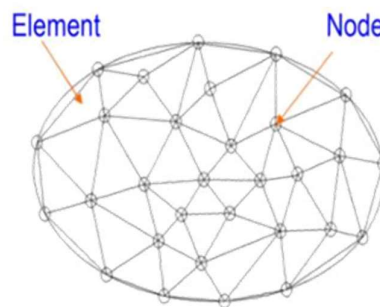


Figure 3-1: Grid based methods (Finite Element Method (FEM))

These advantages make the FEM a more generic, systematic, powerful, and easily adaptable numerical method than other more sophisticated numerical methods. The advantage of adopting the finite element approach is that once the model is established, numerous cases may be studied, and the sensitivity of assumptions can be checked. Furthermore, for those buried pipe applications that are difficult to analyze using typical analysis techniques, a finite element analysis may be conducted. Katona & Center (1976) pioneered the use of the finite element method to solve buried pipe related problems.

Finite element analysis may be a useful and effective approach for analyzing the behavior of buried pipelines under a range of geometric and loading conditions. There are commercially available user-friendly computer programs (e.g., Abaqus etc.) that may be used to model the soil–pipe system and produce trustworthy findings.

3.2.2 Non-linear FEM

The non-linear FEM can be conducted using non-linear material property, non-linear geometry and/or non-linear boundaries. If the model is loaded beyond its elastic limit and the predicted deformation is high, non-linear FEM provides an excellent result. In every model there are three kinds of non-linearities: a) Geometric nonlinearities, b) Material non-linearities, c) Boundary nonlinearities. Few nonlinearities in the model have also been experienced in this analysis. This study was conducted with the introduction of non-linear geometry to provide the second ordered effect. For contact analyses, non-linear boundaries are modelled by applying an elastic-perfectly plastic frictional formulation. The contact between the non-connected FE meshes reveals the boundary nonlinearities in the model. In all soil and pipeline model, Material non-linearities can be discovered. Soil and pipe were modeled as with both elastic and plastic behavior.

3.2.3 3-Dimensional FEM

It is more appropriate to simulate the real scenario by using three-dimensional models for the evaluation of axial and bending deformations in pipes than a 2D or plain strain model. A realistic and convenient 3-dimensional FEM was also developed in this study using Abaqus Program.

3.3 Numerical Modelling of Soil-Pipe System

The size of soil domain has been formed as a cuboid with a buried pipeline at its center of width. Figure 3.2 represents the schematic 3D diagram of soil and pipeline model with their proper dimensions.

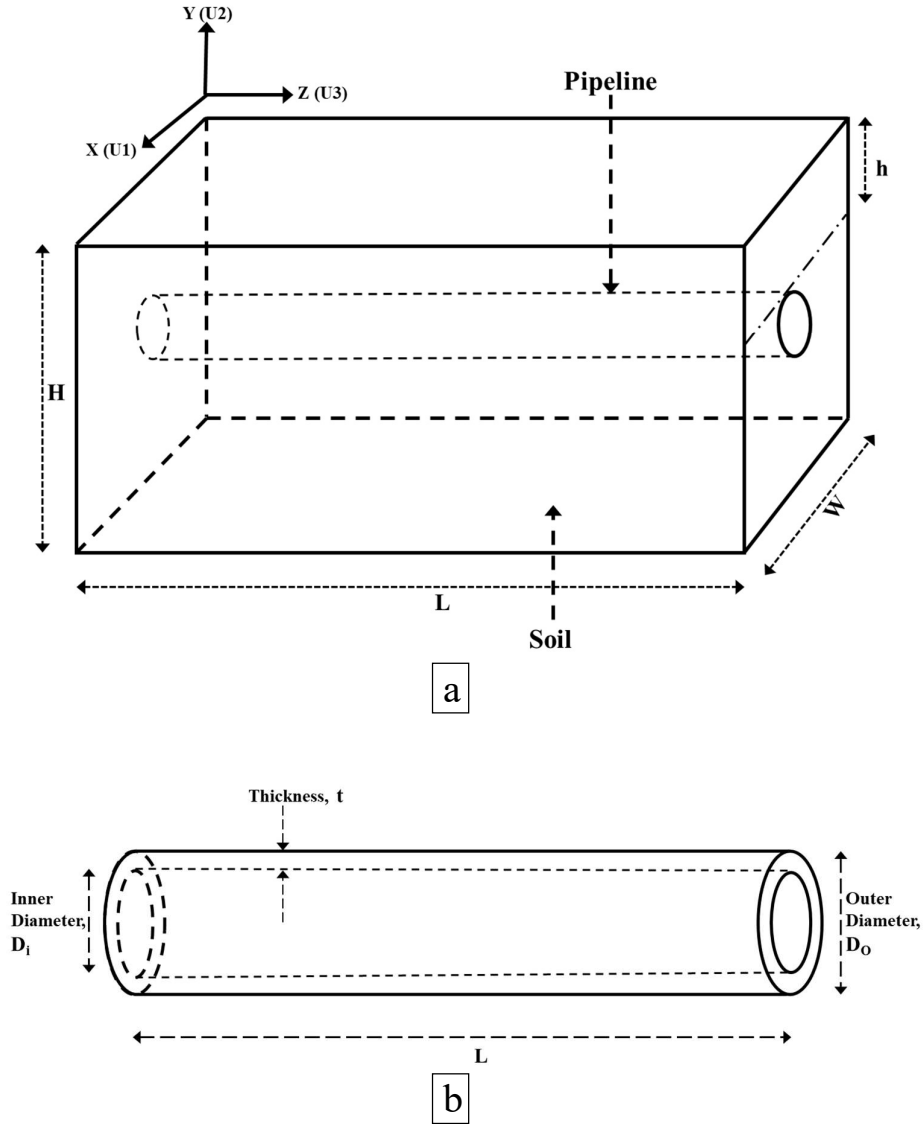
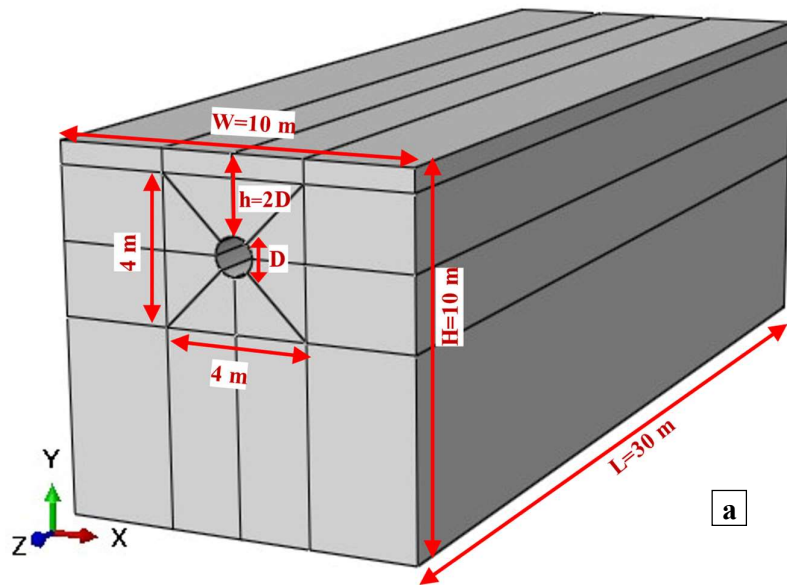


Figure 3-2: Schematic 3D diagram of a) soil and b) pipeline model

A few analyses were carried out to examine the effect of the length of the model (taken as 20, 30, 50, and 100 m), and a minimum variation was found in the seismic response of buried pipe. Hence, following the length of pipelines as found in various FEM related works in case of seismic analysis, the length (L) of soil model as well as pipeline was

considered as 30 meters [Alamatian et al. (2013); Kazemi and Saffari (2015); Meesawasd et al. (2016); Somboonyanon and Halmen (2016)]. Also, to save the computational time and memory, soil-pipe model length was limited to 30 m only. To provide an affordable space in which the pipeline with soil could fail when FEA was performed, the width (W) and height (H) of the soil were both set at 10 meters. The pipeline was aligned with the soil model in the center of the soil width according to the buried depths of the pipeline (h), measured from the top surface of the soil to the crest of the pipe, such as 1D, 2D, 3D, 4D, and 5D (D is the outer diameter of the pipe). The maximum buried depth of 5D m for the pipeline was selected because the live load is insignificant compared to dead loads in deeply buried pipelines (Trott, 1984). While pipes are buried at a minimum depth of 0.9 to 1.2 meters, it is possible to clearly investigate the behavior of pipelines by evaluating measurements taken at depths above or below these limits.

The pipeline model was defined as a 3-dimensional deformable shell because of the small thickness of the pipeline and the soil model was defined as a 3-dimensional deformable solid body as in Fig. 3-3 in the complete ABAQUS environment.



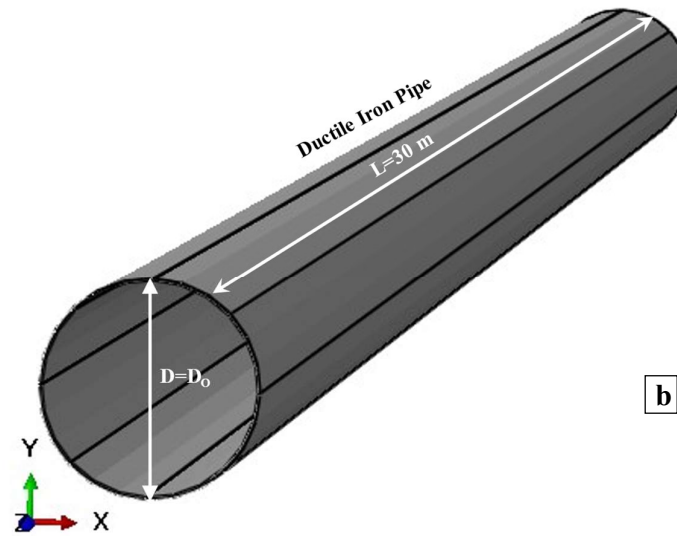


Figure 3-3: 3D FE models: (a) soil as deformable solid (b) pipeline as deformable shell, in the complete ABAQUS environment.

3.3.1 Constitutive Relation for Soil

In any numerical approach, the most difficult part is to characterize its materials. Even in FE analysis, a proper constitutive relation is necessary to solve the stress equation. Various approaches are available for constitutive model such as: Viscous model, Elastoplastic model etc. Tests on soil samples reveal elastoplastic behavior of soil. Few basic and practical soil constitutive models are available such as Hooke's law, Linear elastic (LE) model, Elastic Mohr-Coulomb (MC), Elasto-plastic Mohr-Coulomb (MC), Drucker-Prager, SANI-Sand, Nor-Sand, Duncan-Chang or Hyperbolic model, (Modified) Cam Clay, Hyper-elastic Model, Hypo-elastic Model, Hardening soil (HS) model, Hardening soil model with small strain stiffness (HS small), Visco-plasticity Theory, Plaxis Soft Soil (Creep) and Plaxis Hardening Soil Model etc. Most of the models are sophisticated and require complex understanding and need several parameters. In the context of simplicity, ease of use, less computational time, few parameters involved and a better understanding by common geotechnical engineers, Elasto-plastic MC model was considered in the current study to characterize the soil behavior. This model is applicable for granular soil. MC model requires only a few parameters that can be readily determined through direct shear tests, unlike other models which require their parameters via proper regulated triaxial tests.

Based on the relevant literatures and the features of FE software, the mechanical behaviors of soil and rock material were incorporated by an elastic-perfectly plastic Mohr-Coulomb (MC) constitutive model. In a soil-pipe interaction event, Yimsiri et al. (2004) demonstrated that Mohr-Coulomb model gives reasonable results. This model has also been successfully applied on soil-pipe interaction problem including large soil deformations (Popescu et al., 2002; Guo & Stolle, 2005).

The Mohr-Coulomb model is an elastic-perfectly plastic model and forms, in fact, a combination of Hooke's law as a first order approximation involving isotropic linear elastic behavior and generalized form of Coulomb's failure criterion, formulated in a plasticity framework (Smith & Griffith, 1982) and demonstrated in Fig. 3-4.

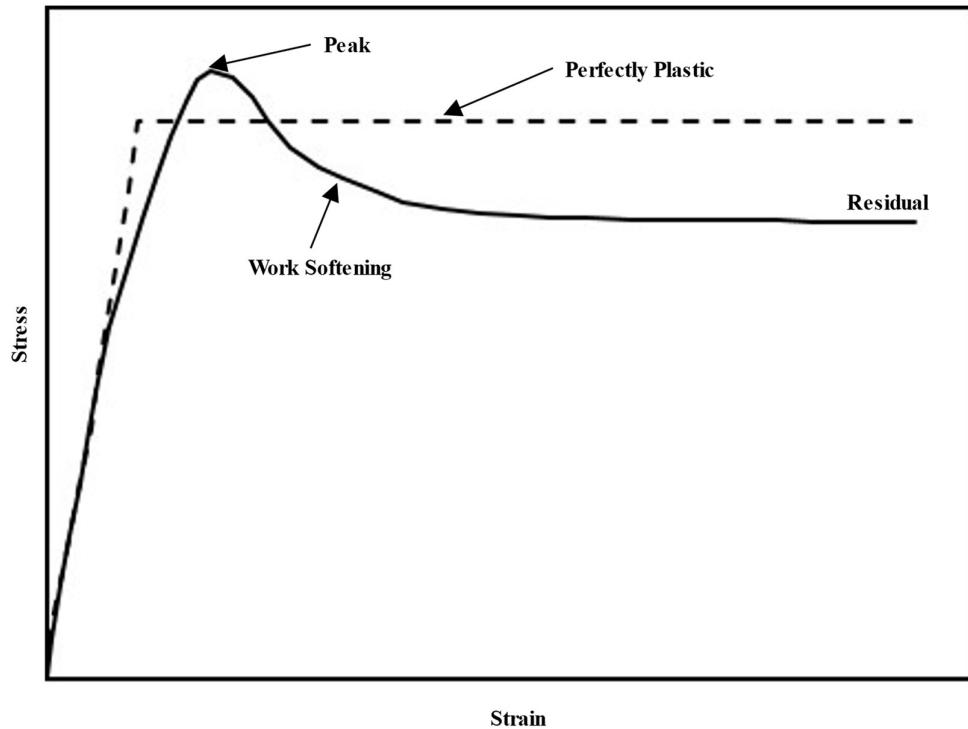


Figure 3-4: Elastic-perfectly plastic assumption of Mohr-Coulomb Model. (After Smith & Griffith, 1982)

According to the Mohr-Coulomb criteria, failure happens when the shear stress at any location in a material exceeds a certain threshold that varies linearly on the normal stress in the same plane. The Mohr-Coulomb model is based on graphing Mohr's circle in the plane of the highest and lowest principal stresses for states of stress at failure. The best straight line that touches these Mohr's circles is the failure line as shown in Fig. 3-5.

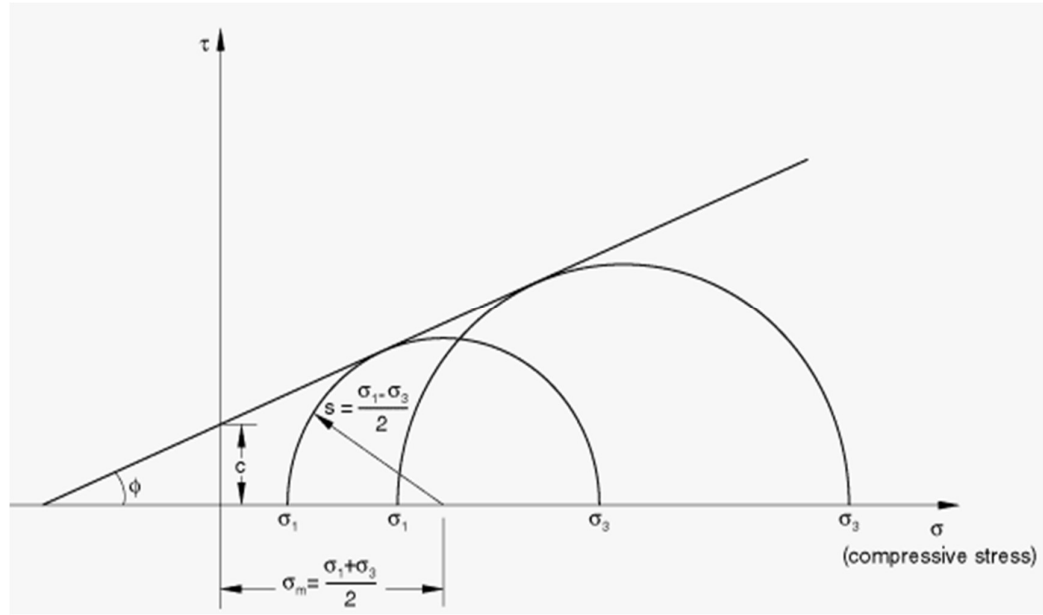


Figure 3-5: Mohr-Coulomb failure model

However, the Mohr-Coulomb model may be defined by the following

$\tau = c - \sigma \tan \phi$, where σ is negative in case of compression.

From the Mohr's circle,

$$\tau = s \cos \phi \text{ and } \sigma = \sigma_m + s \sin \phi ,$$

where $s = \frac{1}{2}(\sigma_1 - \sigma_3)$, the maximum shear stress; σ_1 , the maximum principal stress;

σ_3 , the minimum principal stress and ϕ is the friction angle.

Substituting for τ and σ , multiplying both sides by $\cos \phi$, and reducing, the Mohr-Coulomb model can be expressed as

$$s + \sigma_m \sin \phi - c \cos \phi = 0$$

$$\text{where } \sigma_m = \frac{1}{2}(\sigma_1 + \sigma_3)$$

This model is more readily expressed in terms of three stress invariants for generic states of stress as

$$F = R_{mc}q - p \tan \phi - c = 0$$

where,

$$R_{mc}(\theta, \phi) = \frac{1}{\sqrt{3} \cos \phi} \sin \left(\theta + \frac{\pi}{3} \right) + \frac{1}{3} \cos \left(\theta + \frac{\pi}{3} \right) \tan \phi$$

ϕ is the slope of the Mohr-Coulomb yield surface in the $p - R_{mc}q$ stress plane (Figure 3-6), defined as the friction angle of the material and which depends on temperature and predefined field variables;

c is the cohesion of the material; and Θ is the deviatoric polar angle which can be expressed as

$$\cos(3\Theta) = \left(\frac{r}{q}\right)^3$$

and

$p = -\frac{1}{3}\text{trace}(\boldsymbol{\sigma})$, is the equivalent pressure stress,

$q = \sqrt{\frac{3}{2}(\mathbf{S} : \mathbf{S})}$, is the Mises equivalent stress,

$r = \left(\frac{9}{2}\mathbf{S} \cdot \mathbf{S} : \mathbf{S}\right)^{\frac{1}{3}}$, is the third invariant of deviatoric stress,

$\mathbf{S} = \boldsymbol{\sigma} + p\mathbf{I}$, is the deviatoric stress.

As illustrated in Fig. 3-5, the friction angle, ϕ governs the shape of the yield surface in the deviatoric plane and it varies from $0^\circ \leq \phi < 90^\circ$.

For $\phi = 0^\circ$, the Mohr-Coulomb model converts to the pressure-independent Tresca model with a perfectly hexagonal deviatoric section and for $\phi = 90^\circ$, the Mohr-Coulomb model transforms to the “tension cut-off” Rankine model with a triangular deviatoric section.

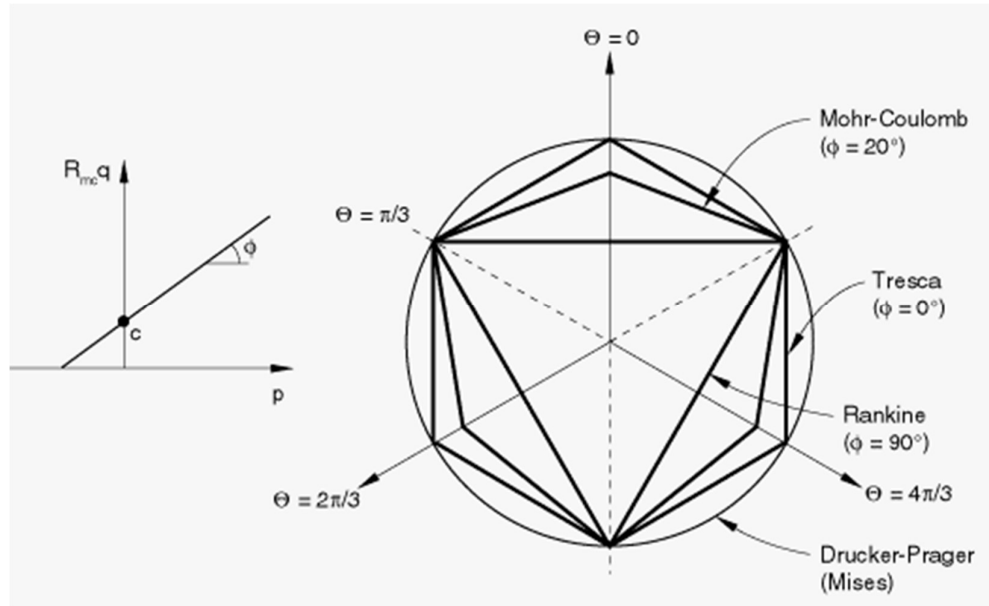


Figure 3-6: Mohr-Coulomb yield surface in meridional and deviatoric planes.

3.3.2 Constitutive Relation for Pipe

A simple constitutive framework, i.e., the Ramberg-Osgood theory, was capable of capturing the main trends of strain localization in a complex microstructure like mild steel, DI, CI etc. The Ramberg-Osgood model was used for the pipe constitutive model because its stress-strain relationship is more compatible with actual pipe material. The material model for the pipe was approximated by the Ramberg-Osgood relation, according to the following equation:

$$E\varepsilon = \sigma + \alpha \left(\frac{|\sigma|}{\sigma_Y} \right)^{n-1} \sigma \quad 3.1$$

Where σ is the Cauchy stress, σ_Y is the yield stress, E Young's modulus, ε is the total strain, and α and n are the specific constants of Ramberg–Osgood model. Figure 3-7 delineates the typical stress-strain curve for ductile metals.

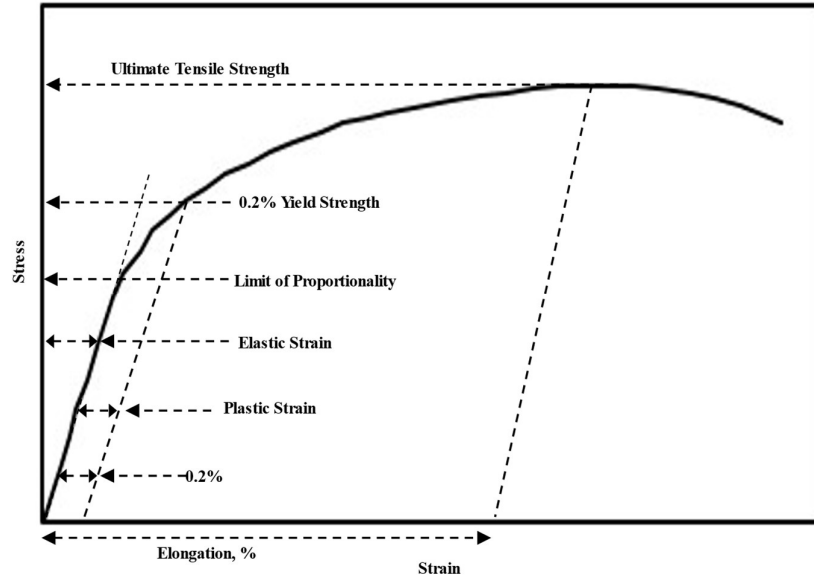


Figure 3-7: Typical stress-strain curve for ductile metals (Collected from-Ductile Iron Society)

3.3.3 Mechanical Properties of Pipe and Soil

The input properties of soil and pipe used in the model are shown in Table 3-1 and Table 3-2. For soil, a small value of cohesion of $c = 0.2$ kPa has been applied which had a negligible impact on the results of simulated interactions between pipe and soil. But it helped avoiding numerical instability. In this study, DN 1000 type DI pipe has been

selected following the guidelines of ISO 2531, and BS EN 545 & 598. The thickness of this pipe (t) was 15 mm and outer diameter (D_o) was 1048 mm.

Table 3-1: Mechanical properties of Kubota Ductile Iron pipe (ISO 2531/ BS EN 545 and 598)

Mechanical property	Parameter	Value
Elastic property	Mass density (kg/m^3)	7050
	Modulus of Elasticity (MPa)	170,000
	Poisson ratio	0.27
Plastic property (T/Y=1.4)	Yield strength (MPa)	350
	Tensile strength (MPa)	490
	Minimum elongation after fracture (%)	10

Table 3-2: Material properties of Sandy soil (Liu et al., 2010; Seed & Duncan, 1985; Nixon & Child, 1989)

Mechanical properties	Parameter	Value
Elastic property	Mass Density (kg/m^3)	1700
	Modulus of Elasticity (MPa)	19
	Poisson ratio	0.2
Plastic property	Friction angle (deg.)	30

3.3.4 Soil-Pipe Interaction

In perspective of the material and geometric nonlinearity of the soil and pipe, and the nonlinear behaviors such as bonding, sliding and separation at the soil-pipe contact interface, a non-linear surface-to-surface contact model was used to simulate the interaction between pipe and soil as shown in Fig. 3-8. Frictional interface between pipeline and soil was also used in the researches by (Cheong et al., 2011; Paolucci et al., 2010; Bolvardi & Bakhshi, 2010).

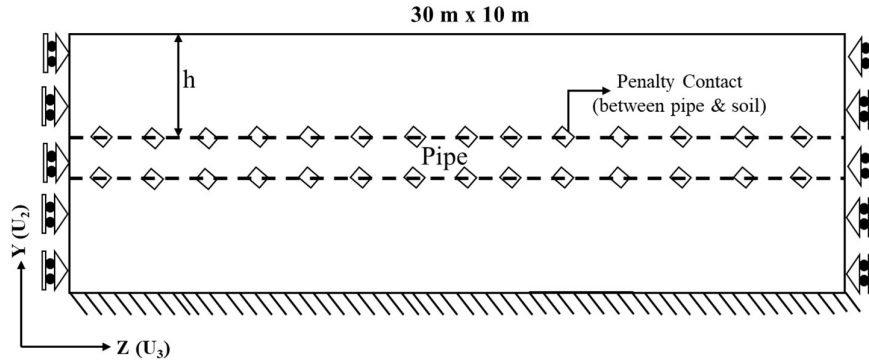


Figure 3-8: Surface-to-surface contact model (Penalty) in between pipe and soil.

The Coulomb friction model with Penalty friction formulation was used in the tangential behavior of contact surface to define the frictional behavior, with friction coefficient as 0.5 for pipe-soil interface, whereas mechanical contact between the circumference border of pipe and the surrounding soil, defined as "hard" contact selected from the pressure-overclosure field with the penalty constraint enforcement method and permissible separation after contact was applied in the normal behavior for better numerical convergence.

The sensitiveness of the selected pipe capacity to adjust the interface friction ratio was examined by a variation of the interface friction ratio of 0.5, 0.7, and 0.9, covering a range of half to full value of interface friction spectrum.

3.3.4.1 Penalty Friction Method

The easiest method which is employed in the solution of contact problems is the penalty friction method. It is employed in the solution of equality constrained optimization problems. The penalty friction method is depicted schematically in Fig. 3-9. The master is the bottom surface, and the slave is the upper surface. The node of the slave surface is restricted to not enter the master surface and the node of master surface can penetrate the slave surface. With no additional degrees of freedom, the penalty friction method approximately enforces the contact constraint through the use of springs. Even though the overclosure has been exaggerated, it is obvious that the stiffness of spring, k resists the slave node from penetrating the master surface.

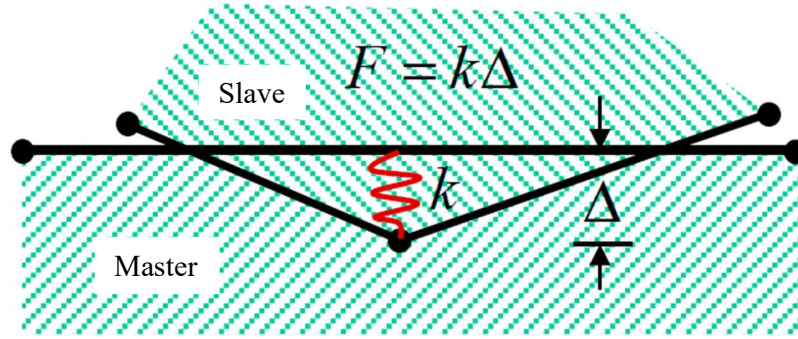


Figure 3-9: Schematic diagram of the penalty method

The penalty friction method is used to model the contact between two bodies in a virtual environment, including frictional forces. The total contact force between the two bodies is modeled using the following equation:

$$F_{\text{contact}} = F_{\text{penalty}} + F_{\text{friction}}$$

Where, F_{contact} is the total contact force, F_{penalty} is the penalty force, and F_{friction} is the frictional force.

The penalty force is modeled using the same equation as in the penalty contact method:

$$F_{\text{penalty}} = K_{\text{contact}} \times \delta_n \times n_{\text{contact}}$$

Where, K_{contact} is the contact stiffness, δ_n is the normal penetration depth, and n_{contact} is the unit normal vector that points from the first body to the second body at the contact point.

The frictional force is modeled using the Coulomb friction model:

$$F_{\text{friction}} = -\mu \times F_n \times t_{\text{rel}}$$

where μ is the coefficient of friction, F_n is the normal component of the contact force, and t_{rel} is the relative tangential displacement vector between the two contacting surfaces.

The relative tangential displacement vector is defined as:

$$t_{\text{rel}} = [v_1 - v_2 - (v_1 - v_2) \times n_{\text{contact}}^2]$$

where v_1 and v_2 are the velocities of the two bodies at the contact point.

By combining the penalty force and the frictional force, the penalty friction method provides a more realistic model of contact between two bodies in a virtual environment.

However, the choice of parameters such as the contact stiffness and coefficient of

friction can have a significant impact on the simulation results and should be carefully calibrated based on experimental data or analytical solutions.

The penalty friction formulation was used in every model analyzed in this study to model a modified Coulomb friction by placing an elastic slip in the sticking stage. The formulations of the penalty friction allow stiffness that enables certain relative movement of actual surfaces in the sticking stage, as an elastic displacement called ‘elastic slip’ shown in Fig. 3-10. Elastic slip influences the frictional behavior before the slipping stage works.

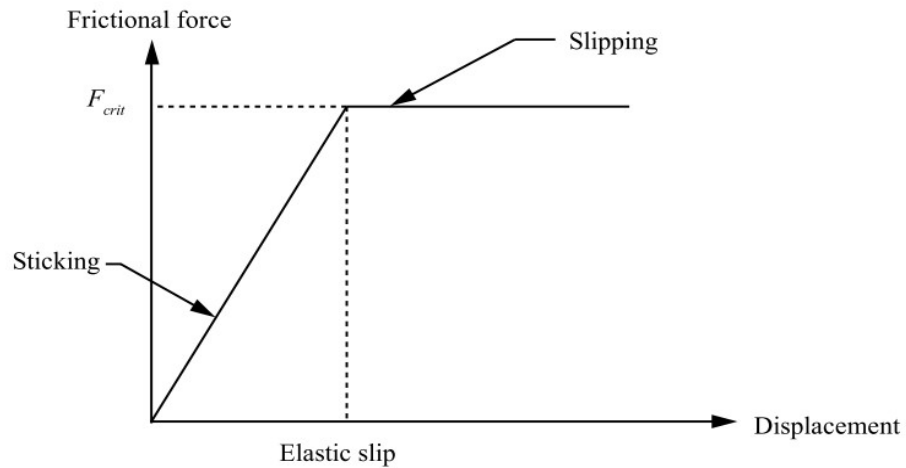


Figure 3-10: A general friction curve with penalty friction formulation

3.3.5 Incremental Loading and time steps

The solution cannot be converged if the loads are applied in a single increment in a non-linear analysis. Therefore, the load must progressively be applied in a sequence of smaller increments. The loads were applied in a sequence of steps in the FEM. In each step, different load, and boundary conditions with linear incrementation follow the process as shown in Fig. 3-11.

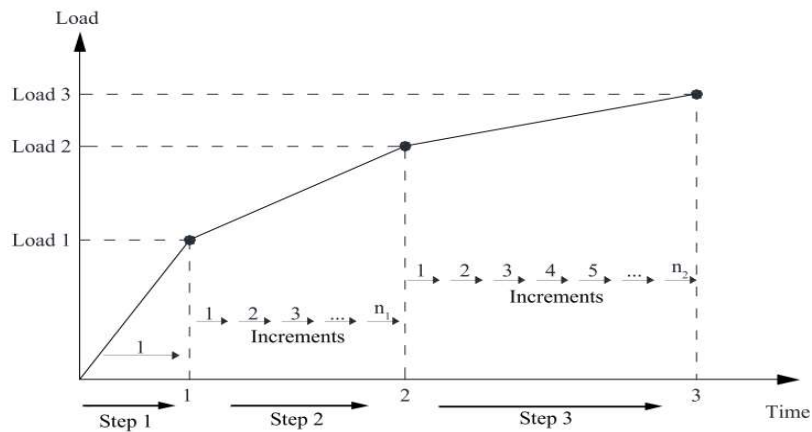


Figure 3-11: Schematic diagram of the distribution of steps and increments, according to (Bower, 2010).

3.3.6 Loads on Pipeline and Soil

The loads and their combinations are critical for any structure, buried structures are of no exception. The loads may be categorized as functional loads (e.g., self-weights, pipe internal fluid pressure), accidental loads (e.g., seismic loads), and environmental loads (e.g., traffic loads). The static and dynamic loads that applied in the buried flexible DI pipeline under static and seismic condition are shown in Table 3-3. A further explanation is made in the following sections.

Table 3-3: Static and seismic loads (BSI., 2006, BSI., 2010, and <https://strongmotioncenter.org>)

Static Loads	Gravity (m/s^2)	9.81
	Traffic load on the soil top surface (kPa)	1100
	Internal water pressure in pipeline (kPa)	100
Seismic Load	Component	Y (Vertical. Comp.)
	Peak ground acceleration (PGA) (g)	- 0.21 at 0.98 sec.
	History Time (sec.)	91.54

3.3.6.1 Static Loads

The static analysis of buried flexible pipelines was done for the total loads, which included the effects of the operational water pressure inside the pipe, the dead load

caused by the soil and pipe, and the live load caused by traffic. Both, dead and live loads acting directly on the pipeline are considered as the resultant vertical load and of static nature.

Unit-weights of both soil and pipelines were defined as gravity loads, while the traffic loads were defined as a uniform pressure over the surface backfill.

In addition, internal water pressure in the pipe was included. The deformability of the buried pipeline would not be significantly affected by the internal fluid pressure. However, to restrain the buried pipeline deformations, it could play a smaller role. Inclusion of fluid pressure helps mitigating the expansion effect (if any) induced by continuous water flow through the buried pipeline which can also increase stiffness of buried pipeline. In the present study, a water pressure of 14.5 psi (100 kPa) was used to test the critical state of a buried pipeline. Considering a full flow condition in the pipe, static water pressure was uniformly distributed around the interior surface of the pipe to simulate the hydrostatic condition as shown in Fig. 3-12.

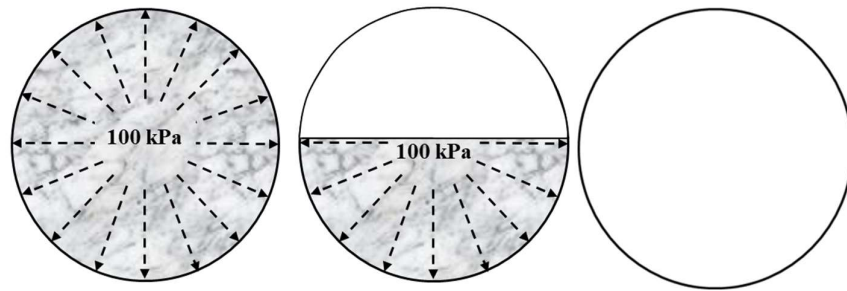


Figure 3-12: Water pressure inside the pipe under full flow, half flow and no flow condition

Traffic loads were considered following the guidelines of BSI 2006 and BSI 2010. The heaviest vehicle load was used to analyze the critical deformation of the pipeline. According to BS 5400-2:2006 (BSI, 2006) and BS 9295:2010 (BSI., 2010), One of the heaviest loads on the main road for all public highways and bridges in the United Kingdom is the 8-wheel HB load. This induces a 112.5 kN load on each wheel which is distributed over a contact area of 0.102 m^2 (1 sq. ft) on the road with a contact pressure of 1100 kPa as shown in Fig. 3-13.

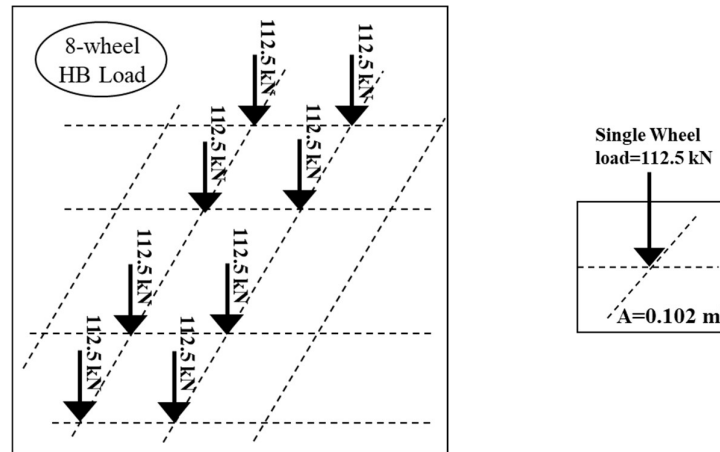


Figure 3-13: 8-Wheel HB Truck Loading with a wheel load on contact area of 0.102 m^2 .

If there are enough 8-wheel HB loads on the road, then a uniform surface load on the road is thought to be as sufficient as 1100 kPa as shown in Fig. 3-14. For this reason, the short-term structural serviceability condition of the underground pipeline was investigated using a uniform surface load of 1100 kPa on soil.

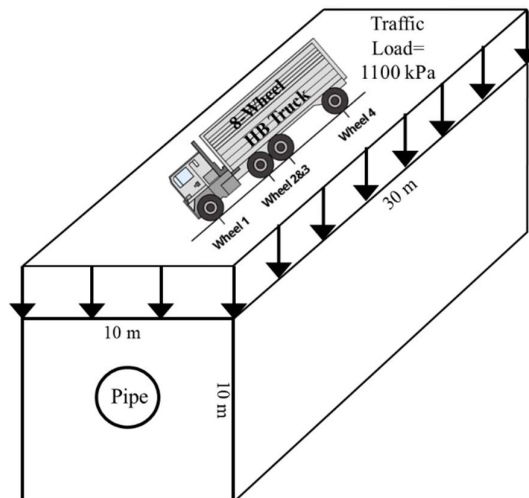


Figure 3-14: A uniform surface load of 1100 kPa on soil.

3.3.6.2 Dynamic Loads

A ground motion component is characterized by acceleration, velocity or displacement time history with three significant factors: amplitude; frequency; and duration of strong ground motion (Hashash et al., 2001). The seismic loading is often applied as an acceleration time-history at the base of a model in numerical simulation. Essentially,

time-history analysis methodologies have been built on the basis of validated FEM methodologies for underground structures subjected to seismic excitations (Abuhajar et al., 2015a; Abuhajar et al., 2015b; Fabozzi & Bilotta, 2016; Tsinidis et al., 2016).

To examine the nonlinear seismic behavior of the pipe a well recorded earthquake, 1940 El Centro Earthquake, was chosen in this study. The input signal was retrieved from the recording of El Centro Valley Irrigation District, Station No. 117 32 47 43N, 115 32 55W during the Imperial Valley Earthquake (1940) in USA. Figure 3-15 represent the acceleration time history of El Centro record with a time increment of 0.02 sec. The peak ground acceleration (PGA) of the ground motion was 0.21g (Vert comp.). The first 12 sec. of this record was used for time history analysis.

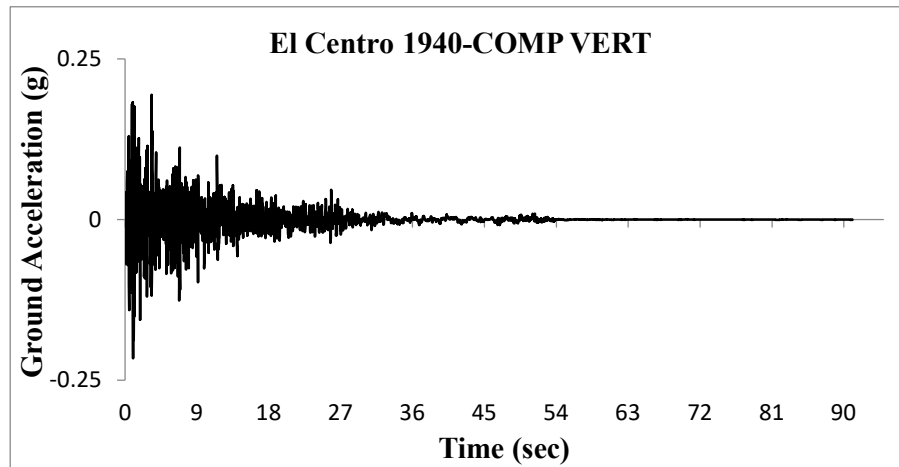


Figure 3-15: The accelerogram [Acceleration time history] (Vert. Comp.) of El Centro Earthquake of 18th May 1940 (<https://strongmotioncenter.org>).

Figure 3-16 shows the Fourier spectrum of this excitation. It was observed from Fig.3-16 that the predominant frequency of the record was around in the range of 1.87 to 10.18 Hz (Vert comp.).

The vertical component of real acceleration time history of El Centro earthquake was applied through Y direction of the model at the base of the numerical model to comprehend how a particular earthquake will affect a buried structure.

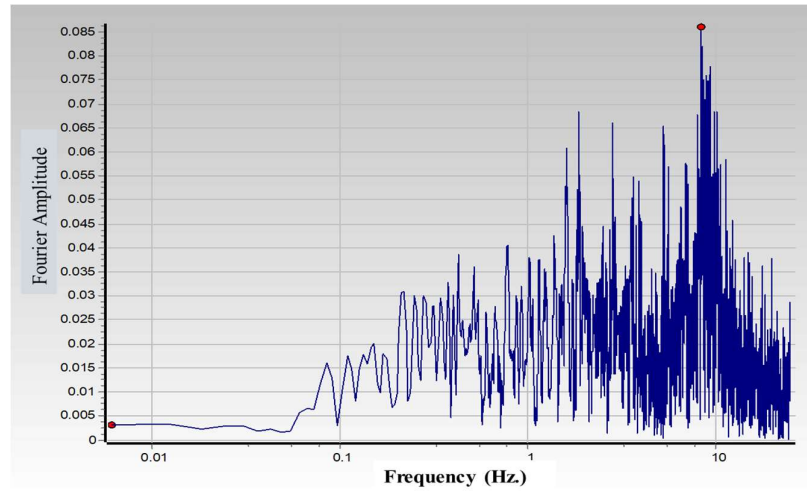


Figure 3-16: Fourier spectrum of Vert comp. (Predominant frequency, 8.43 Hz) for the recording of El Centro Valley Irrigation District Station during the Imperial Valley Earthquake (1940)

3.3.7 Boundary Conditions

The static boundary conditions were used to restrain horizontal displacement of boundary surfaces of soil model. These boundary conditions were also applied to prevent vertical and horizontal displacements of the base of the soil model to simulate the soil bed as bed rock and the top surface of the soil was set to be a free surface. The static boundary conditions applied to the soil and pipeline model are summarized in Table 3-4. U1, U2, U3 denote displacements; UR1, UR2, UR3 denote rotations; and A1, A2, A3 denote accelerations in the X, Y, and Z directions of the 3D model, respectively.

Table 3-4: Displacement (U), Rotational (UR) and Acceleration (A) constraints

Entity	Sub-Entity	Initial step and Static step	Dynamic step
Pipe both ends	Roller	U1,U3	U1,U3
	Hinge	U1,U2,U3	--
	Fixed	U1,U2,U3 UR1,UR2,UR3	--
Soil bottom		U1,U2,U3	U1,U3
Soil Front-Back Sides		U1,U3	U1,U3
Soil Left-Right Sides		U1,U3	U1,U3
Acceleration time history			A ₂ (Y direction)

3.3.7.1 Boundary Conditions for soil continuum

The four-vertical faces of the 3D soil model were supported by roller to restrain the horizontal displacement (i.e., $U_1 = U_3 = 0$) only as shown in Fig. 3-17. Furthermore, roller support for these faces are practical because infinite or semi-infinite soil medium may be expected to move in vertical direction with a substantial portion of the soil body (Rao, 1999).

The bottom face of the 3D soil model was kept as fixed (i.e., $U_1 = U_2 = U_3 = 0$) to restrain both horizontal (i.e., $U_1 = U_3 = 0$) and vertical displacement (i.e., $U_2 = 0$), mimicking a bed rock as shown in Fig. 3-17.

This concept is compatible with many findings from literature (Lee, 2010; Cheong et al., 2011; Sahoo et al., 2014a). These studies employed a roller support on all FEM faces which allowed displacement in any direction except to the normal direction.

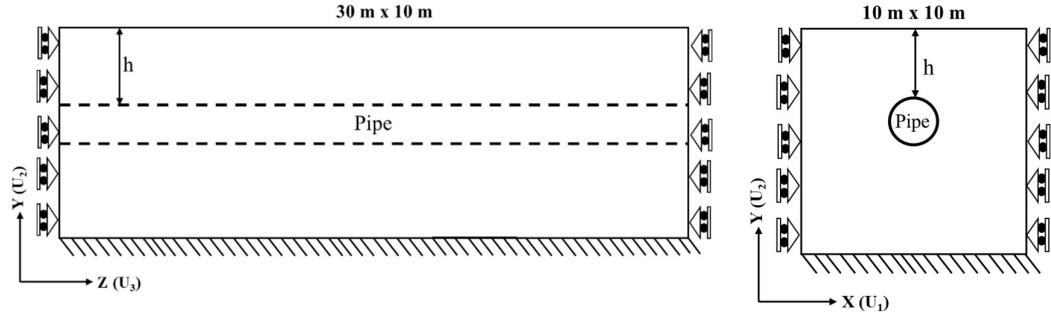


Figure 3-17: Boundary Conditions for soil continuum

3.3.7.2 Boundary Conditions for pipeline

The boundary conditions for the buried pipe were considered as per the below criteria.

- Roller support at both end ($U_1=U_3=0$) as shown in Fig. 3-18.
- Hinge support at both end ($U_1=U_2=U_3=0$) as shown in Fig. 3-18.
- Fixed support at both end ($U_1=U_2=U_3=U_{R1}=U_{R2}=U_{R3}=0$) as shown in Fig. 3-18.

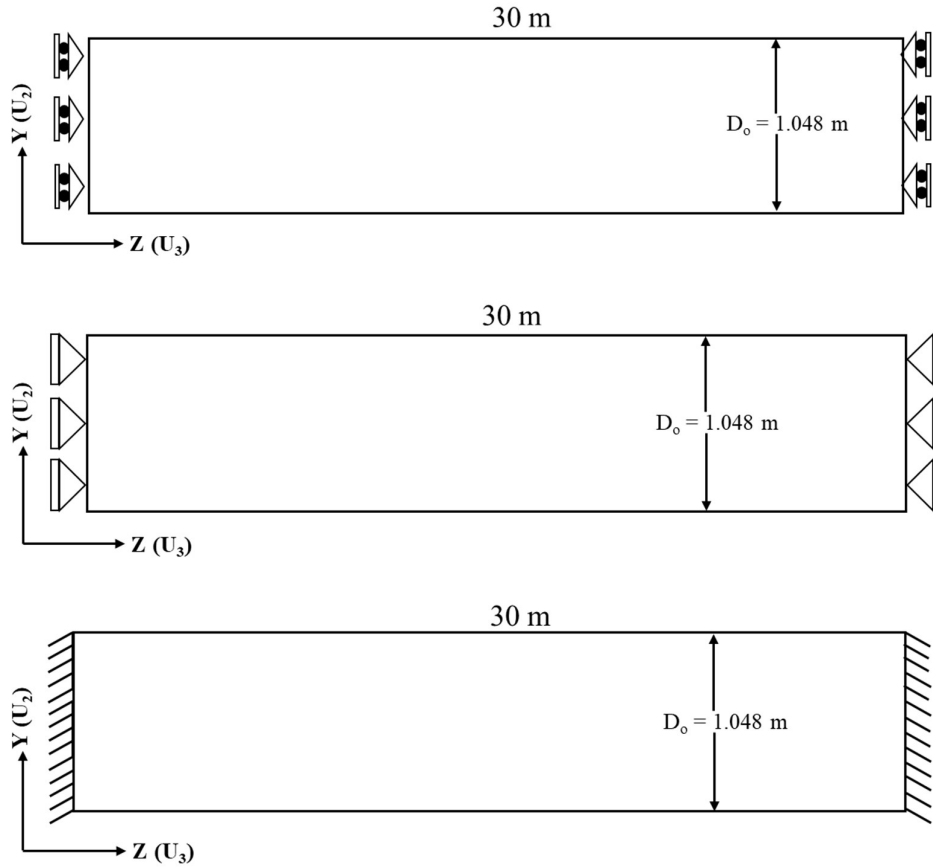


Figure 3-18: Boundary Conditions for pipe end

To select a boundary condition for both pipeline ends, two typical cases were followed: (1) a roller support to simulate the infinite length effect of a buried pipeline for its continuous length, and (2) a hinge or fixed support to simulate the finite length effect of a buried pipeline in between two structures.

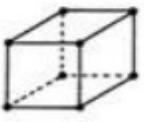

The roller support allows the buried pipeline to displace comparatively easily with soil. Whereas, a finite pipeline length is practical when there is a presence of structures at the end of a buried pipeline. The ends of the pipeline remain constrained by the connection between two structures. Hence, the restrained ends of the buried pipeline should be hinged or fixed in all directions (i.e., $U_1=U_2=U_3=0$ or, $U_1=U_2=U_3=UR_1=UR_2=UR_3=0$).

3.3.8 The Type and Shape of Element

A first order (or linear) interpolation, with 3D shell element consisting of 4 nodal points with reduced integration and hourglass control, titled as **S4R**, for pipe was selected. The

first-order (or linear) interpolation are proven to show better convergence for contact analysis, particularly for the surface-to-surface interactions in a soil-pipe system (Hellgren & Lundberg, 2011). For soil, 3D solid element consisting of 8 nodal points linear brick with reduced integration and hourglass control, titled as **C3D8R**, was selected (very suitable for large deformation analysis). Table 3-5 illustrates these element types and shapes.

Table 3-5: Selected type and shape of element for 3D-FE soil-pipe model

Name of element	Element types	Element shapes	Technique	Geometric orders	Element numbers	Element shape
Soil	C3D8R	Hexahedral	Structured	First-order (or linear)	9000	
Pipeline	S4R	Quadrilateral			960	

3.3.9 Mesh Accuracy

Due to tiny meshing making calculations more accurate than coarse meshing but increasing computational time, the convergence test for determining an adaptive mesh size is the most effective way for verifying errors as well as accuracy in computed displacement or stress results as well as the response of the pipe. Because a good number of elements is an essential component in the quality of the analysis, increasing mesh density in 3D models enhances analysis accuracy and precision. For this reason, a coarse mesh to a fine mesh by local seeding was investigated here to determine the optimal number of elements depending on the available computational capability. When elements were subdivided into smaller ones, a process called "h-refinement" was used to determine adaptive mesh size of the elements (Lee, 2010). For the h-refinement mesh technique, the maximum mesh size was 2m as a coarse mesh, and the smallest mesh size was 0.1m as a fine mesh, respectively. Five cases were considered as 4980, 8085, 9960, 14910, and 19920 elements to study the mesh accuracy in the 3D FE model. It was found that 9960 elements are enough to validate the mesh accuracy because this case shows almost the same displacement results as the largest number of elements case (19920) as shown in Fig. 3-19.

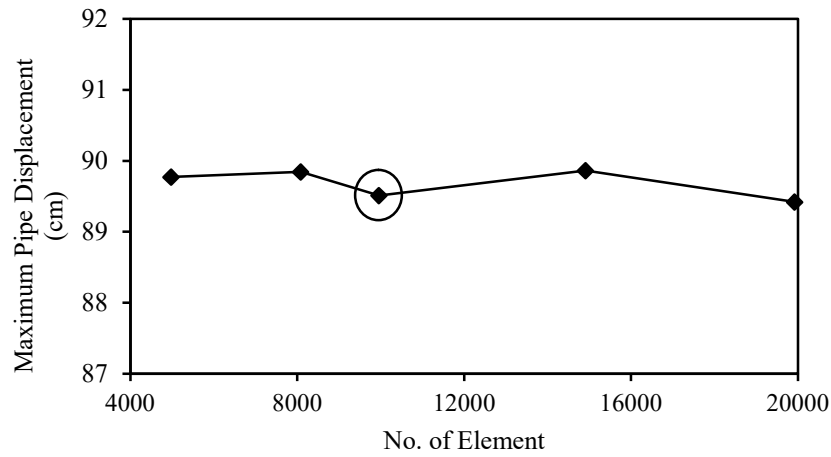


Figure 3-19: Effect of the element size on the Displacement of pipe

After checking the mesh accuracy, the finite element mesh of pipe was discretized to 32 segments along the circumference and 30 segments along the length of the pipeline, resulting in a total of 960 elements for the pipeline shell. The finite element mesh of soil outside the pipeline was optimized within 2 m from the center of pipe and needed a total of 9000 elements for the whole soil.

3.3.10 The size of element

The mesh size should be finer around the pipe hole within the soil and progressively the mesh size may bigger with increasing distance from the pipe hole to achieve the cost effective finite element result (Georges & Shephard, 1990). Since the soil response is more significant around the pipe, finer mesh should be used in this region. To measure strain and stress more precisely, a 2 m finer mesh zone (with respect to pipe center) was created in soil around the pipeline as shown in Fig. 3-20.

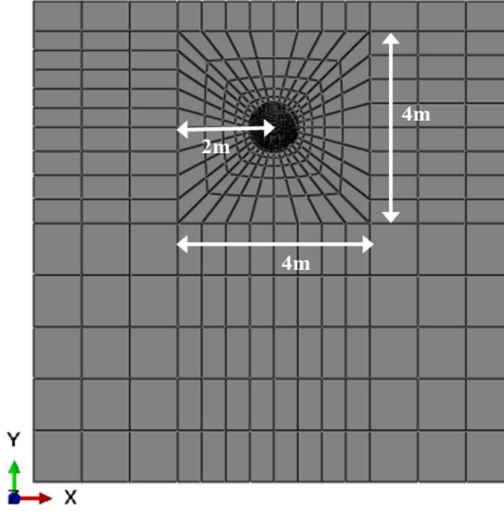


Figure 3-20: Meshing of soil box around pipe.

Near the pipe, the mesh was refined to accommodate for the severe stress gradients and plasticity experienced in the soil. In the cross-sectional view, the size of the elements of the pipe was 0.1 m along the circumference of the pipe and along the radial direction, the size of the elements in the soil varied from 0.1 m to 0.5 m, gradually increasing away from the soil-pipe interface up to the boundaries of the aforementioned 4m X 4m region and then continues uniformly at 0.5 m in both directions from the exterior side of the 4 m X 4 m box up to the exterior boundary of the soil model. The element size is kept uniform at 1 m in the longitudinal direction (along the length) for both the pipe and the soil model and for the remaining part.

3.3.10.1 The Evaluation of Finite Element Mesh Adequacy

The size of the elements should fulfill recommended requirements to ensure stability and accuracy of the numerical solution.

(Kim et al, 2002; Kuhlemeyer & Lysmer, 1973) demonstrated that the element size (Δl), should be around 1/10 to 1/8 of the wavelength associated with the highest-frequency of the input wave to accurately perform the wave propagation through a model:

$$\Delta l \leq \frac{\lambda}{10} \text{ to } \frac{\lambda}{8} \quad 3.2$$

where λ is wavelength of the input wave in the model and can be expressed by the following relation:

$$\lambda = \frac{V_s}{f_{max}} \quad 3.3$$

where, V_s is the shear wave velocity in the soil and pipe respectively and f_{max} is the highest frequency (pre-dominant frequency) of the input motion found from the Fourier analysis of the input motion. The theoretical shear wave velocity of S waves can be determined by

$$V_s = \sqrt{\frac{E}{2(1+\nu)\rho}} \quad 3.4$$

where E and ν are Modulus of Elasticity and Poisson ratio, respectively, and ρ is the mass density. V_s is the shear wave velocity in the soil and pipe, respectively. Substituting Equation (3.3) into Equation (3.2) gives:

$$\Delta l \leq \frac{V_{s,min}}{10f_{max}} \quad 3.5$$

In this FEA - after evaluating the shear wave velocity in the soil and pipe system, and using pre-dominant frequency of the input motion, and wavelength of the input wave - the maximum and minimum element sizes were obtained as shown in Table 3-6. Moreover, A sensitivity analysis was carried out to ensure that the mesh size did not affect results accuracy.

Table 3-6: Element sizes for soil and pipe

Approximate local size of meshed elements	Min. Element size (m)	Max. Element size (m)
Soil	0.8	8.5
Pipe	1.5	10.5

3.4 FE Model Performance

To validate the used FE model performance, it should be compared with established work. For FE model performance validation purpose, keeping all the mechanical properties, geometries, and arrangements same for both soil & pipe, an experimental model of Pires & Palmeira (2021) have been numerically simulated using this finite element model for static response only. The parameters used for both the experimental and numerical models are shown in Table 3.7.

Table 3-7: Parameters used for both the experimental and numerical models

Mechanical property		Parameters	Unit	Value
Soil (Sand)	Elastic property	Mass Density	ton/m ³	1.67
		Young’s modulus	kN/m ²	4600
		Poisson’s Ratio	---	0.3
	Plastic property	Friction angle	°	37
		Dilation Angle	°	7
		Cohesion	kN/m ²	0.1
Pipe (PVC)	Elastic property	Mass Density	ton/m ³	1.67
		Young’s modulus	kN/m ²	3100000
		Poisson’s Ratio	---	0.4
	Plastic property	Yield Strength	MPa	350
		Tensile Strength	MPa	490
A Surcharge on 250 mm strip at the center line of soil top surface along the pipeline			kPa	5~160
Soil Continuum Dimension: L=1500 mm, H=1000 mm, W=700 mm				
Pipe Dimension: L=700 mm, Outer Dia.=200 mm, t=3.2 mm				
Buried Depth: 400 mm				

Figure 3-21 shows the cross-section of the 3D FE model used in this research for experimental validation. Also, Figure 3-22 depicts a 3D view of the Experimental Model of Pires and Palmeira (2021). The study by Pires and Palmeira (2021) used a PVC pipe in their experimental model. Though the seismic response of buried PVC pipe is too high compared to the DI pipe used in this study, the FE model performance considering PVC pipe shows a similar trend to the experimental one.

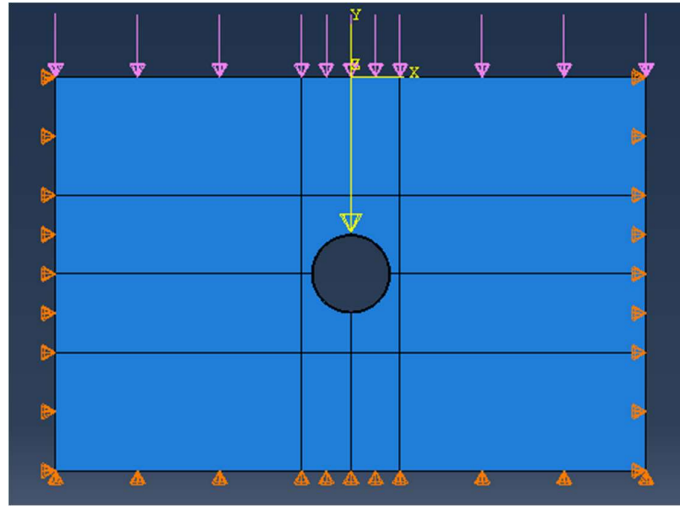


Figure 3-21: Cross section of FE Model



a



b

Figure 3-22: a) Front view of Experimental Model, b) PVC Pipe (Pires & Palmeira, 2021)

The variations of pipe deflection with surface surcharge are depicted in fig. 3-23 from both FE analysis and experimental results. The Fig. 3-23 presents the reduction (ΔD) in pipe diameter along the vertical direction (in Y-direction) normalized by the initial pipe diameter (D) with surcharge in tests and FE analysis respectively. It can be seen that vertical displacement of pipe from FE result is only 5% higher than that of the experimental studies. As such it can be said that the finite element model considered here is predicting the performance very well.

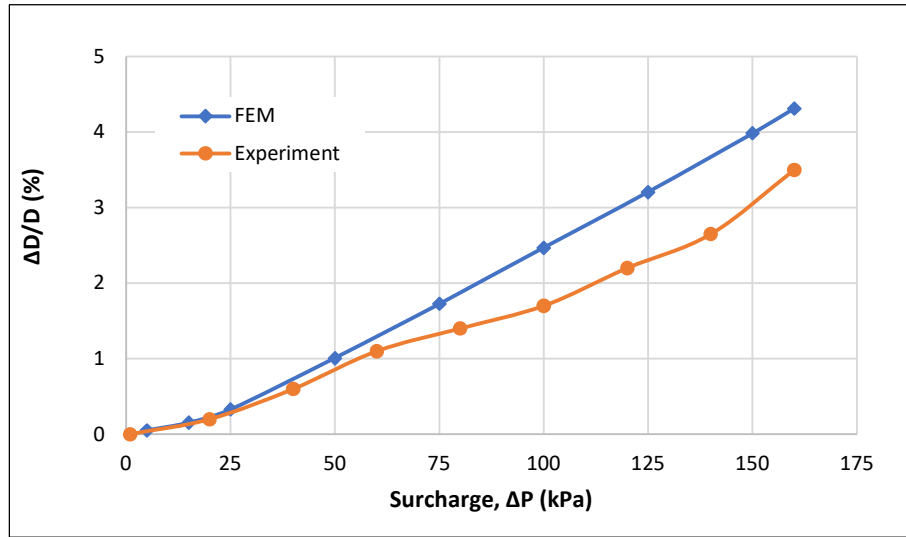


Figure 3-23: Comparison between numerical result and experimental result (Pires & Palmeira, 2021)

As there was no comparable experimental work found in the literature dealing with real seismic excitations, this model was compared with an experimental work by Pires and Palmeira (2021) to investigate the static response only.

3.5 Summary

A sensitivity analysis is performed to examine the effects of internal pressure, traffic load, depth of pipe laying, diameter and wall thickness of pipe, pipe end restraints and soil type with different density, modulus of elasticity, friction angle, Poisson's ratio etc., interface friction co-efficient, D/t ratio, h/D ratio, unidirectional seismic excitation and discussed to achieve a better comprehension of the seismic behavior of DI pipelines under seismic loads.

Chapter 4. RESULTS AND DISCUSSIONS

4.1 General Overview

In this chapter, pipe-soil responses under static and dynamic (seismic) loads are quantified based on the FEA of a 3D soil-buried pipe model. The effect of model geometry (e.g., pipe diameter, thickness, buried depth etc.), soil properties (e.g., density, modulus of elasticity, angle of internal friction, Poisson's ratio etc.), support conditions (roller, hinge, fixed etc.), contact properties, loading conditions (traffic load, fluid pressure etc.), on the seismic response of buried DI pipe are presented and discussed. Figure 4-1 shows the monitoring lines where maximum responses (vertical displacement and deformation, stress and strain) of the pipe were extracted.

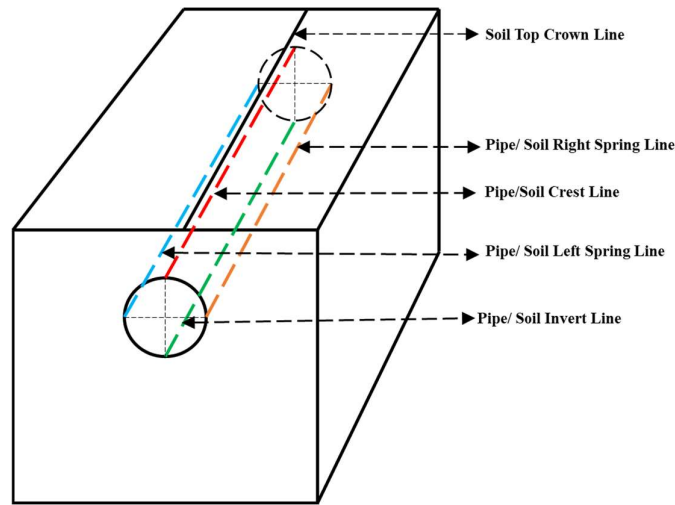


Figure 4-1: The location of monitoring lines.

The seismic response under prescribed ground motion was evaluated along the pipe length at crest, invert, left and right spring lines of the pipe as shown in Fig. 4-1. The pipeline was deformed into an oval shape along its entire length by imposed static loads (gravity, traffic load); water pressure, and seismic loads, which allowed the crest line of the pipeline to respond with the maximum response. The crest line of a buried pipe is the highest point of the pipe, where the overburden soil exerts the maximum load on the pipe. Since the crest line is subjected to the highest loads, it experiences the maximum responses. However, the stiffness and lateral resistance of soil vary depending on its

location with respect to the pipe. At the crest line, the soil is less confining and less supportive of the pipe than the soil located closer to the sides of the pipe. Therefore, the ability of soil to resist deformation and support the pipe is reduced at the crest line, resulting in higher induced stresses and strains. Furthermore, the stiffness of the soil decreases at the crest line, leading to greater deformation and displacement of the pipe. Therefore, the crest line of a buried pipe is considered a critical location for evaluating its seismic response, and it is essential to analyze the behavior of pipe and stability at this location during seismic events.

4.2 Static and Seismic Response of Pipe

4.2.1 Response under Static and Seismic Load

In this section, the behavior of buried pipeline under static load including gravity load, traffic load, water pressure; seismic load was discussed. The observed maximum vertical displacement, stress, plastic strain etc. are graphically depicted to analyze the behavior of buried pipeline at the end of static and seismic steps respectively. All the analysis considering the influential parameters was conducted by taking the roller support at both ends of the pipe and the buried depth of the pipe to 2D for higher response found at that depth and to take advantage of the 4 m by 4 m box around the pipe.

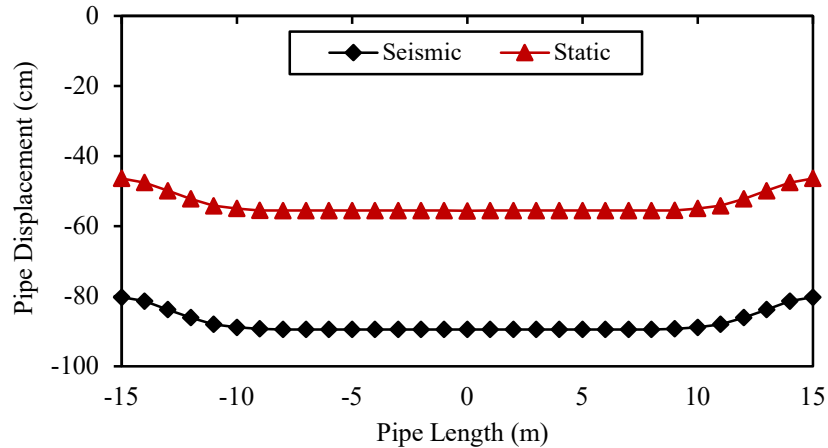


Figure 4-2: Displacement response of pipe

From Fig. 4-2, it is observed that at the middle portion of pipe, the maximum pipe displacement was measured at 55.60 cm and 89.51 cm for static and seismic conditions, respectively. At the pipe end, minimum pipe displacement was noticed for both

conditions. Since the pipeline ends were restrained by roller boundary conditions, which do not allow the pipe to move uniformly with the soil movement, particularly at the pipe end rather than the middle portion of the pipe, the maximum response was found at the middle portion rather than the pipe ends. When subjected to seismic loads, the ground experiences shaking, which can cause significant lateral and vertical movements of the soil surrounding the buried pipe. This can result in a greater displacement of the pipe compared to the displacement under static loads. As seismic loads are characterized by high-frequency, short-duration vibrations, it can further amplify the displacement of the buried pipe.

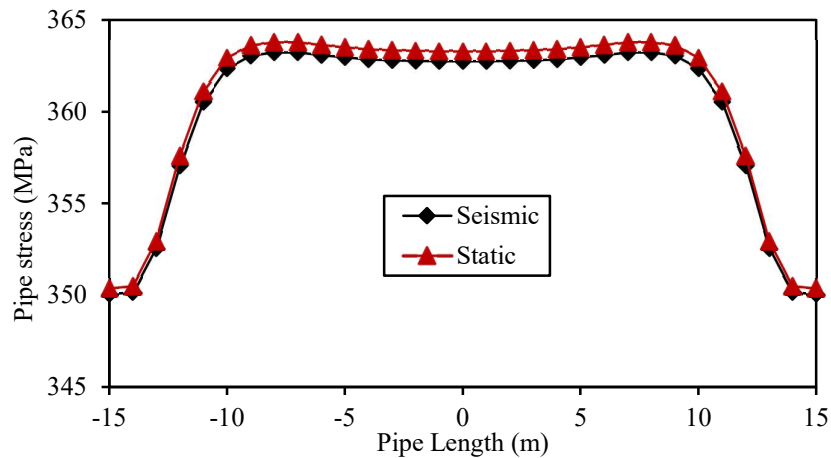


Figure 4-3: Stress response of pipe

Observing Fig. 4-3, it is found that the maximum stress developed in the pipe through the crest line was 363.78 MPa and 363.22 MPa at the location 8m away from both pipe ends, as well as the minimum stress was found to be 350.4 MPa and 350.06 MPa at the pipe end for static and seismic cases, respectively due to the roller support at the pipe end. The maximum stress was found at the middle portion of the pipe, as the displacement was higher at that location. It is also observed that the stress variation is negligible for both cases. Though, it is not necessarily true that stress and strain variation in buried pipes is negligible for static and seismic loads but the stress and strain variations may differ depending on the nature and intensity of the applied loads and roller support at the pipe end. The pipe follows the soil movement due to roller support, which may cause the same stress magnitude in static and seismic cases. All the stress found on the pipeline is greater than the yield stress (350 MPa) of ductile iron because pipe experiences more stresses due to traffic load as it is shallowly buried. It

could be inferred that the maximum stress generated by a pipeline at the crest and comparatively lower stress at the invert positions makes the flexible pipeline buckle in these locations. In this way a buckling is produced at the crest as well as at the invert of the pipeline and a flexible pipeline is completely collapsed when stress is reached to a critical buckling stage if there is not enough strength for resistance to static and seismic loads. This collapse of a flexible pipeline is most likely to occur near the joint at the crest and invert positions, where the stresses are highest and buckling is most likely to occur.

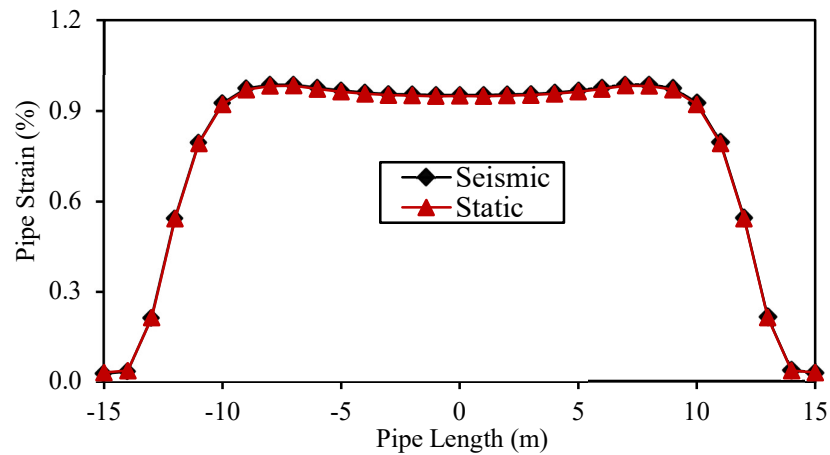


Figure 4-4: Strain response of pipe

Analyze the Fig. 4-4, it is noticed that at the same location of maximum stress, the maximum pipe strain was found for static and seismic cases due to the same reason as discussed earlier for stress response. Since the observed strain (approximately 1%) is significantly lower than the allowable plastic strain of DI pipe (10%), there is no plastic strain and deformation in the considered pipe.

The pipe displacement for seismic case is 61 % greater than the static case. Because, under seismic loads, the soil may undergo significant lateral and vertical movements, leading to greater displacement of the buried pipe. Since roller support was used as a boundary condition for pipe ends, the buried pipeline may be moved relatively easily with soil. Also, due to the nature and intensity of the applied loads, all other pipe responses i.e., stress, strain shows no significant variations for static and seismic cases. Also, all the response patterns maintain the same trend in both cases.

Hence, the effect of seismic loads on buried pipe analysis is significant because these dynamic loads can be much larger than static loads and can cause significant deformation, displacement, and damage to buried pipes. The large dynamic forces and

ground motions caused by earthquakes can result in significant stress and strain on the pipe, leading to pipe failure, leaks, and other damage.

4.2.2 Effect of Boundary Conditions

Three different boundary conditions for both pipe ends were evaluated in this study: 1) roller support 2) hinge support and 3) fixed support. A roller support at both pipe ends restrains displacement in the direction perpendicular to the surface. A hinge support on both pipe ends restrains displacement in the direction perpendicular and parallel to the surface. Also, a fixed support at both pipe ends restrains displacement in all directions, including translational and rotational displacement. The displacement, stresses and strains along the crest line of pipe using roller support, hinge support, and fixed support as the boundary conditions are shown in Fig. 4-5, 4-7 and 4-9. It is observed from these graphs that for all support conditions, the pipe response was found at almost the same magnitude as in the middle part along the length of the pipe, up to an approximately 5 m distance from pipe ends. One reason for this could be the restrained boundary conditions which do not allow the pipe to move uniformly with the soil movement, particularly at the pipe end rather than the middle portion of the pipe. Thus, the pipeline ends were restrained by roller boundary conditions, which allowed certain displacement (as roller support allows vertical movement) and certain stress and strain at the pipeline end but permitted the maximum displacement, stress, and strain at the mid portion of the pipeline through the entire length. Thus, roller support can mimic practically the infinite-length effect of pipelines (Lee, 2010). Again, the pipeline ends were constrained by hinge and fixed boundary conditions, which allowed zero displacement (as hinge and fixed support allow no movement at the pipe end), maximum stress, and maximum strain at the pipeline end (due to no movement of the pipe end, huge stress and strain developed here), but permitted maximum displacement, minimum stress, and minimum strain at the mid portion of the pipeline through the entire length. Thus, hinge and fixed support can mimic practically the finite-length effect of pipelines (Lee, 2010).

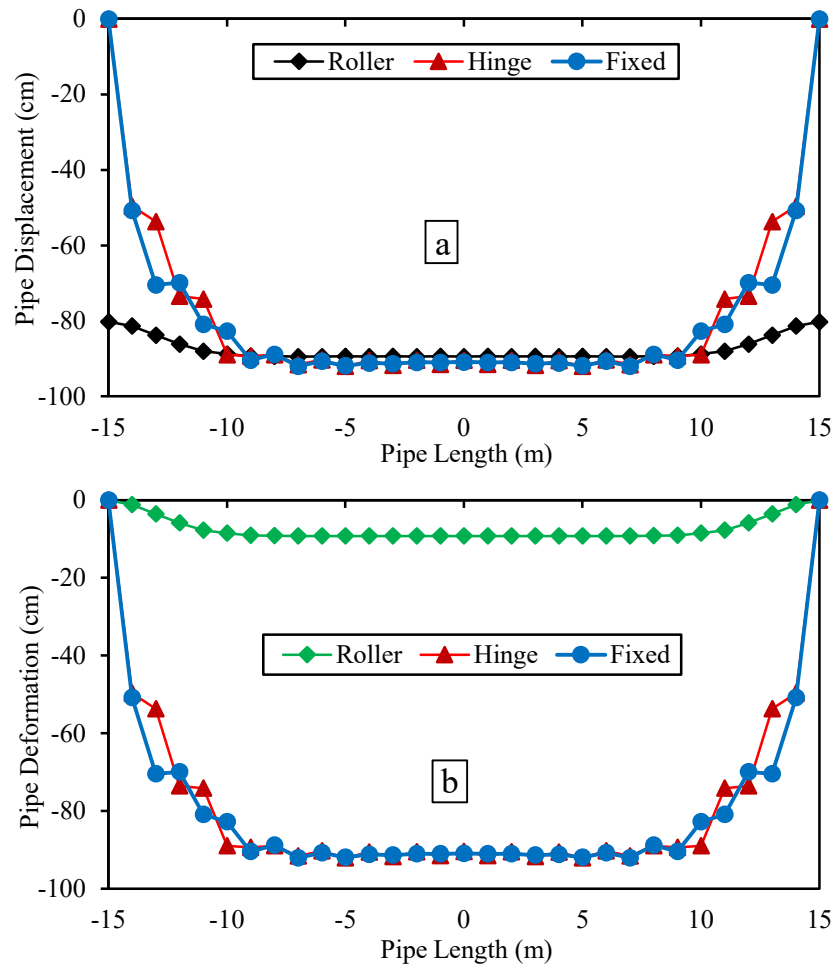


Figure 4-5: Effect of pipe end support on vertical displacement of buried pipeline (along crest line): (a) total displacement, (b) net deformation

The total displacement refers to the change in position of the pipe relative to its initial location in soil. The net deformation refers to the change in shape of the pipe due to external loads. Both displacement and deformation can be important factors to consider when designing or evaluating the performance of buried pipes in soil. From Fig. 4-5 (a), It is clearly noticed that the pipeline response to displacement for roller support shows a maximum value of 89.51 cm in the mid zone and a certain pipe displacement of 80.26 cm at the pipe end, which is due to no vertical constraint at the pipe end for roller support. The pipe displacement is zero at the pipe end and the maximum pipe displacement is 92.08 cm and 92.04 cm for hinge and fixed support, respectively.

In Fig. 4-5 (b), maximum pipe deformations in the middle portion of the pipe for roller, hinge and fixed support are 9.25 cm, 92.08 cm, and 92.04 cm, respectively. The freedom of vertical movement of the pipe leads to much lower maximum deformation at

the mid-length of the pipe for roller support compared to hinge and fixed supports. Since the pipe follows the soil movement relatively well at the mid-length of the pipe due to the imposed overburden pressure of the soil, traffic load, and seismic load; at the pipe end, the pipe goes for vertical movement or not depending on the degree of constraints, causing the zone of maximum displacement to remain almost the same at the mid-length of a shallowly buried pipe. Here, all pipeline responses were taken along the crest line of the pipeline because of the maximum magnitude at that location. The pipe displacement and deformation curve for hinge and fixed support follows the same trend. This is possibly because of the degree of constraints at the pipe end.

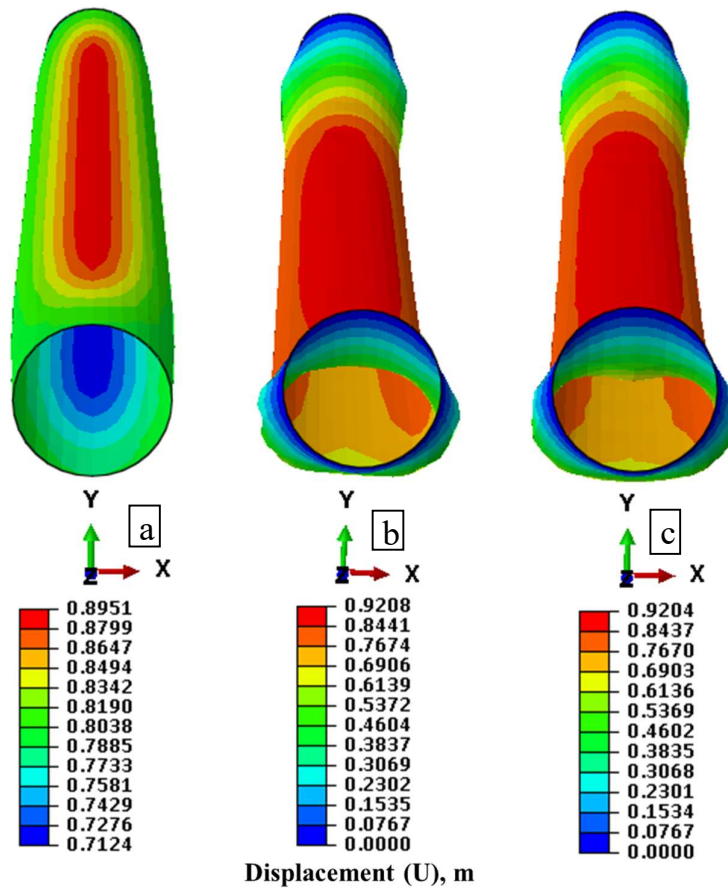


Figure 4-6: Displacement contour of DI pipe for a) roller, b) hinge, and c) fixed support at the pipe end

Figure 4-6 shows the Displacement contour of pipe for roller, hinge, and fixed support condition. Due to no vertical constraints applied at the pipe ends for the roller support, the pipe is displaced with the soil movement in the vertical direction and the deformed shape of the pipe remains almost straight. In the case of hinge and fixed support

conditions, there is a noticeable bend near both ends of the pipe due to the translational and/or rotational constraints, for which huge stress and strain are developed at and near the pipe end by external loads. Analyzing the deformed shape of the pipe, it is found that the circular cross section remains circular at the pipe ends i.e., no deformation occurred at the pipe ends and at the middle portion, the pipe section is ovalized and deformed slightly for roller support and ovalized and deformed extensively for hinge and fixed support due to external loads and corresponding support conditions. Hence, the maximum displacement as well as deformation is found in the middle portion, through the crest line of the pipe. When the distinct changes between the four monitor lines of pipe during an earthquake event are compared, the pipeline is deformed starting from the top crest position (crest line), moving on to the two sides of the pipeline (left and right spring line) and then moves to the bottom invert position (invert line), and finally, the circular cross section of the pipe forms an oval shape.

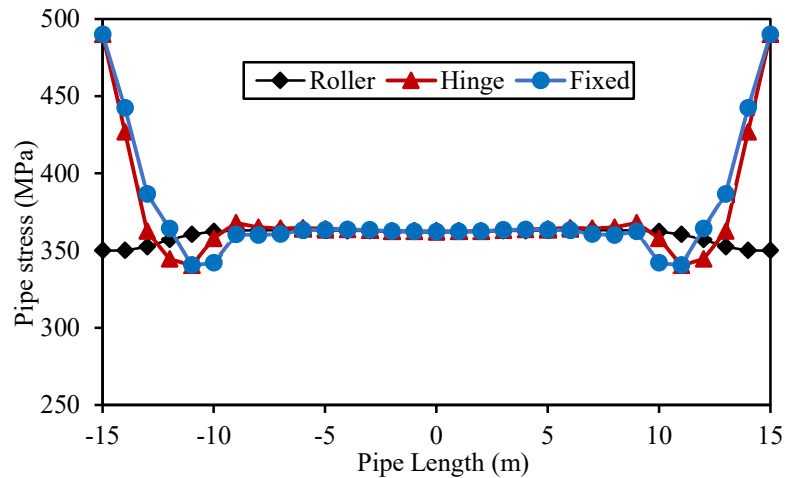


Figure 4-7: Effect of pipe end support on stress of buried pipeline (along crest line)

Figure 4-7 illustrates that the stress response of a pipe shows the same pattern as the displacement response of the pipe for hinge and fixed support. The stress response of a pipe with hinge or fixed support is similar because both types of support limit the axial movement of the pipe at the ends and allow for more freedom of movement towards the middle of the pipe. This results in maximum stress at the ends of the pipe and minimum stress at the mid-length of the pipe. From Fig. 4-7, it is observed that the maximum stress in the pipe is 363.22 MPa at the location 8m away from pipe end and the minimum stress is 350.06 MPa at the pipe end for the roller support. The combination

of the bending moment and the lack of support at the mid-length of the pipe leads to maximum stress, while the freedom of movement at the pipe ends due to roller support results in minimum stress. For hinge and fixed support, the maximum stress in the pipe is 490 MPa at the pipe end and the minimum stress is around 340.5 MPa, 4m away from the pipe end. The combination of the bending moment and the resistance to axial movement provided by the hinge or fixed support leads to maximum stress at the pipe ends, while the lack of resistance to axial movement at the mid-length of the pipe results in minimum stress. All the stress magnitude found exceeds the yield limit (350 MPa) of the pipe except near the pipe end (3 to 5 m away from the pipe end) and particularly at the pipe end it reaches the ultimate strength (490 MPa) in case of hinge and fixed support. For shallowly buried pipe, the effect of traffic load as well as seismic load is higher rather than deeper depth, hence, the stress magnitude may exceed the yield limit and also reach to ultimate capacity of pipe.

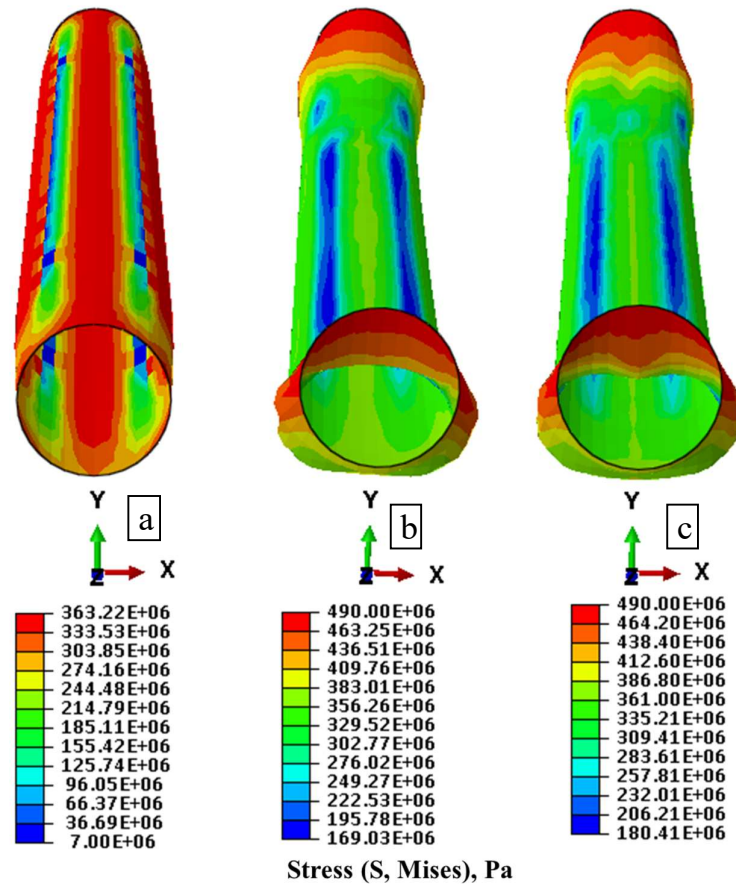


Figure 4-8: Stress contour of DI pipe for a) roller, b) hinge, and c) fixed support at the pipe end

Figure 4-8 shows the stress contour of DI pipe for roller, hinge, and fixed support conditions. A significant stress intensity was found at the crest, invert, left and right spring line of the pipe. Furthermore, in case of hinge and fixed support, the maximum stress intensity was found at the ends of the pipe rather than the middle portion because of the translational and or rotational constraints and vice-versa for roller support due to only horizontal translational constraints.

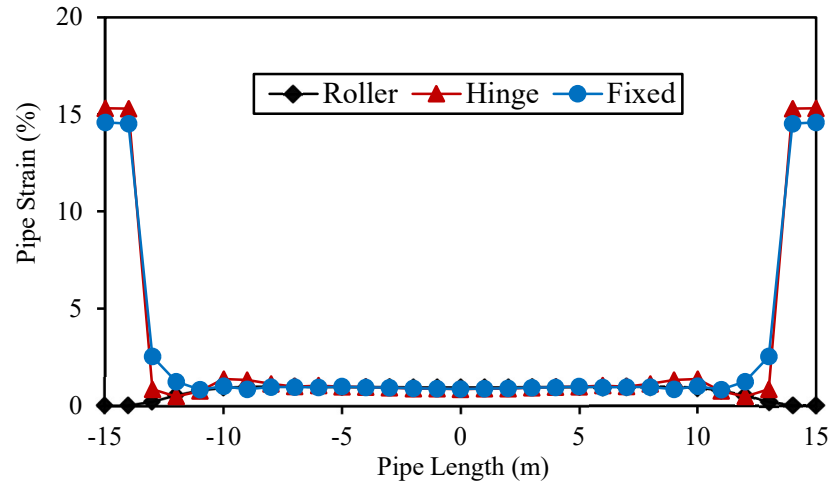


Figure 4-9: Effect of pipe end support on strain of buried pipeline (along crest line)

Figure 4-9 shows that the strain response of a pipe shows the same trend as the stress response of the pipe for hinge and fixed support. Hinge and fixed supports restrict axial movement at the ends, leading to strain concentration and maximum strain at the ends, while allowing more freedom of movement towards the middle of the pipe, resulting in minimum strain at the mid-length of the pipe, leading to a similar strain response trend. From Fig. 4-9, it is noticed that the maximum plastic strain in the pipe is around 1 % at the location 8m away from pipe end and no plastic strain at the pipe end for the roller support. Roller support allows the pipe to move freely along the vertical direction at the pipe ends, resulting in minimum strain, while maximum strain is found at the mid-length of the buried pipe due to the bending moment developed by external loads. For hinge and fixed support, the maximum plastic strain in the pipe is around 15 % at and close to the pipe end and the minimum plastic strain is around 1 %, 4 m away from the pipe end. For roller support conditions, the developed plastic strain at any location is sufficiently lower than the minimum elongation limit (10%) of the pipe. The maximum plastic strain generated at and close to the pipe ends is higher than the minimum

elongation (10 %) and at any location is lower than the minimum elongation (10 %) of the pipe for hinge and fixed support conditions. The pipe failure occurs due to crossing the minimum limit of elongation (10%) at the pipe end in the case of hinge and fixed support.

The maximum displacement and stress magnitude generated in the pipe increases by up to 2.87 % and 34.9 % respectively for hinge support; also, it increases by up to 2.83 % and 34.9 % respectively for fixed support with respect to roller support. The observed plastic strain in the pipe was 90.1% lower (roller); 53.1 % higher (hinge); 45.9 % higher (fixed) than the minimum elongation (10%) of pipe.

4.3 Parametric Study

Effect of different parameters on the seismic response of pipes were observed and reported in the following sections.

4.3.1 Effect of Buried Depth of Pipe (Embedment Ratio, h/D)

Different burial depths of pipes were considered to investigate their prominent role in the seismic response of buried pipes. To examine the effect of an increase in burial depth (h) on pipe responses, five dynamic analyses have been performed for a pipe of outer diameter $D = 1048$ mm and thickness $t = 15$ mm. The pipe was modeled at buried depths, $h = 1D, 2D, 3D, 4D$ and $5D$. For all these cases, roller support at both ends of the pipe was applied. Since buried pipeline may be moved substantially with the soil if an indefinite length of pipeline is considered, it makes sense to use a roller support as the boundary condition between the ends of the pipeline (Lee, 2010). The normalized response against normalized buried depth (h/D) is depicted from Fig. 4-10, 4-12 and 4-14.

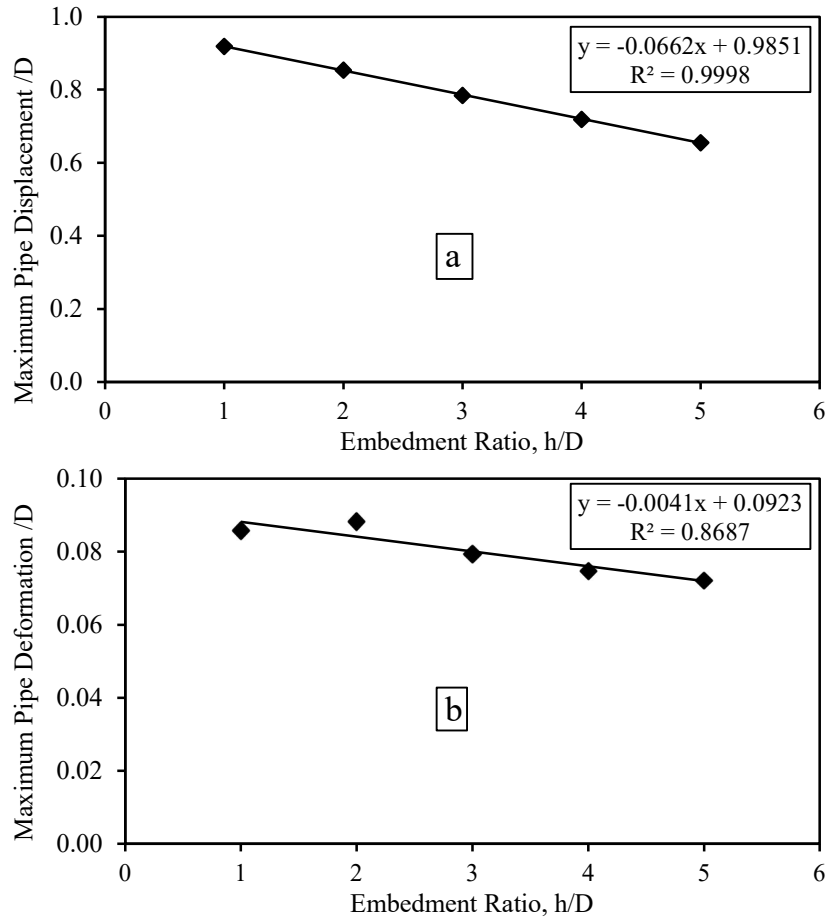


Figure 4-10: Effect of embedment ratio (h/D) on seismic response of pipe: (a) total displacement, (b) net deformation

The maximum pipe displacement and deformation are normalized by pipe diameter (D). The displacement of the pipe is maximum at a burial depth equal to the diameter ($1D$) of pipe, minimum at $5D$ and decreases with the increase in h/D (Figure 4-10a). A possible reason for this could be the effect of traffic load on the pipe: traffic load intensity on pipe decreases as h increases (Nath, 1994). Such results are in line with those reported by (Sahoo et al., 2014b). They reported that at a burial depth equal to the pipe diameter, the maximum magnitude of final displacement was observed at the end of the seismic period. From Fig. 4-10b, it is observed that maximum pipe deformation was noticed at a depth of $1D \sim 2D$, and minimum at a depth of $5D$, respectively. Since the maximum displacement and deformation were found at shallow depths ($1D \sim 2D$), it may not be safe to install pipeline at that depth to ensure structural safety.

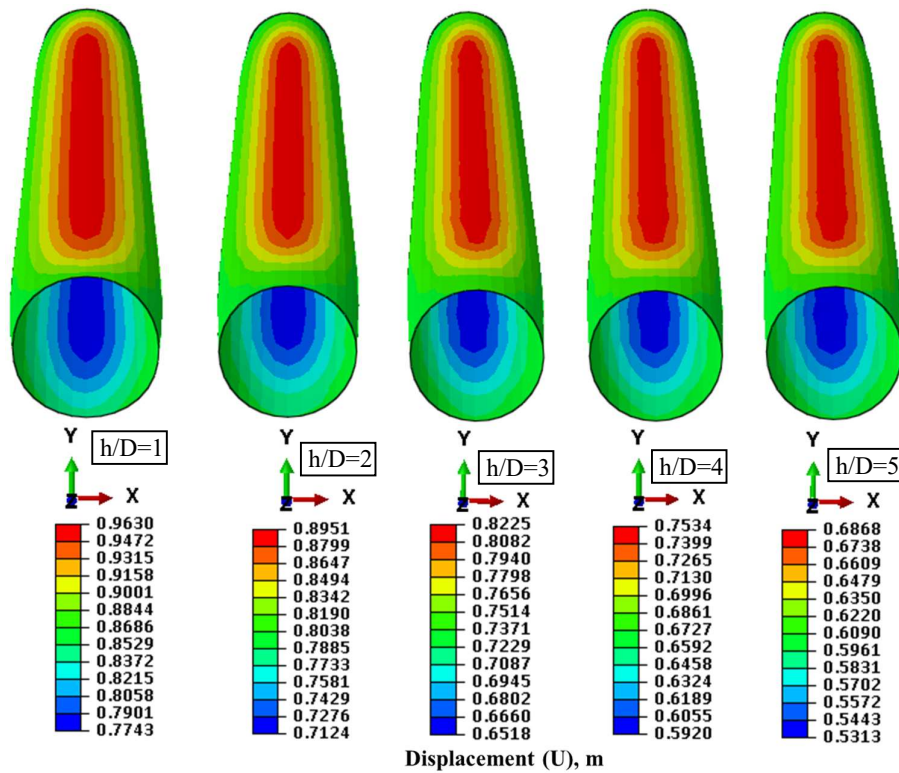


Figure 4-11: Displacement contour of DI pipe for $h/D=1\sim5$

The displacement contour of the pipeline under seismic loading for various h/D are presented in Fig. 4-11. Displacement contours indicate that, in each case, the final displacement is greater in the middle portion and gradually decreases toward the end of the pipeline. Also, the displacement pattern along the pipeline at each burial depth is identical in nature. It is also noticeable that the greatest displacement (red color band) happens at the crest of the pipeline.

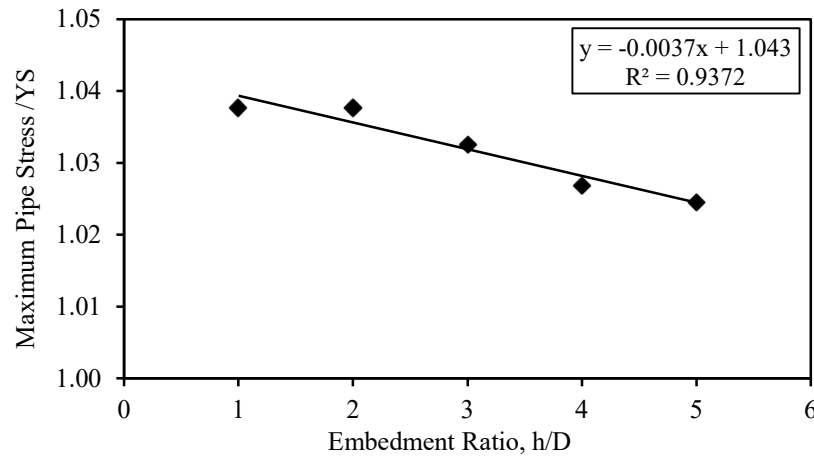


Figure 4-12: Effect of embedment ratio (h/D) on seismic response (stress) of pipe

The maximum pipe stress is normalized by yield strength of DI pipe (YS). Figure 4-12 presents the maximum stress occurred in the buried pipe at each individual normalized buried depth, h/D . The highest stress magnitude occurred for $h/D = 1 \sim 2$. But at deeper depths, the pipe stress decreases for $h/D = 5$. This is probably due to the overburden pressure of a lower height of backfill soil and a higher effect of traffic load at shallow depth and a higher height of backfill soil and a lower effect of traffic load at higher depth, along with the seismic load. All the stress values in all cases were found higher than the limit of the yield stress (350 MPa) of the pipe due to the nature and intensity of the applied loads.

However, the stress variation in pipe for different h/D , is not significantly large. Because at shallow depth, traffic load may dominate, and at deeper depth, overburden pressure from backfill soil may dominate, causing insignificant stress variation with depth. The stress variation shows a decreasing trend with an increase in buried depth due to the following reasons: Deeper soil is stiffer, providing better support against external loads and reducing soil deformation, resulting in lower stress on the pipe. Deeper soil has more mass and provides a damping effect that reduces stress induced by seismic loads by reducing vibration susceptibility. Deeper soil has increased lateral resistance, which improves pipe support against seismic loads and reduces soil deformation, resulting in lower stress on the pipe.

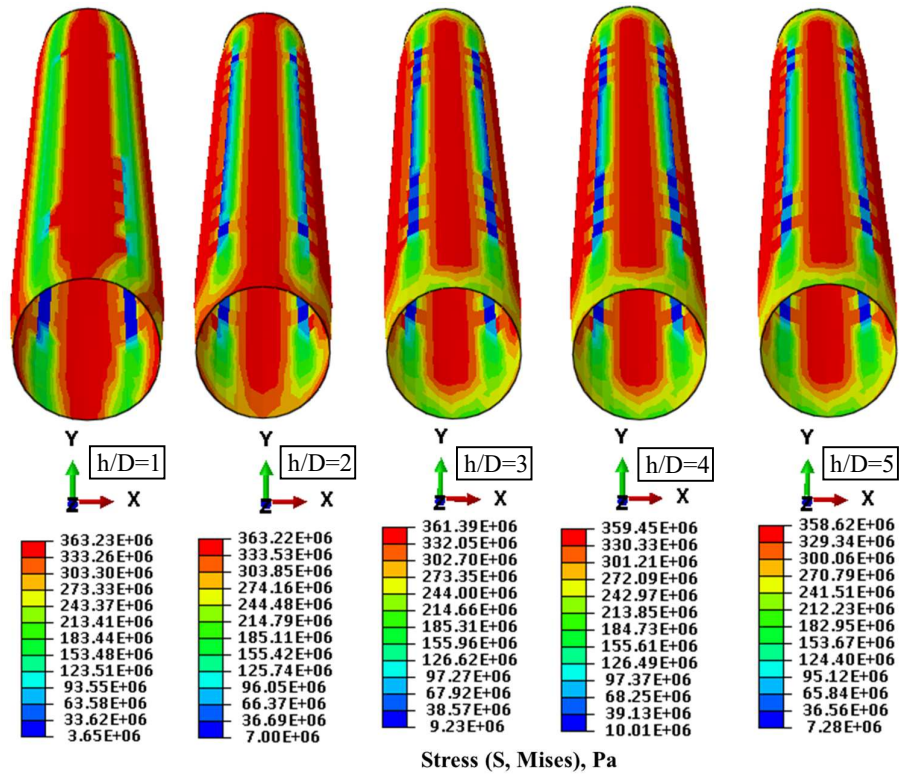


Figure 4-13: Stress contour of DI pipe for $h/D=1\sim5$

The stress contour of the pipeline under seismic loading for various h/D are presented in Fig. 4-13. It can be observed that the maximum stress (red color band) is formed on the crest line of the pipe in all cases. Also, the significant stress intensity (red color band) was observed at the crest, invert, left and right spring lines of the pipe. During an earthquake event, the pipeline is deformed starting from the top crest position (crest line), moving on to the two sides of the pipeline (left and right spring line) and then moves to the bottom invert position (invert line), and finally, the circular cross section of the pipe forms an oval shape.

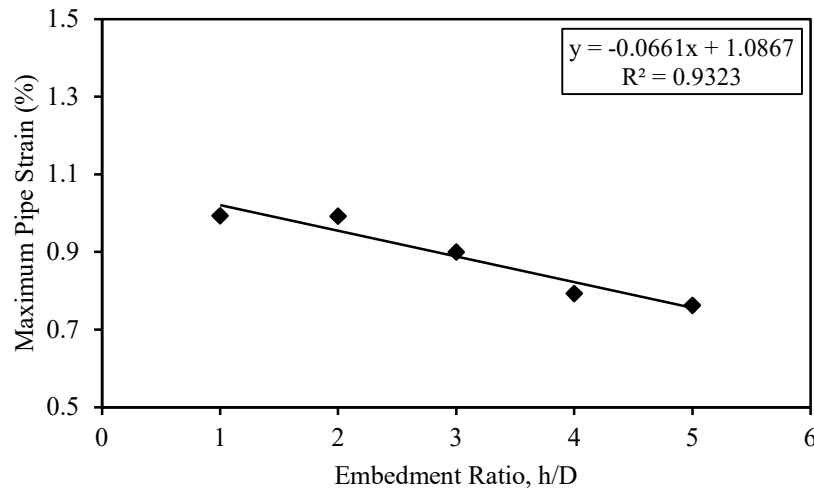


Figure 4-14: Effect of embedment ratio (h/D) on seismic response (strain) of pipe

Figure 4-14 shows that as h/D increases, the pipe strain (ε_p) decreases. Since the effect of traffic load is higher at shallow depths and vice-versa. It can also be noticed that the maximum pipe strain was found at $h = 1D \sim 2D$, and the minimum pipe strain was found at $h = 5D$. It is to mention that the maximum strain is significantly smaller than the minimum elongation of the ductile iron pipe (10%).

Overall, the increases in the embedment ratio (h/D) from 1 to 5, decreases pipe displacement, deformation, stress and strain by 28.7 %, 15.8 %, 1.3 % and 23.2 %, respectively.

4.3.2 Effect of D/t Ratio of Pipe

Increasing the pipe diameter would increase the soil displacement around it and decrease the resistance of the pipe to seismic waves as the perimeter of the pipe is increased under the earthquake load.

The increased thickness of pipes reduces the displacement of the soil around them. The rise in the thickness of the pipe raises the pipe hardness and reduces the displacement between the pipe and the soil.

The D/t ratio is the ratio of the outside diameter of the pipe (D) to its wall thickness (t). A D/t spectrum from 48 to 144 was considered in this study. This spectrum of D/t values is typical for onshore applications (oil, gas or water pipelines) (Vazouras et al., 2010). Three pipe outer diameters of 1255 mm, 1048 mm, 842 mm and three corresponding pipe thicknesses of 17 mm, 15 mm, 13 mm respectively were considered

to examine the effect of diameter to thickness ratio (D/t) on the seismic response of pipe.

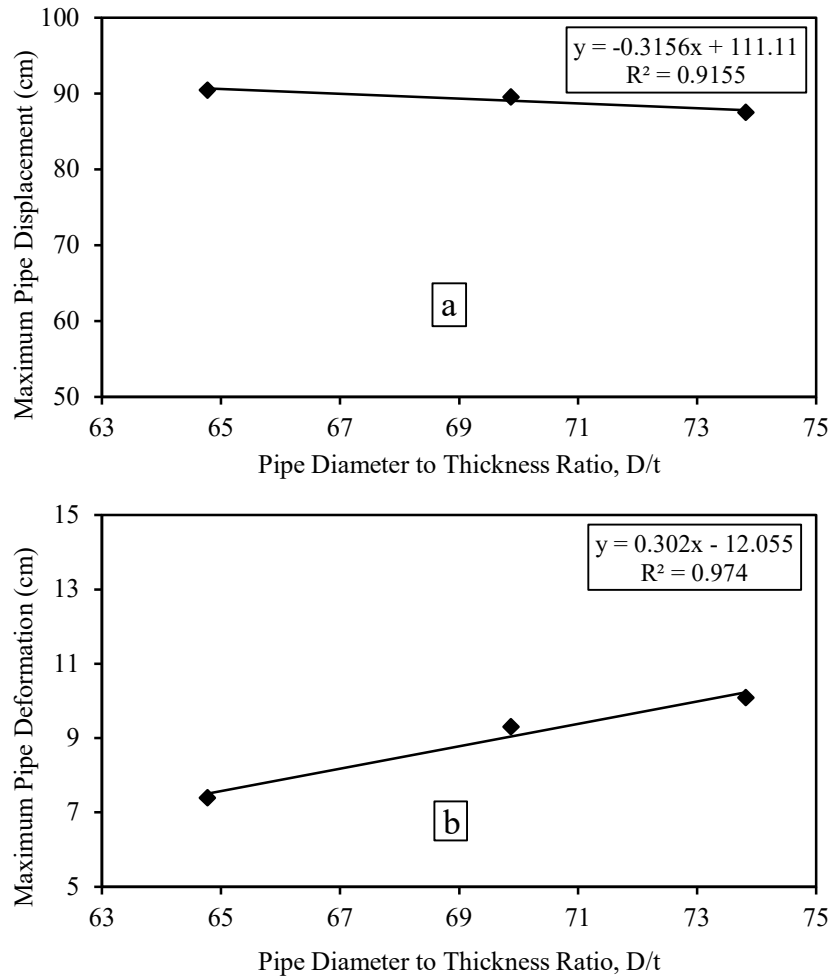


Figure 4-15: Effect of diameter-to-thickness ratio of pipe on seismic response of pipe (a) total displacement (b) net deformation

Figure 4-15a illustrates that the pipe displacement drops with a rise in the D/t ratio of pipe. Generally, for larger pipe dimensions, both the pipe's diameter and thickness increase simultaneously for practical reasons. The stiffness of a pipe increases as its dimensions increase. As a result, a higher D/t ratio reduces pipe displacement. The maximum pipe displacement was found at 90.45 cm with an 842 mm diameter and a 13 mm thickness. In addition, the minimum pipe displacement was measured at 87.53 cm for the 1255 mm diameter and 17 mm thickness. But the fact is that this variation is not significantly large due to the shorter range of the D/t ratio considered. From Fig. 4-15b, it is observed that highest magnitude of deformation is 10.09 cm for largest D/t (73.8) and lowest one is 7.39 cm for lowest D/t (64.8). It may be due to the higher diameter of

the pipe, which deforms the pipe more under a given load. However, for higher pipe deformation, the larger diameter of the pipe plays a vital role.

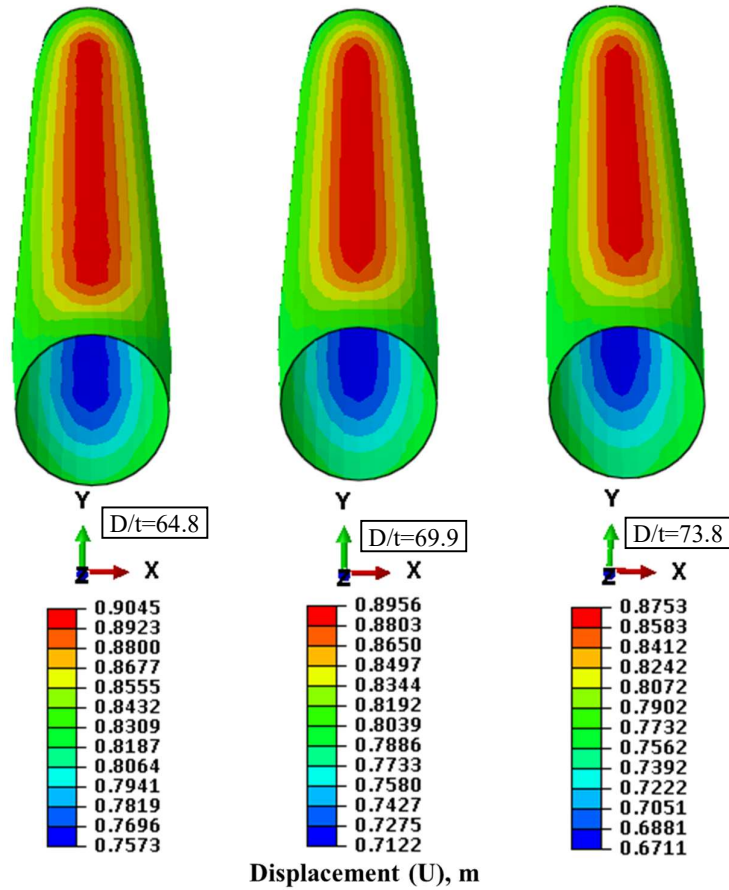


Figure 4-16: Displacement contour of DI pipe for various D/t (64.8 to 73.8)

Figure 4-16 represent the displacement contour of the pipe under different D/t ratios. The contour diagram clearly shows that the maximum pipe displacement (red color band) was found at the crest line of pipe.

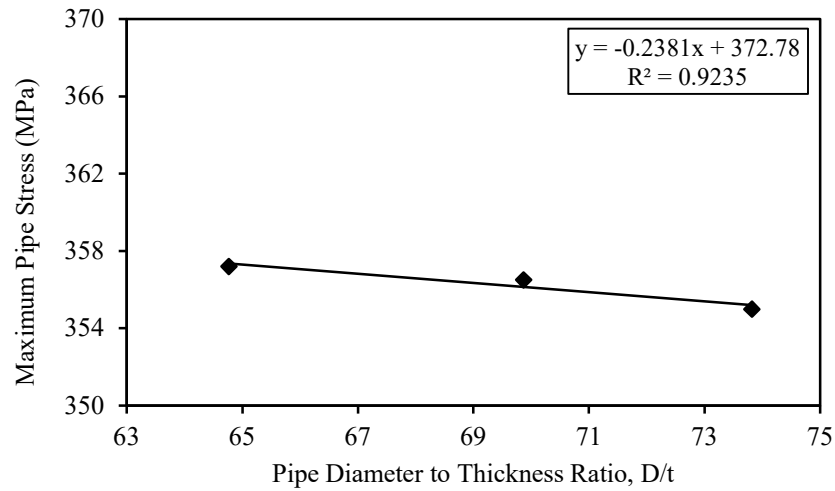


Figure 4-17: Effect of diameter-to-thickness ratio of pipe on seismic response (stress) of pipe

The pipe stress also decreased due to an increase in the D/t ratio of pipe, shown in Fig. 4-17. The maximum pipe stress was 357.2 MPa for diameter 842 mm and thickness 13 mm whereas the minimum pipe stress was 355 MPa for diameter 1255 mm and thickness 17 mm. A higher D/t ratio means that the pipe is less flexible and more stiffer. For this reason, the pipe responses decrease with an increase in the D/t ratio. An interesting observation is that all the maximum pipe stresses were found higher than the limit of yield stress of ductile iron pipe, i.e., 350 MPa due to the nature and intensity of the applied loads.

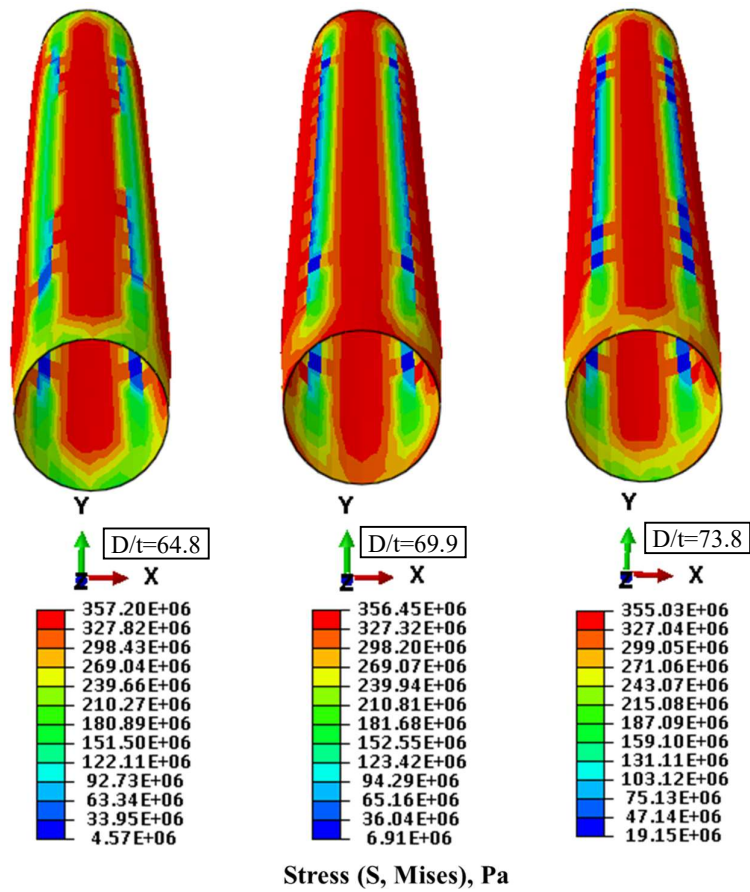


Figure 4-18: Stress contour of DI pipe for various D/t (64.8 to 73.8)

Figure 4-18 represent the stress contour of the pipe under different D/t ratios. The contour diagram clearly shows that the maximum pipe stress (red color band) was found at the crest line of pipe. Also, large magnitude of stress (red color band) was found at the crest, invert, left and right spring lines of the pipe.

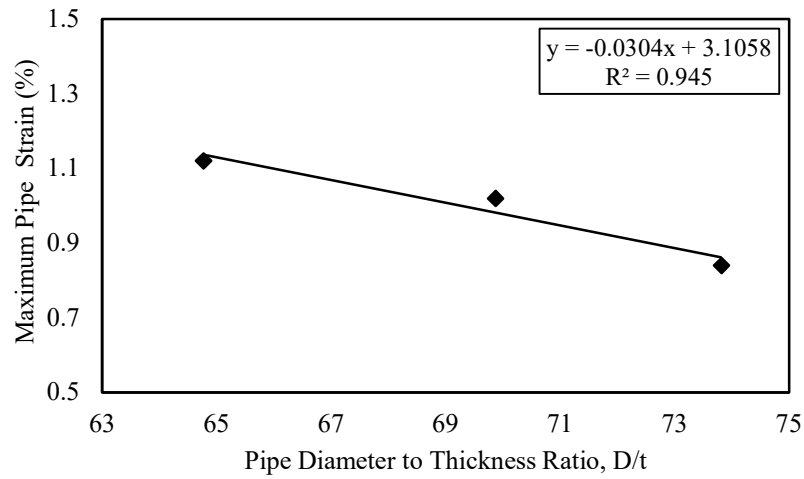


Figure 4-19: Effect of diameter to thickness ratio of pipe on seismic response (strain) of pipe

From Fig. 4-19, it is clearly noticed that by increasing the D/t ratio of pipe, the plastic strain of the pipe is reduced. The maximum pipe strain was found at 1.12 % for a pipe diameter of 842 mm and pipe thickness of 13 mm, as well as the minimum pipe strain was observed at 0.84 % for a pipe diameter of 1255 mm and pipe thickness of 17 mm. It is worth noting that all the pipe strain values were significantly lower than the value of minimum elongation after fracture (10%). Therefore, this provides evidence that there is much less plastic strain in the pipe for the selected D/t ratios of pipe. This appears to imply that larger pipe dimensions are appropriate for water supply in terms of structural safety.

The increase in pipe diameter to wall thickness ratio (D/t) from 65 to 74 by up to 1.14 times, reduces pipe displacement, stress and strain by 3.23 %, 0.62 % and 25 % respectively.

4.3.3 Effect of the Operational Water Pressure

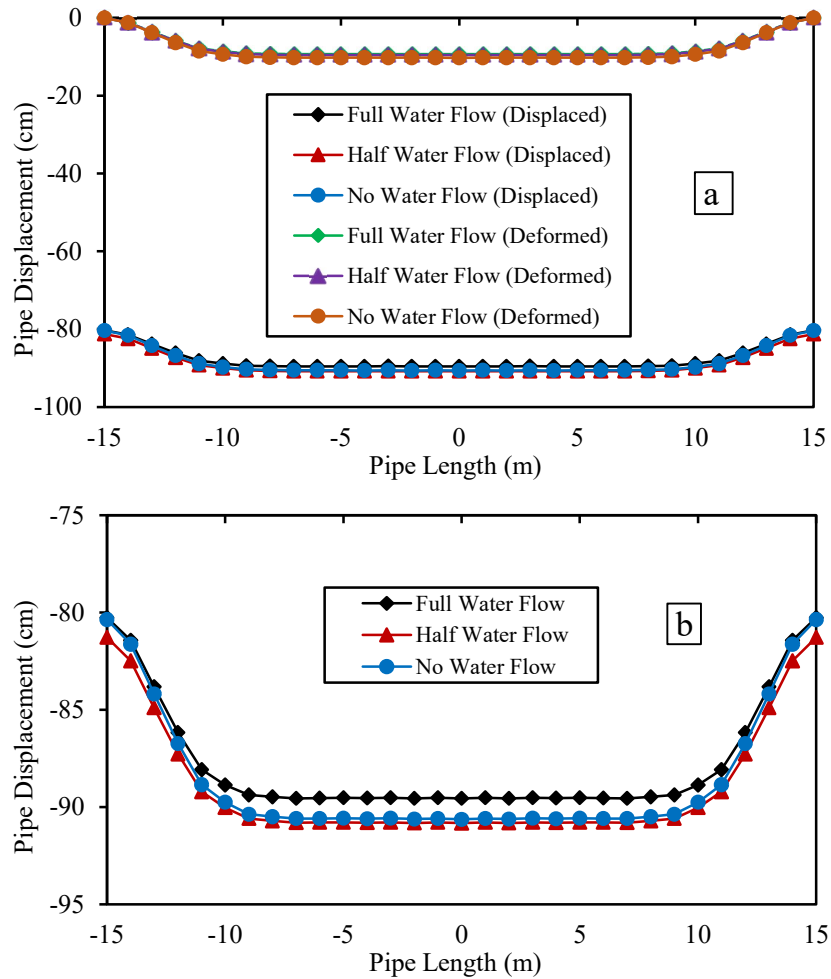
The flow of fluid (water in this FEA) inside the pipe generates hoop stress σ_c that acts in the radial direction of the pipe cross section. This stress can be varied during the operation of the buried pipeline. For example, hoop stress at full flow and half flow will be entirely different compared to no flow (when pipe is empty). As such it would be interesting how these conditions contribute to response of buried pipelines. To investigate those 3 analyses was carried out adopting $D = 1048$ mm, $t = 15$ mm and incorporating roller support as boundary condition for both ends of the pipe. The pipe

was buried at a depth of $h = 2D$ in dry sand deposit. Three operational conditions: (i) full flow of water; (ii) half flow of water; and (c) empty or no flow condition, were considered. Under full flow conditions, the operational water pressure (100 kPa) causes a maximum hoop stress of 3.5 MPa on the inner surface of pipe. The calculation of hoop stress was performed using the well-known Mariotte's formula (Equation 4.1).

$$\sigma_c = \frac{pD}{2t} \quad 4.1$$

where, p = fluid pressure, D = diameter, and t = thickness. For a pipe with $D = 842$ mm & $t = 13$ mm, σ_c will be 3.24 MPa. For a pipe with $D = 1048$ mm & $t = 15$ mm, σ_c will be 3.5 MPa. For a pipe with $D = 1255$ mm & $t = 17$ mm, σ_c will be 3.7 MPa.

Based on FEA results, the effect of flow conditions on the seismic responses of pipe are presented in Fig. 4-20, 4-22 and 4-24.



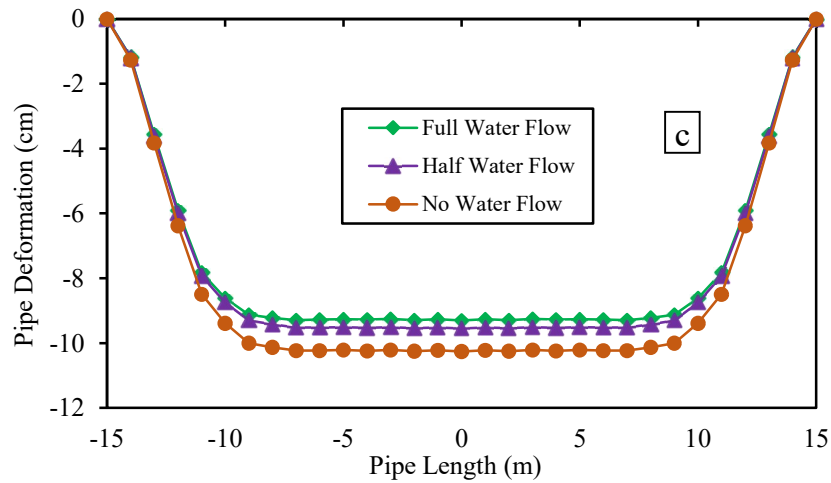


Figure 4-20: Effect of inside water pressure on seismic response of pipe: (a) displacement with deformation; (b) enlarged view of total displacement; (c) enlarged view of net deformation

Displacement as well as deformation responses along the crest line are given in Fig. 4-20. Figure 4-20 (a) compares displaced and deformed crest lines for full, half and no flow conditions. As can be seen, in each case, the final displacement is higher in the mid-span of the pipe, and progressively reduces towards the end. In general, the displacement patterns for different flow conditions are identical in nature. As can be seen from Fig. 4-20 (b), an enlarged view for displacement, the maximum and minimum pipe displacement are 89.56 cm (midspan) and 80.26 cm (end), for full flow conditions. For half flow and no flow conditions, the maximum pipe displacement is 90.83 cm and 90.63 cm, respectively, and the minimum pipe displacement is 81.28 cm and 80.37 cm, respectively. It is evident that maximum displacement under full flow is slightly smaller than half and no flow case. This can perhaps be attributed to the radial outward pressure exerted by the fluid on the inner surface of pipe, which contributed to preventing the displacement, deformation, stress, and strain of the pipe. The deformation, as can be seen in Fig. 4-20 (c) (enlarged view), was found to be as maximum as 10.3 cm for no water flow condition, and as minimum as 9.3 cm for full water flow condition. For half water flow, it was found to be 9.5 cm.

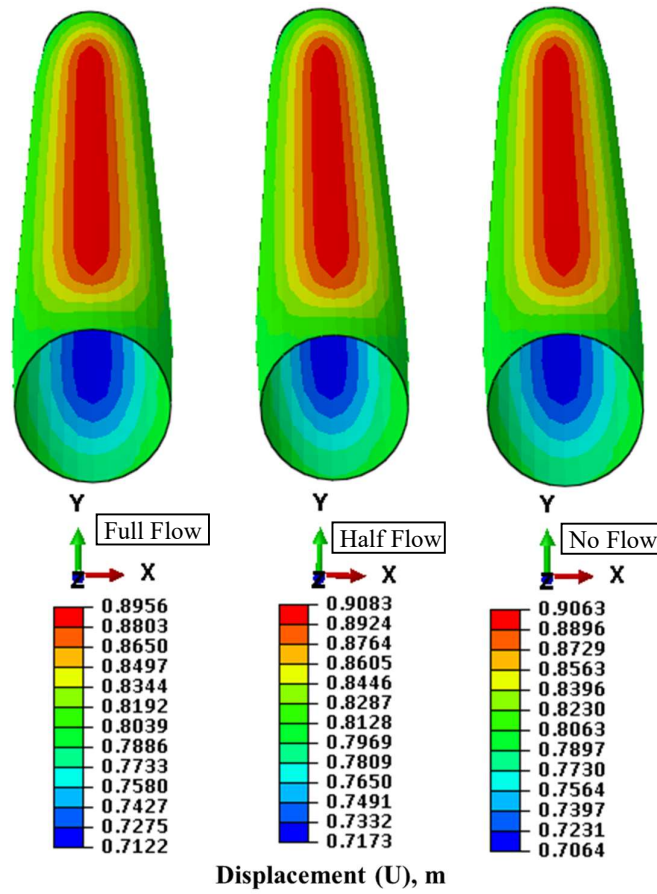


Figure 4-21: Displacement contour of the ductile iron pipe for different flow conditions (full, half and no flow)

Figure 4-21 presents the displacement contours of the buried pipe for full flow, half flow, and no flow conditions, respectively. The maximum pipe response (red color band) is found to happen at the crest line of the pipe.

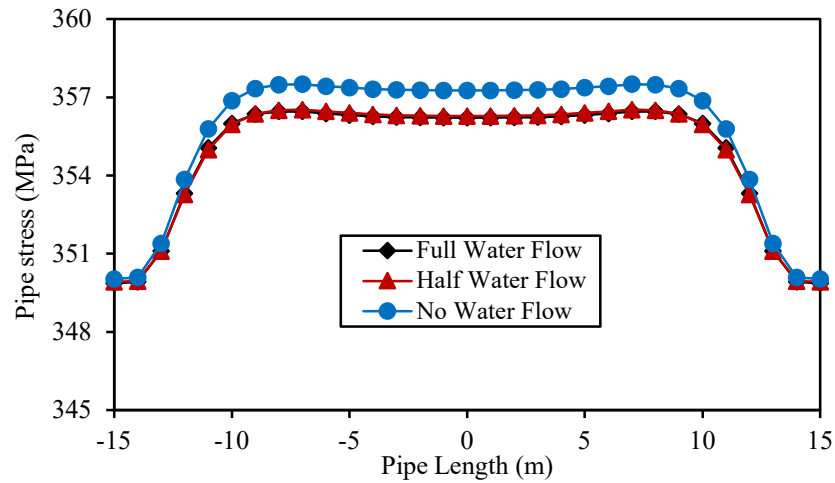


Figure 4-22: Effect of inside water pressure on seismic response (stress) of pipe

Figure 4-22 compares stress generated in pipe along the crest lines for full, half and no flow conditions. From Fig. 4-22, it can be seen that the pipe stresses are maximum at the midspan region and minimum at the pipe end for any given flow conditions. For full flow condition, the maximum pipe stress is 356.45 MPa and the minimum stress is 349.86 MPa. For half flow and no flow condition, the maximum pipe stress is 356.5 MPa and 357.5 MPa and the minimum stress is 349.92 MPa and 350.03 MPa, respectively. The fact that the stress variation in all cases is not significant may be due to the nature and intensity of the applied load. However, the stress distribution for the full flow condition is found to be slightly smaller than the other two cases. The reason can again be attributed to the internal water pressure, as explained earlier. If compared with the yield stress (YS) of the pipe, the stress at the pipe end reaches the yield limit, whereas the stress is higher than the YS at any other location along the length. This is true for other flow conditions. For half flow and no flow cases, the pipe experiences relatively greater stress and displacement, so these cases should be considered carefully.

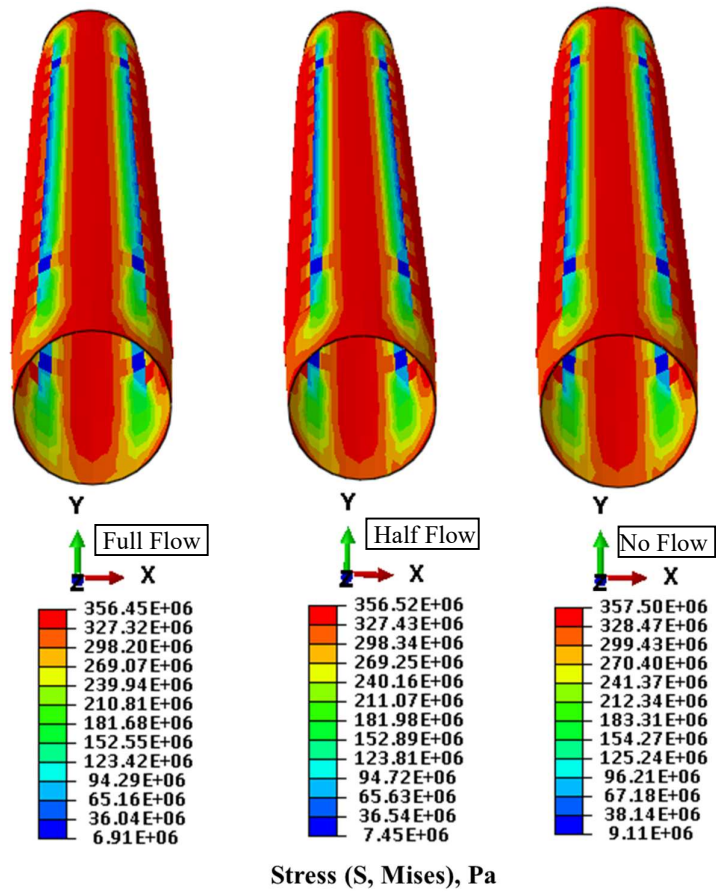


Figure 4-23: Stress contour of the ductile iron pipe for different flow conditions (full, half and no flow)

Figure 4-23 presents the stress contours of the buried pipe for full flow, half flow, and no flow conditions, respectively. The maximum pipe response (red color band) is found to happen at the crest line of the pipe. The significant pipe stresses (red color band) are concentrated at the invert, left, and right spring lines of the pipe as well.

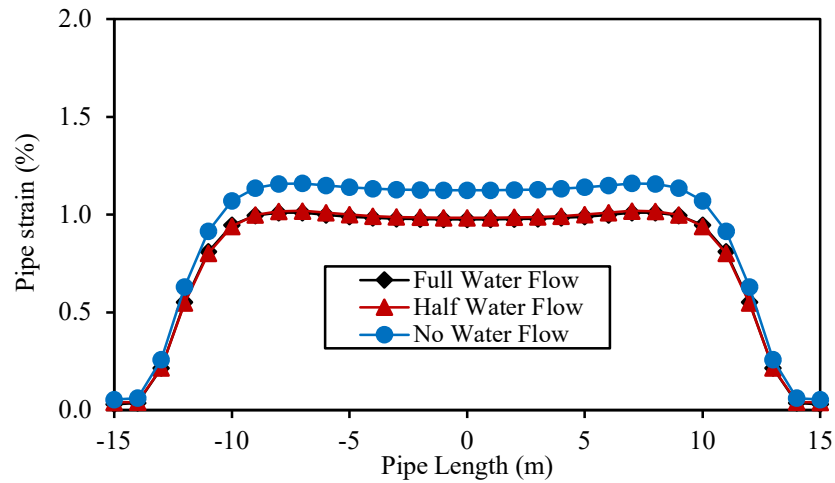


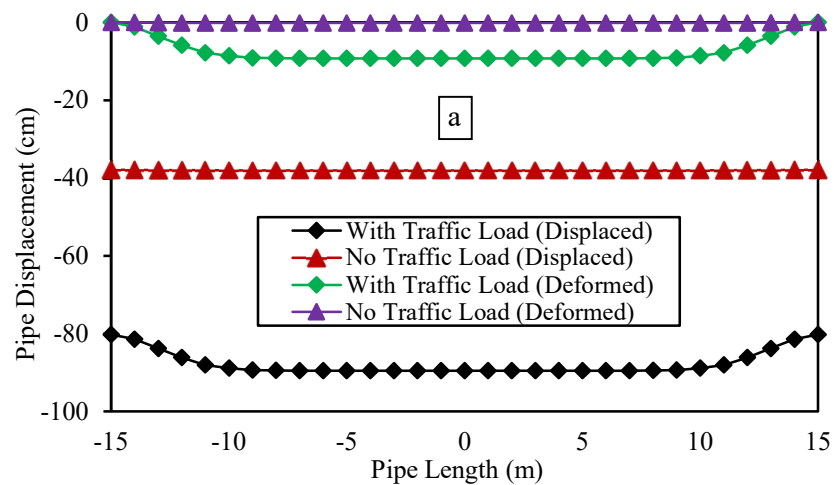
Figure 4-24: Effect of inside water pressure on seismic response (strain) of pipe

Figure 4-24 compares strain induced in the pipe along the crest lines for full, half, and no flow conditions. A maximum plastic strain of 1.2% can be noticed at the mid-length of the pipe for no water flow condition. In contrast, a plastic strain of about 1% was found at the same place for full water and half water flow conditions. In any flow condition, the strain magnitudes are negligible due to the roller boundary conditions. If compared, the induced plastic strains in the pipe are much lower than the minimum pipe elongation (10%).

Overall, if compared with no flow condition, the maximum displacement and stress magnitude developed in the pipe decreases by 1.2% and 0.29% respectively for full flow condition and increases by 0.22 % and decreases by 0.28 % respectively for half flow condition. The observed plastic strain in the pipe was about 90% lower (full flow and half flow) and 88.4% lower (no flow) than the minimum elongation (10%) of pipe. Hence, it is important to consider operational water pressure in the analysis of buried pipes because the water pressure can significantly affect the structural behavior and stability of pipe. When water flows through a pipe, it generates internal pressure that can increase the load on the pipe and affect its deformation, stress, and strain. Therefore, the analysis of a buried pipe must account for the operational water pressure to ensure that the pipe can withstand both static and dynamic loads, including seismic events.

4.3.4 Effect of Traffic load

To investigate the effect of traffic load on the seismic response of pipelines like displacement, stress, strain, etc., two analyses on pipe with an outer diameter of 1048 mm, a thickness of 15 mm, and a burial depth of 2D in a dry sand deposit with and without traffic load and full water flow inside the pipe have been performed. A uniform surface load of 1100 KPa (as traffic load) on soil top surface is considered to inspect the short-term structural serviceability condition of the buried pipeline considering the pipeline lies in the traffic area. Generally, the dead load on the buried pipeline is considerably higher than the live load since the effects of the live load (traffic load) reduce quickly with an increase in soil depth (Lee, 2010). Even though the live load becomes more critical than a dead load for the shallow buried depth of the pipeline, (Nath, 1994). The effect of traffic load on the pipe response is easily understood by considering traffic load and no traffic load cases.



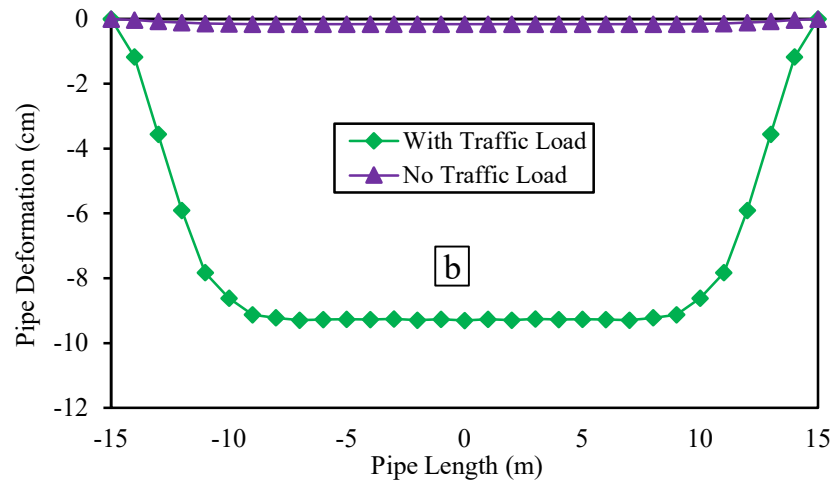


Figure 4-25: Effect of traffic load on seismic response of pipe (a) displacement with deformation, (b) net deformation

The pipe displacement is 89.56 cm due to traffic load, which is higher and uniform in the middle region of the pipe up to the closest to the pipe end and then gradually decreases to 80.26 cm at the pipe end, as shown in Fig. 4-25 (a). For the no traffic load case, the pipe displacement is about 38 cm, which is almost uniform throughout the pipe length and is about 42.4 % of the displacement found in the traffic load case. As the pipe was installed at the shallower depth of 2D, the pipe faces greater displacement due to traffic load. In traffic load cases, the maximum pipe deformation was found to be 9.3 cm in the middle of the pipeline, and there was no noticeable deformation in the pipe without traffic load as shown in Fig. 4-25 (b).

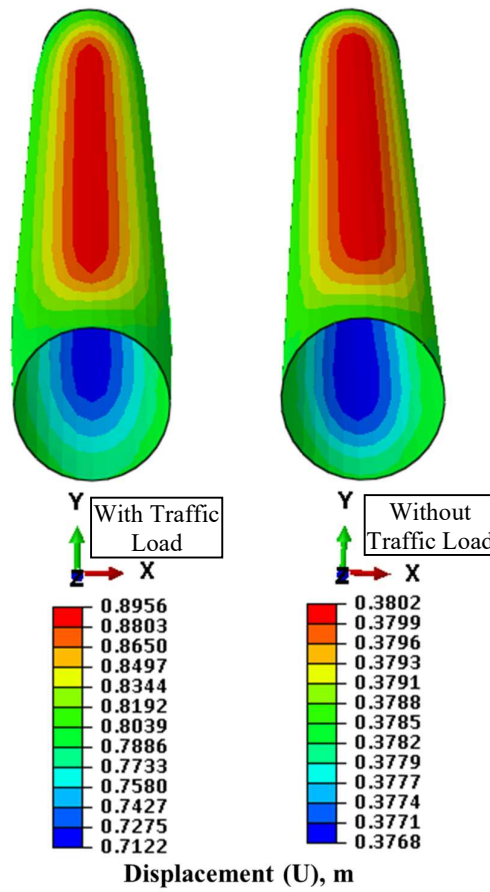


Figure 4-26: Displacement contour of the ductile iron pipe with a traffic load of 1100 kPa and without traffic load

Figure 4-26 represents the displacement contour of the pipe due to traffic load and without traffic load. Considering traffic load and no traffic load, maximum displacement (red color band) was found at the crest line of the pipe.

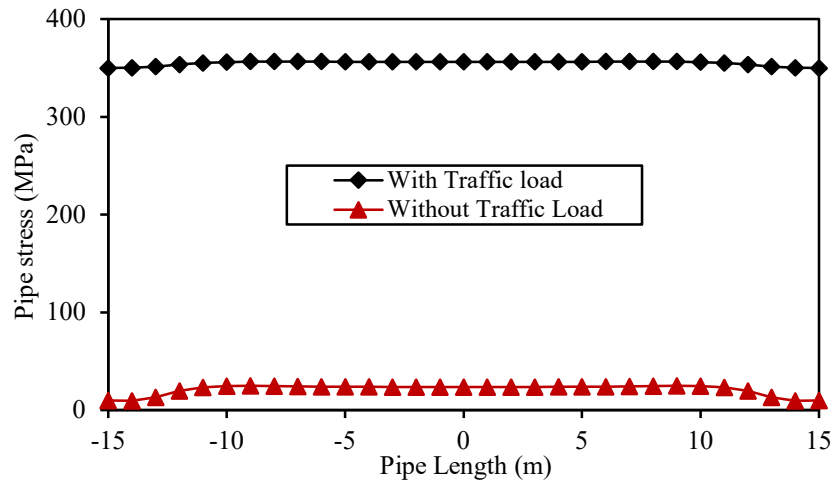


Figure 4-27: Effect of the traffic load on seismic response (stress) of pipe

If the pipe travels in the traffic area, traffic loads are frequently put on the pipes, as well as water pressure and soil pressure. These loads are of minimal importance when the depth of the burial is extremely low. However, when the pipes are shallowly buried, they can play a critical function. Pipe stress is thus investigated under traffic charges and no traffic charges, to understand how traffic loads affect the stress distribution developed in the pipes. Figure 4-27 clearly shows that pipe stress follows a similar trend to that of traffic and no traffic load. But there is a significant gap in stress distribution observed in the case of traffic and no traffic load. For the same reason, the maximum stress was found at midspan to be 356.45 MPa including traffic load and the maximum stress was found to be 25 MPa (about 7% of the stress found including traffic load) excluding traffic load. Most interestingly, all the stress magnitudes considering traffic load were equal or slightly greater than the yield limit (350 MPa).

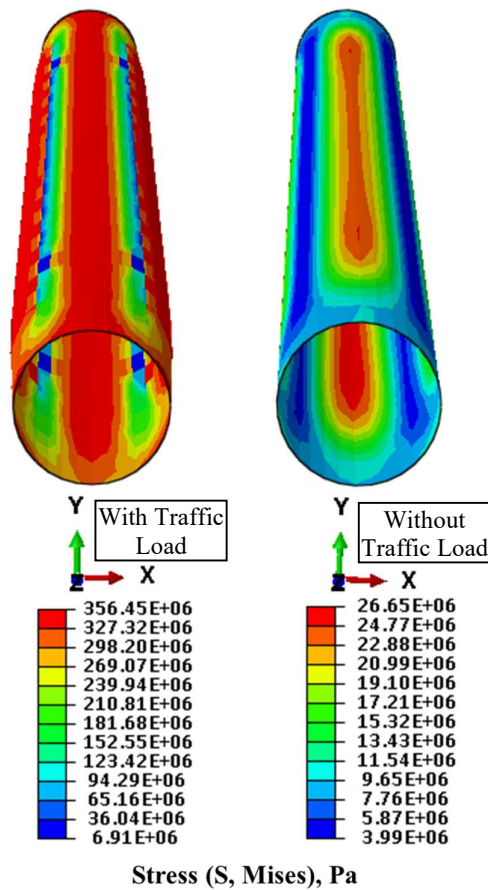


Figure 4-28: Stress contour of the ductile iron pipe with a traffic load of 1100 kPa and without traffic load

Figure 4-28 represents the stress contour of the pipe due to traffic load and without traffic load. Considering traffic load, maximum response (red color band) was found at the crest line of the pipe and significant stress intensity (red color band) was observed at the invert, left and right spring lines of the pipe. Due to no traffic load conditions, maximum response (red color band) was found at the crest line of the pipe, and significant stress intensity (red color band) was observed at the invert lines of the pipe only because of overburden soil pressure.

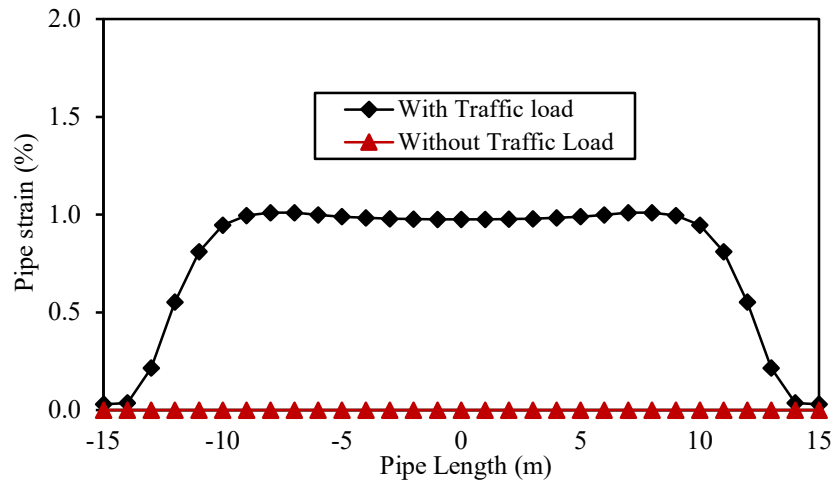


Figure 4-29: Effect of the traffic load on seismic response (strain) of pipe

Figure 4-29 highlights that the plastic strain in the pipe is 1 % due to traffic load, which is higher and uniform in the middle region of the pipe up to the closest to the pipe end and then gradually decreases to almost 0% at the pipe end. In the case of no traffic load, there is no plastic strain observed in the pipe. In the case of traffic load, the observed strain in the pipe was much lower than the minimum elongation limit (10%).

The greatest displacement and stress values occurred in the pipe considering the traffic load (1100 kPa) on the soil significantly increased by 135.7% and dramatically increased by (1326 %) respectively compared to the no traffic load case. The observed plastic strain in the pipe due to traffic load was 90 % lower than the minimum elongation (10%) of pipe. If the pipe travels in the traffic area, traffic load should be considered to ensure the structural safety of the pipe.

4.3.5 Effect of Soil Density

To examine the effect of soil density on the seismic response of the pipe, four dynamic analyses consisting of four different dry densities of soil from 1700 kg/m^3 to 2160 kg/m^3 (1700, 1850, 2000, and 2160 kg/m^3) have been performed. The maximum pipe displacement and deformation are normalized by pipe diameter (D). The density ratio indicates the ratio between the density of the pipe and the density of the soil. The density ratio is inversely proportional to the soil density. Increasing the soil density surrounding a pipe leads to a stiffer soil that provides better support, resulting in decreased pipe displacement, deformation, stress, and strain under external loads.

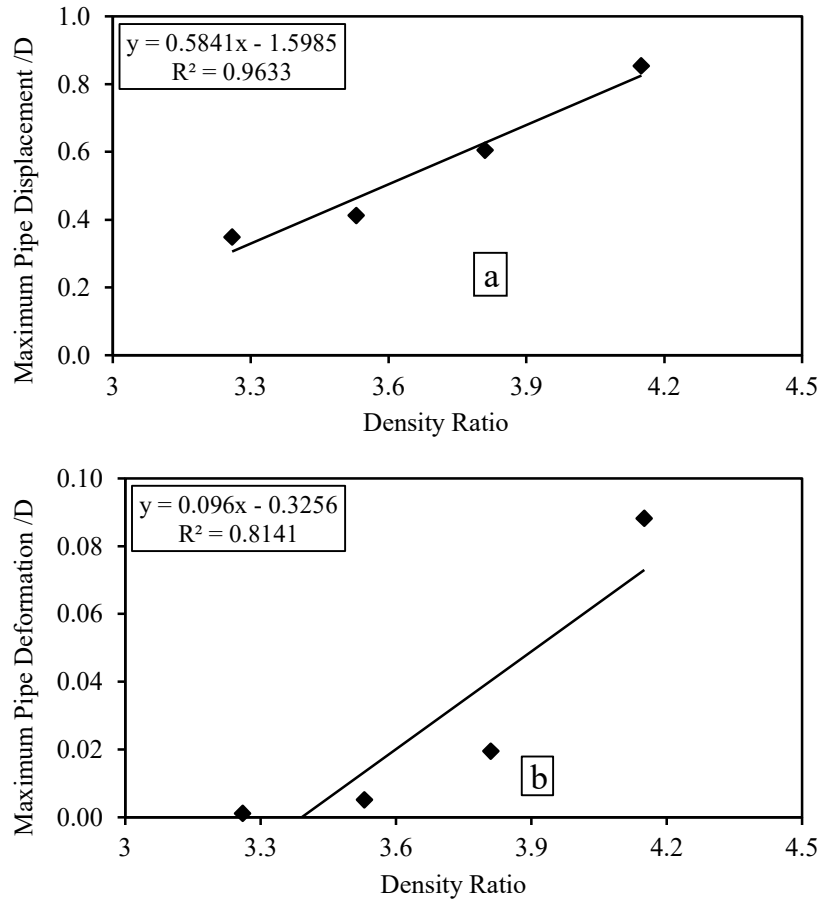


Figure 4-30: Effect of soil density on seismic response of pipe: (a) total displacement, (b) net deformation

Figure 4-30 (a) shows the normalized maximum pipe displacement with different density ratios. From this figure, it was observed that due to an increase in the density ratio, the maximum pipe displacement increased and vice-versa. The maximum pipe displacement was found for a dry density of 1700 kg/m^3 , and the minimum pipe displacement was seen for a dry density of 2160 kg/m^3 . Because of higher densities of sand, the pipeline experiences lower displacement, which is the most common phenomenon in nature. Also, from Fig. 4-30 (b), higher and lower magnitudes of deformation were depicted for dry densities of 1700 kg/m^3 and 2160 kg/m^3 , respectively.

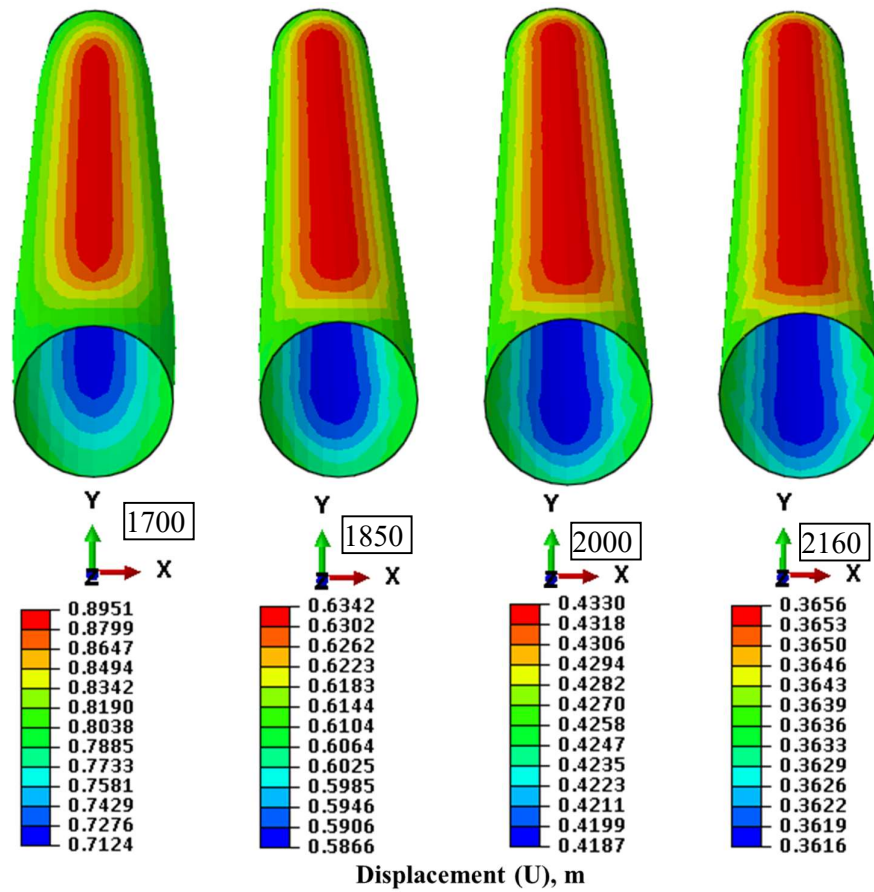


Figure 4-31: Displacement contour of DI pipe due to variation in dry densities (1700 kg/m³ to 2160 kg/m³) of soil

Figure 4-31 depicts the displacement contour of a ductile iron pipe caused by variations in soil density. In all cases, the maximum displacement (red color band) was noticed in the crest line of the pipe.

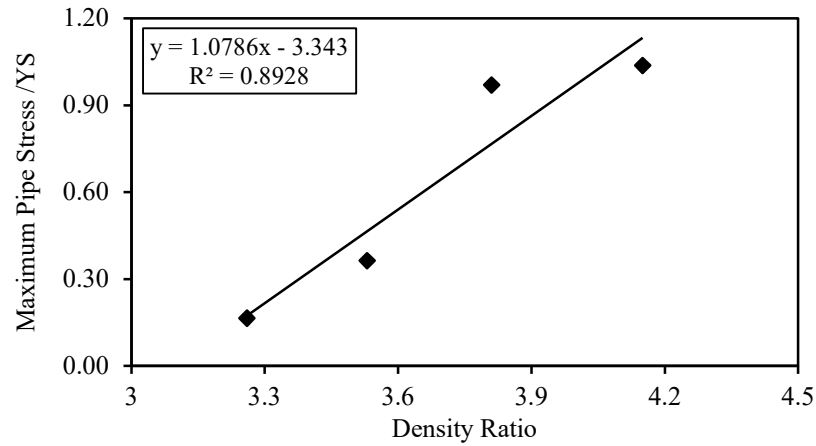


Figure 4-32: Effect of soil density on seismic response (stress) of pipe

The maximum pipe stress is normalized by yield strength of pipe (YS). From Fig. 4-32, it is depicted that maximum pipe stress increases as the density ratio increases. The maximum pipe stress was developed for a dry density of 1700 kg/m^3 and the minimum pipe stress was developed for a dry density of 2160 kg/m^3 . The distribution of stress in pipes follows the same trend as pipe displacement. This is due to the higher density of sand and the lower stress developed in the pipe as the maximum external load is carried by the dense sand. It is obviously observed that all pipe stresses were within the limit of yield stress of ductile iron pipe, i.e., 350 MPa, except for the pipe stresses for the soil density of 1700 kg/m^3 .

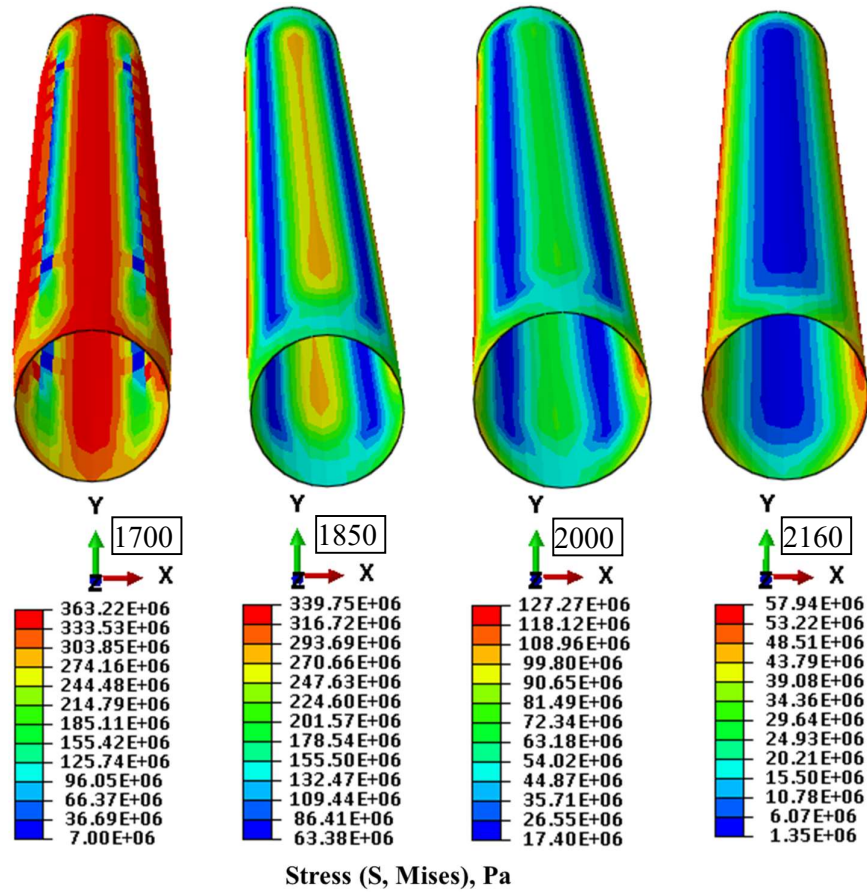


Figure 4-33: Stress contour of DI pipe due to variation in dry densities (1700 kg/m^3 to 2160 kg/m^3) of soil

Figure 4-33 depicts the stress contour of a ductile iron pipe caused by variations in soil density. The maximum stress (red color band) was observed in the crest line of the pipe with a soil density of 1700 kg/m^3 and 1850 kg/m^3 , respectively. In contrast, the maximum stress was found in the left and right spring line of pipe for soil density of 2000 kg/m^3 and 2160 kg/m^3 , respectively.

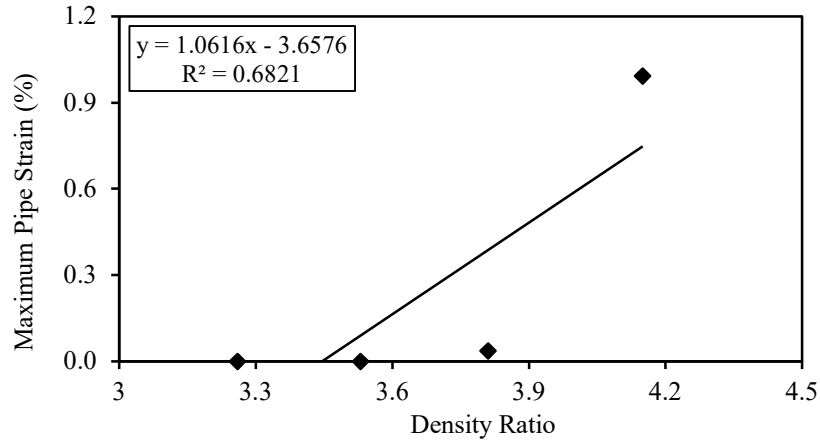


Figure 4-34: Effect of soil density on seismic response (strain) of pipe

From Fig. 4-34, it was noticed that higher pipe strain was found for higher density ratio and vice versa. The maximum plastic strain in the pipe was detected at 1% for a soil density of 1700 kg/m^3 and no plastic strain in pipe was found for other densities of sand. The distribution of pipe strain also follows the same trend as pipe stress for the same reason. In all the cases, the observed plastic strain in the pipe was within the minimum limit of elongation after fracture (10%) of the pipe.

The maximum displacement, stress and strain developed in the pipe decreased by up to 59.2%, 84% and 100% respectively, due to an increase in soil density (from 1700 to 2160 kg/m^3 by 1.27 times). Hence, the soil backfills surrounding the pipe should have a higher density to ensure the structural safety of buried pipes.

4.3.6 Effect of the Angle of Internal Friction of Soil

The friction angle of the soil is another variable considered in this study. To investigate the impact of soil friction angle on the seismic response of the pipe, four dynamic analyses with 4 different friction angles of soil (30° , 35° , 40° , and 45°) were performed for a pipe with an outer diameter of 1048 mm , a thickness of 15 mm , roller support at both pipe ends, and a burial depth of $2D$ depth.

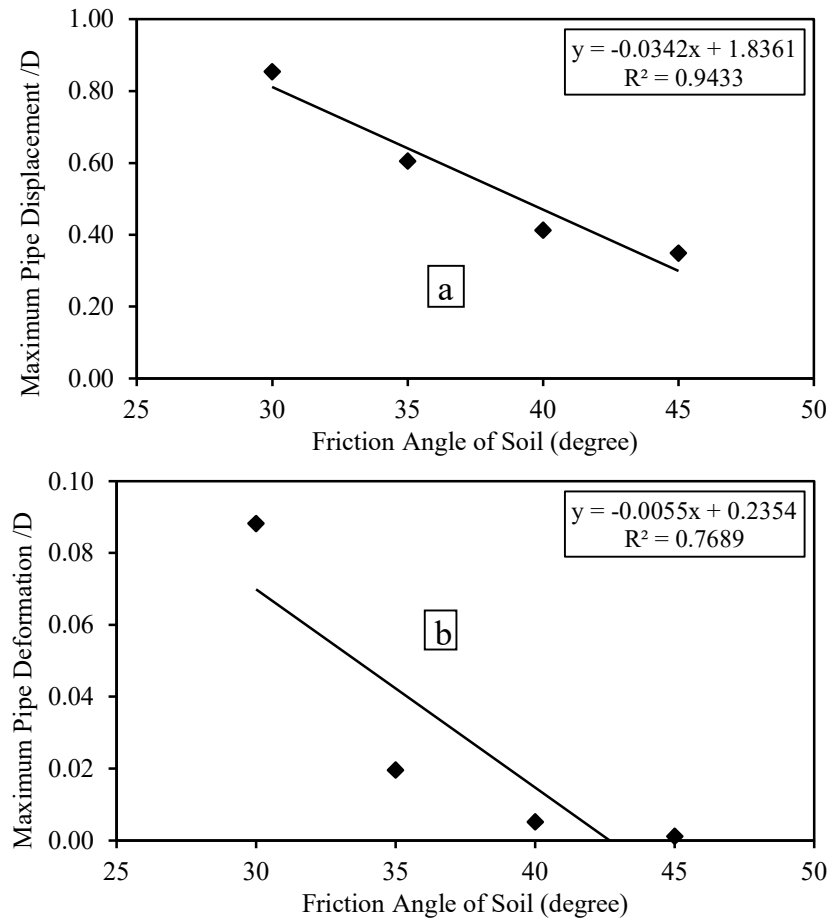


Figure 4-35: Effect of friction angle of soil on seismic response of pipe (a) total displacement (b) net deformation

The maximum pipe displacement and deformation are normalized by pipe diameter (D). It is found from Fig. 4-35(a) that the magnitude of final displacement of the pipe decreases gradually due to an increase in the angle of internal friction of the soil. By increasing the friction angle of the sand, the state of the sand changes from loose to dense. Thus, the forces applied to the pipe by the sand are reduced, with a rise in the friction angle of the sand. It can be seen from this graph that the maximum pipe displacement was found for a friction angle of 30°, whereas the minimum pipe displacement was found for a friction angle of 45°. Fig. 4-35(b) depicts that maximum and minimum pipe deformation were observed for friction angles of soil of 30° and 45°, respectively, for the same reason.

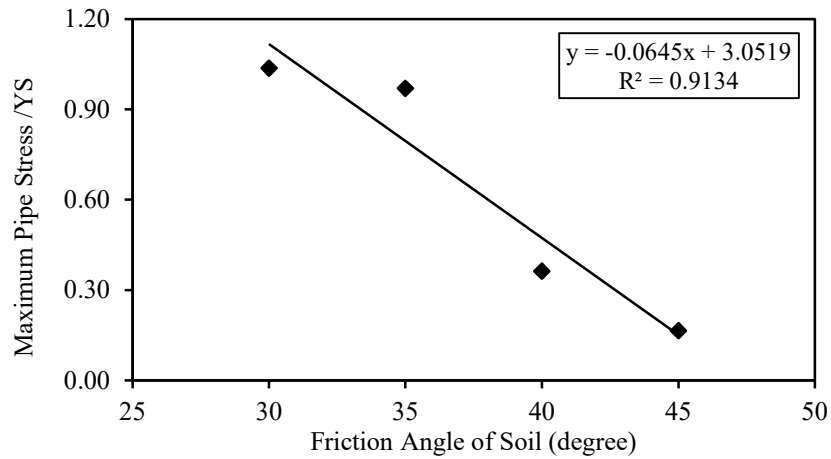


Figure 4-36: Effect of friction angle of soil on seismic response (stress) of pipe

The maximum pipe stress is normalized by yield strength of pipe (YS). It is obvious from Fig. 4-36 that the pipe stress decreases while the friction angle of the soil increases for the same reason as discussed earlier. It is clearly observed that the maximum stress was found for the friction angle of soil of 30° and gradually reduced for the friction angle of soil of 45°. All cases in the following graph showing stress on the pipeline are less than the yield stress of the ductile iron pipe (350 MPa) except the pipe stress for the friction angle of the soil of 30° due to the nature and intensity of the applied loads.

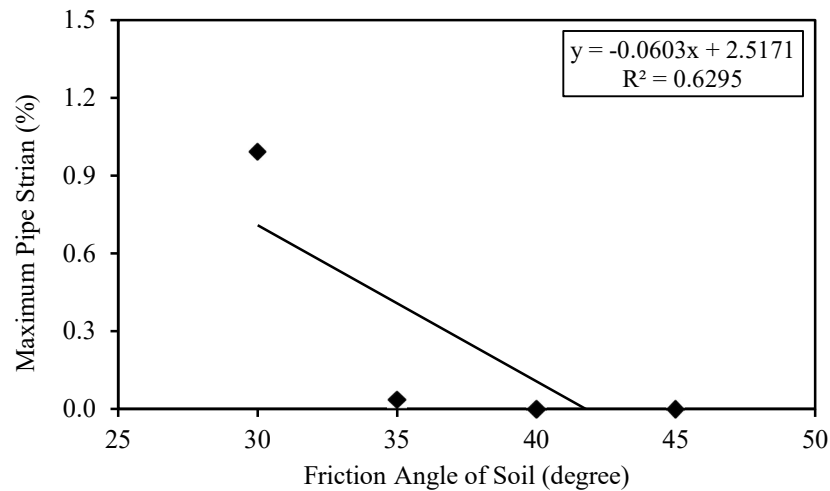


Figure 4-37: Effect of friction angle of soil on the seismic response (strain) of pipe

Figure 4-37 illustrates that the pipe strain follows a descending trend due to an increase in the friction angle of the soil. From Fig. 4-37, the maximum pipe strain was observed

at 1% for 30° and no considerable pipe strain was observed for 40° and 45°. All of the strains are significantly less than the minimum elongation (10%) of the pipe after fracture.

The maximum displacement, stress and strain developed in the pipe decreased by up to 59.2%, 84% and 100% respectively, due to an increase in the friction angle (from 30° to 45° by 1.5 times) of the soil.

Figure 4-31 and 4-33 show the displacement and stress contours of a ductile iron pipe caused by variations in friction angle of soil. In all cases, the maximum displacement was noticed in the crest line of the pipe. The maximum stress was observed in the crest line of the pipe with a friction angle of soil of 30° and 35°, respectively. In contrast, the significant stress was found in the left and right spring line of pipe for friction angle of soil of 40° and 45°, respectively.

Hence, it can be said that, higher density and friction angle of soil may be recommended for the structural safety of pipe.

4.3.7 Effect of Soil Stiffness

The type and properties of the soil around the pipe are a very effective parameter because the greater soil stiffness (E) around the pipe, the less soil movement around the pipe and, hence, its earthquake resistance is greater. This is because the void between the soil particles is reduced due to its compaction.

To evaluate the effect of the modulus of elasticity of soil on the seismic response of the pipe, 4 dynamic analyses, consisting of 4 different moduli of elasticity (19, 24, 48, and 96 MPa), for a pipe of 1048 mm in outer diameter, 15 mm in thickness with roller support at both pipe ends and a burial depth of 2D m depth, have been performed. The rigidity ratio indicates the ratio between the E of the pipe and the E of the soil. The rigidity ratio is inversely proportional to the soil E.

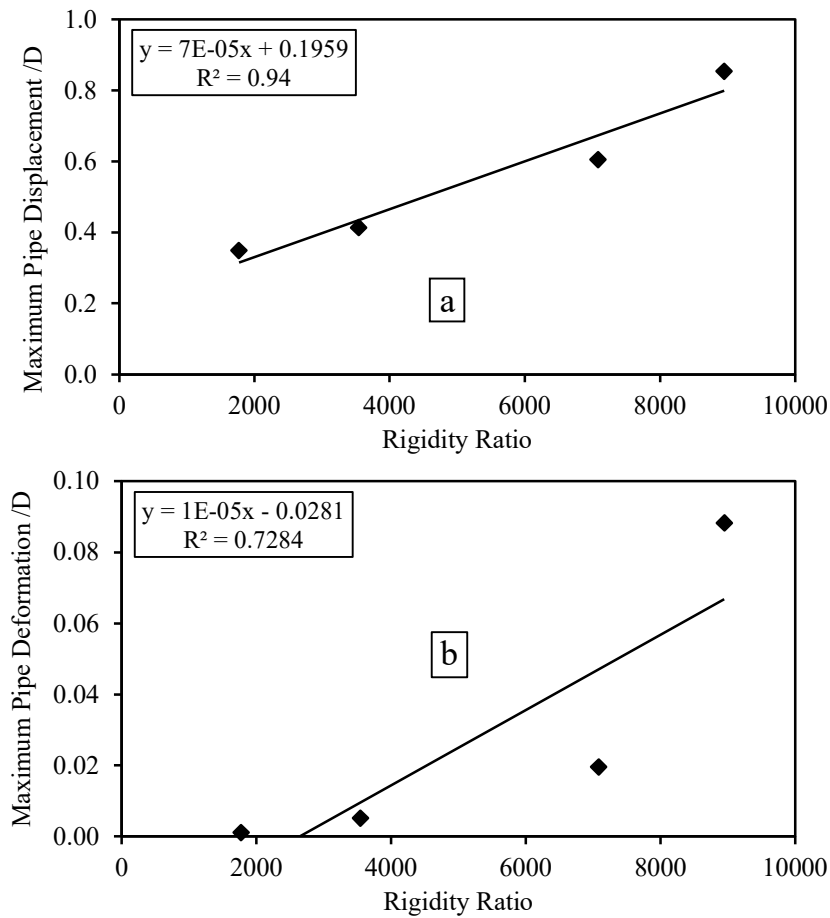


Figure 4-38: Effect of modulus of elasticity of soil on seismic response of pipe (a) total displacement (b) net deformation

The maximum pipe displacement and deformation are normalized by pipe diameter (D). Figure 4-38 (a) highlights that the pipe displacement follows an ascending trend with an increase in the rigidity ratio. The maximum and minimum pipe displacements were found for E to be 19 MPa and 96 MPa, respectively. One reason for this could be the degree of denseness of the soil. If the degree of denseness of the soil is increased by increasing the modulus of elasticity of the soil, the corresponding pipe displacement will also be reduced. Similarly, from Fig. 4-38 (b), it is clearly noticed that a higher and lower value of pipe deformation were found for E of 19 MPa and 96 MPa, respectively. Increasing the modulus of elasticity of the soil surrounding a buried pipe can decrease the displacement of pipe because a higher modulus of elasticity indicates that the soil is stiffer and more resistant to deformation. This increased soil stiffness provides better support for the pipe, reducing its tendency to deform or displace under external loads.

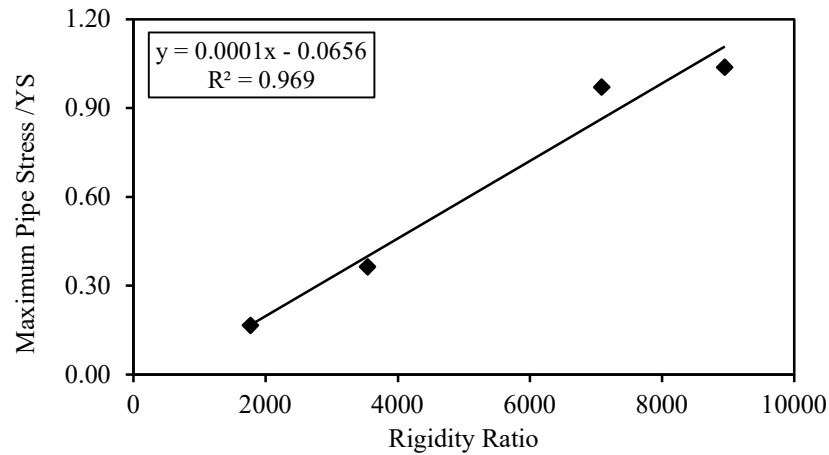


Figure 4-39: Effect of modulus of elasticity of soil on seismic response (stress) of pipe

The maximum pipe stress is normalized by yield strength of pipe (YS). From Fig. 4-39, it is noticed that the stress developed in the pipe was significantly increased due to an increase in the rigidity ratio, for the same reason. All the stress values of the pipe were below the yield stress (350 MPa) of ductile iron pipe except the stress magnitude for the modulus of elasticity of the soil at 19 MPa, due to the nature and intensity of external loads. Additionally, a stiffer soil distributes the external loads more evenly across the surface of pipe, reducing the stress and strain on the pipe.

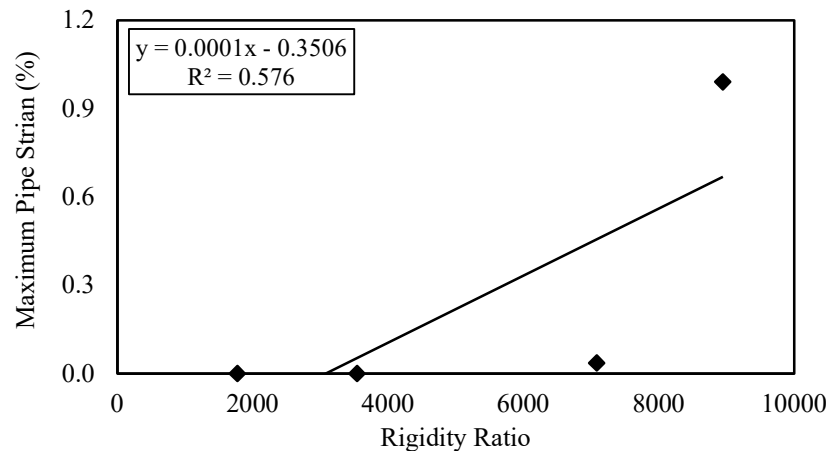


Figure 4-40: Effect of modulus of elasticity of soil on seismic response (strain) of pipe

An analysis of Fig. 4-40 illustrates that by increasing the rigidity ratio, the pipe strain increases. As shown in this graph, for an E of 19 MPa, the pipe strain was 1 %, whereas for other cases, it was almost null. A notable fact is that the total amount of plastic strain

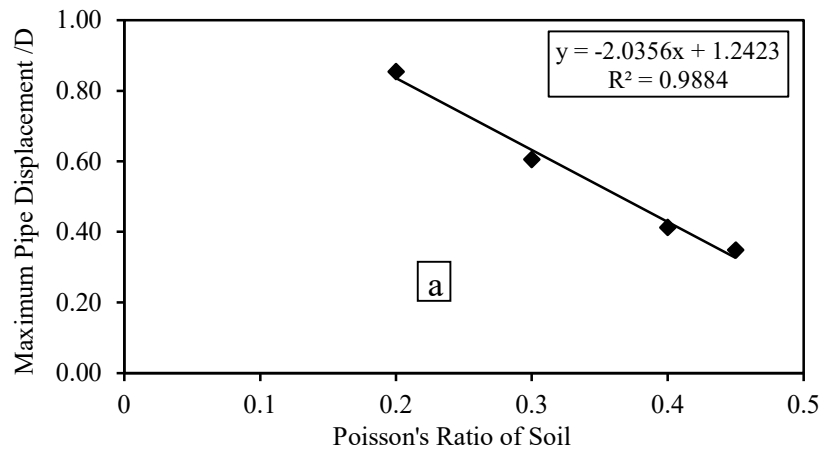
discovered in the pipe is significantly less than the minimum elongation of pipe after fracture (10%).

The maximum displacement, stress and strain developed in the pipe decreased by up to 59.2%, 84% and 100% respectively, due to an increase in the modulus of elasticity (from 19 to 96 MPa by ~5 times) of soil.

Figure 4-31 and 4-33 show the displacement and stress contours of a ductile iron pipe caused by variations in modulus of elasticity of soil. In all cases, the maximum displacement (red color band) was noticed in the crest line of the pipe. The maximum stress (red color band) was observed in the crest line of the pipe with a modulus of elasticity of soil of 19 MPa and 24 MPa, respectively. In contrast, the significant stress (red color band) was found in the left and right spring line of pipe for modulus of elasticity of soil of 48 MPa and 96 MPa, respectively.

4.3.8 Effect of the Poisson's Ratio of Soil

Since the material non-linearity of soil was considered in this study, Poisson's ratio of soil may be an important parameter for analysis. To determine the effect of Poisson's ratio of soil on the seismic response of the pipe, four dynamic analyses with 4 different Poisson's ratios of soil (0.2, 0.3, 0.4, and 0.45) were performed for a pipe with an outer diameter of 1048 mm, a thickness of 15 mm, roller support at both pipe ends, and a burial depth of 2D.



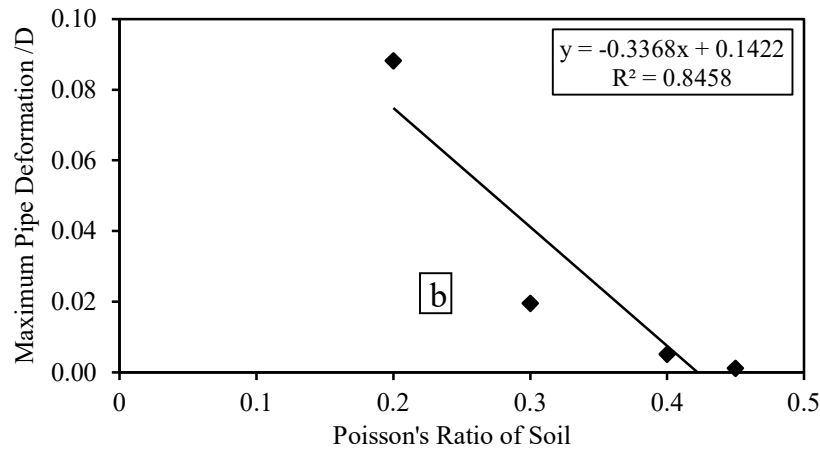


Figure 4-41: Effect of Poisson's Ratio of soil on seismic response of pipe (a) total displacement, (b) net deformation

The maximum pipe displacement and deformation are normalized by pipe diameter (D). An analysis of Fig. 4-41 (a) illustrates that the pipe displacement becomes lower when the Poisson's ratio of soil increases. As the Poisson's Ratio of the soil increases, the porosity in the soil continuum decreases, resulting in less influence of the surrounding soil on the pipe, resulting in a decrease in pipe displacement and deformation as well. Analyzing Fig. 4-41 (b), it is found that the maximum pipe deformation was found for a Poisson's ratio of 0.2, which gradually reduces up to a Poisson's ratio of 0.45.

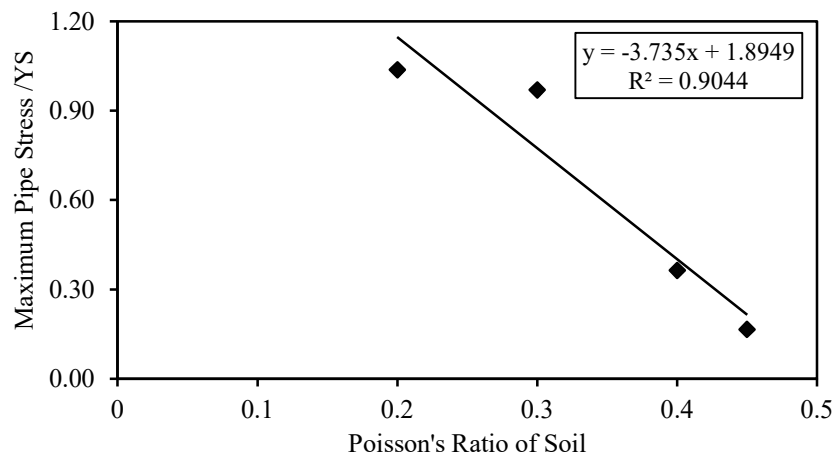


Figure 4-42: Effect of Poisson's Ratio of soil on seismic response (stress) of pipe

The maximum pipe stress is normalized by yield strength of pipe (YS). From Fig. 4-42, it was found that by increasing the Poisson's Ratio of the soil, the pipe stress decreases for the same reason. Most interestingly, in each case, the stresses developed in the pipe

did not cross the yield limit (350 MPa) of the pipe, except for the pipe stress due to the Poisson's Ratio of soil of 0.2.

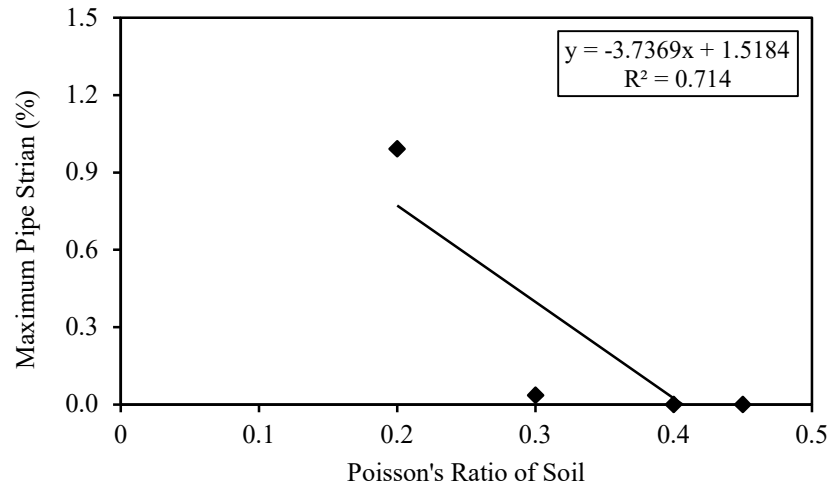


Figure 4-43: Effect of Poisson's Ratio of soil on seismic response (strain) of pipe

From Fig. 4-43, it is quite clear that the magnitude of strain on pipelines decreases with an increase in Poisson's ratio of soil due to a decrease in porosity in the soil. Furthermore, the results show that the maximum pipe strain occurs at a Poisson's ratio of soil of 0.2 to 1%, and no considerable pipe strain occurs for other Poisson's ratios of soil. A higher Poisson's ratio indicates that the soil is more resistant to lateral deformation, resulting in lower induced strains on the pipe. An important point to note is that the developed plastic strain in the pipe is within the minimum elongation limit (10%) of the pipe.

The maximum displacement, stress and strain developed in the pipe decreased by up to 59.2%, 84% and 100% respectively, due to an increase in the Poisson's ratio (from 0.2 to 0.45 by 2.25 times) of soil.

Figure 4-31 and 4-33 show the displacement and stress contours of a ductile iron pipe caused by variations in Poisson's ratio of soil. In all cases, the maximum displacement (red color band) was noticed in the crest line of the pipe. The maximum stress (red color band) was observed in the crest line of the pipe with a Poisson's ratio of soil of 0.2 and 0.3, respectively. In contrast, the significant stress (red color band) was found in the left and right spring line of pipe for Poisson's ratio of soil of 0.4 and 0.45, respectively. Therefore, an increase in the Poisson's ratio of the soil can improve the seismic response of a buried pipe and increase its stability.

4.3.9 Effect of Interface Friction Co-efficient

To explore the impact of interface friction co-efficient (μ) on pipeline seismic response, 3 analyses on pipe with a diameter of 1048 mm, thickness of 15 mm and burial depth of 2D have been performed.

The sensitiveness of the pipe capacity to adjust the interface friction ratio was examined by a variation of the interface friction ratio of 0.5, 0.7, and 0.9, covering a range of 0.5 to 1 of interface friction co-efficient [Leeuw (2022); Somboonyanon (2016)].

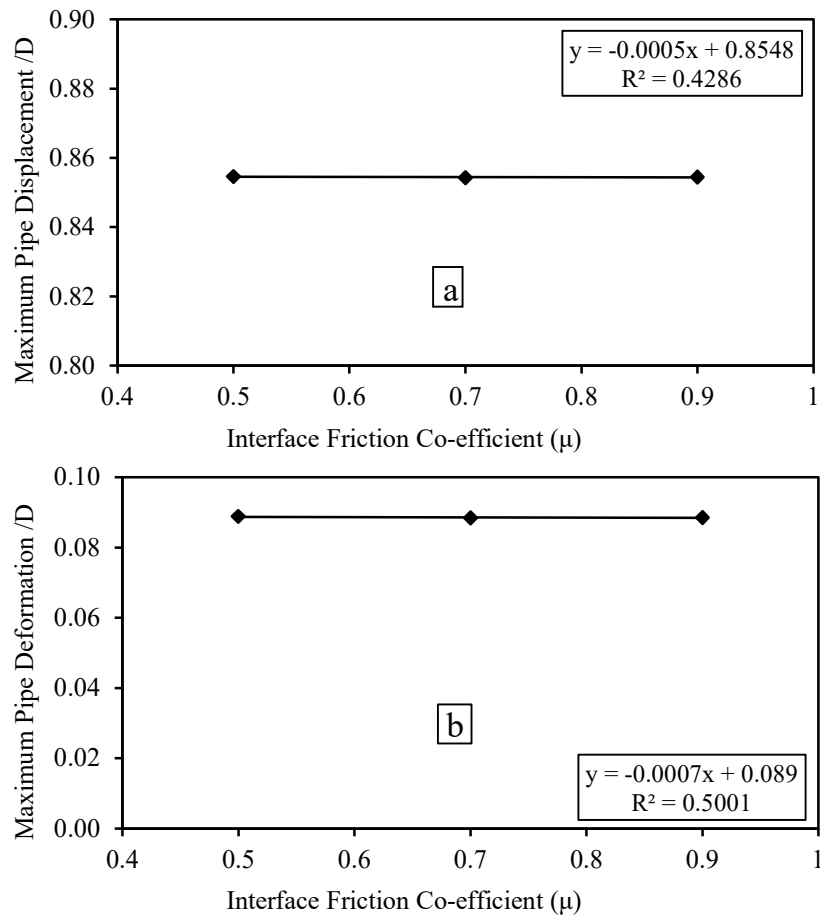


Figure 4-44: Effect of interface friction co-efficient (μ) on the seismic response of pipe: (a) total displacement (b) net deformation

The maximum pipe displacement and deformation are normalized by pipe diameter (D). It is illustrated in Fig. 4-44 that the variation of interface friction co-efficient shows negligible effect on the maximum pipe displacement and deformation as well. Though a slight decreasing trend is observed in the pipe displacement and deformation due to an increase in μ .

A higher interface friction coefficient (μ) means that the pipe is more firmly anchored in the soil, and this can reduce the likelihood of the pipe experiencing excessive displacement or deformation during seismic events. The frictional forces at the pipe-soil interface can resist the lateral movement of the pipe, reducing the induced strains and stresses. As a result, a higher interface friction coefficient can lead to a more stable and less vulnerable buried pipe system during seismic events.

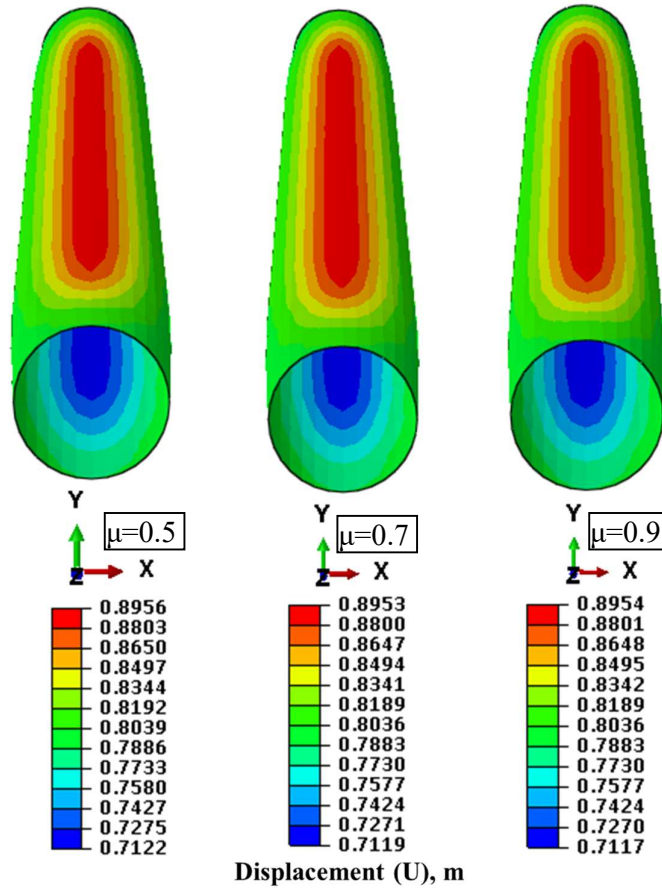


Figure 4-45: Displacement contour of the ductile iron pipe for different interface friction co-efficient ($\mu = 0.5$ to 0.9)

Figure 4-45 highlights the pipe displacement contour due to variations in the interface friction co-efficient. In all cases, the maximum (red color band) pipe displacement was found in the crest line of the pipe.

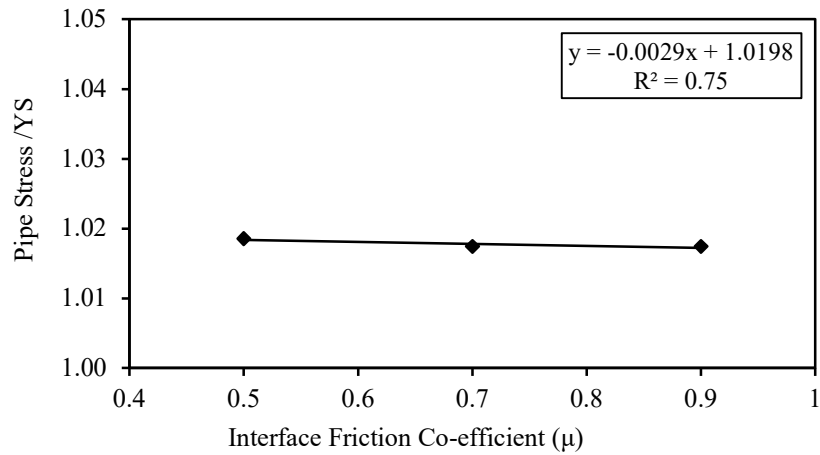


Figure 4-46: Effect of interface friction co-efficient (μ) on the seismic response (stress) of pipe

The maximum pipe stress is normalized by yield strength of pipe (YS). From Fig. 4-46, it is noticed that the change in interface friction co-efficient shows very little variation in the pipe stress as observed earlier in the displacement case. From Fig. 4-46, maximum and minimum pipe stresses were observed for a μ of 0.5 and 0.9, respectively. It was noticed that all the pipe stress values were above the yield limit (350 MPa) of the pipe due to the nature and intensity of the external loads.

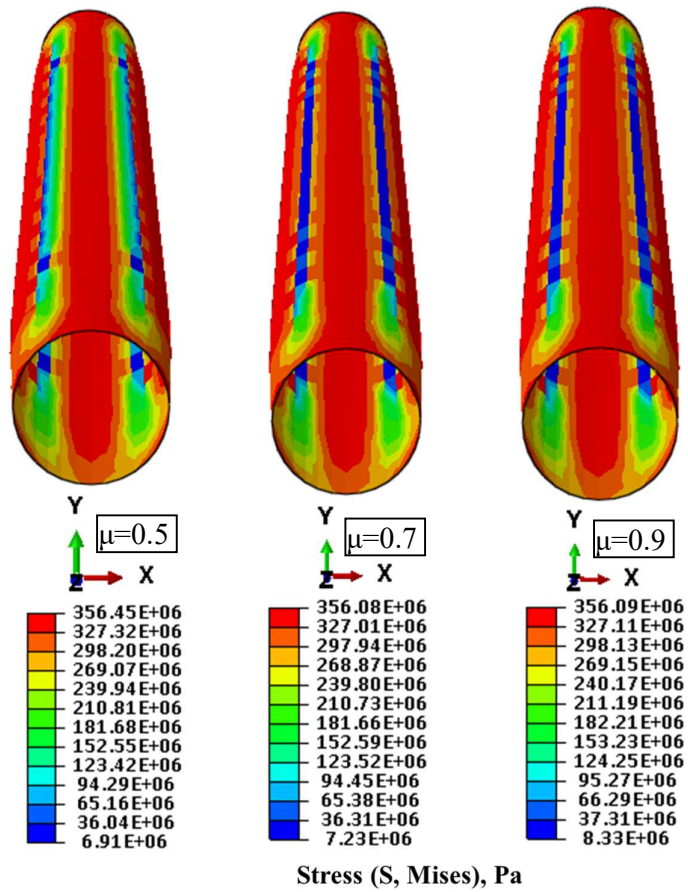


Figure 4-47: Stress contour of the ductile iron pipe for different interface friction coefficient ($\mu = 0.5$ to 0.9)

Figure 4-47 highlights the pipe stress contour due to variations in the interface friction coefficient. In all cases, the maximum pipe stress (red color band) was found in the crest line of the pipe. Also, the significant stress intensity (red color band) was also observed at the invert, left and right spring lines of the pipe.

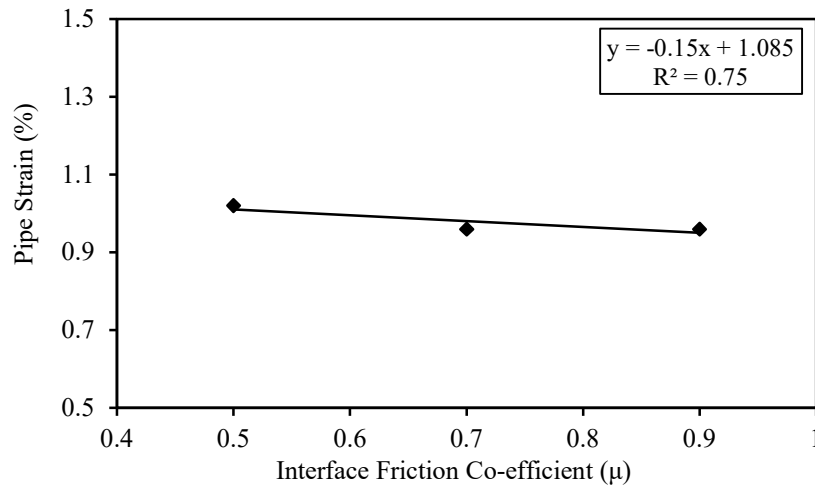


Figure 4-48: Effect of interface friction co-efficient (μ) on the seismic response (strain) of pipe

From Fig. 4-48, it was found that the plastic strain curve of the pipe follows the same trend as for displacement or stress response. The maximum strain was at 1.02 % for $\mu=0.5$ and the minimum strain was at 0.96% for $\mu=0.9$. It can be said that the observed plastic strain values of the pipe are sufficiently lower than the minimum elongation (10%) of the pipe.

When considering the soil-pipe interaction, the magnitude of maximum displacement, stress, and strain on the pipe decreases by 0.03%, 0.11%, and 5.9 %, respectively, as interface friction between the soil and the pipe increases via an interface friction co-efficient or ratio from 0.5 to 0.9 by up to 1.8 times.

Therefore, a proper assessment of the interface friction coefficient is necessary to ensure the stability and safety of buried pipes during seismic events.

4.4 Summary

A sensitivity analysis was conducted to investigate the effects of internal water pressure, traffic load, buried depth of pipe, diameter and wall thickness of pipe, pipe end boundary conditions and soil types with different density, modulus of elasticity, friction angle, Poisson's ratio; interface friction co-efficient, diameter to thickness ratio (D/t) of pipe, embedment ratio (h/D), unidirectional seismic excitations (vertical component) on the seismic behavior of Ductile Iron pipelines subjected to traffic load, water pressure and the El Centro seismic record. The FEM was used for all the analyses in this research work. The results were provided herewith in the form of spatial displacement,

von mises stress, plastic strain etc. of the pipe due to seismic time history. The results reveal that buried depth, seismic excitations, water pressure, soil types, pipe end support condition, soil-pipe interface friction and traffic loads play a significant role in the pipe response. The interesting findings of this research are that higher density, modulus of elasticity, friction angle, Poisson's ratio of soil; full flow condition; higher diameter, higher wall thickness of pipe; higher buried depth of pipe is recommended for the structural safety of pipe. Also, soil-pipe interaction, seismic excitations, traffic load, and pipe end restraints may be a crucial factor in the response analysis of pipes. The outcomes of this study may be utilized to build performance-based design techniques for underground pipelines.

Chapter 5. CONCLUSION AND RECOMMENDATION

5.1 General Overview

In this study, the seismic response of the Ductile Iron pipe used for water supply system was investigated. 3D Finite element analyses considering soil-pipe interaction were carried out using Abaqus Program (version 6.14) to study the effects of some influential parameters on the pipe response. A sensitivity analysis is performed to examine the effects of internal pressure, traffic load, buried depth of pipe, diameter and wall thickness of pipe, pipe end boundary conditions and soil type with different density, modulus of elasticity, friction angle, Poisson's ratio etc., interface friction co-efficient, D/t ratio, h/D ratio, unidirectional seismic excitation and discussed to achieve a better comprehension of the seismic behavior of pipelines under seismic loads. Load-controlled analyses were carried out to determine the ultimate capacity of the pipe under seismic load. The outcomes are in the form of spatial vertical displacement and deformation, von Mises stress, plastic strain, etc. of the pipe subjected to the acceleration time history of the EL Centro seismic record. The results reveal that buried depth, seismic excitation, water pressure, soil types, pipe end support condition, soil-pipe interface friction and traffic loads are important determinants of the pipe response.

5.2 Conclusions

- 1) Seismic excitation plays a vital role in the pipe response.
- 2) The maximum pipe response due to seismic excitations was noticed at the crest line of the pipe.
- 3) When the distinct changes between the four monitor lines of pipe during an earthquake are compared, the pipeline is deformed starting from the top crest position (crest line), moving on to the two sides of the pipeline (left and right spring line) and then moves to the bottom invert position (invert line), and finally, the circular cross section of the pipe forms an oval shape.
- 4) The maximum pipe response (displacement, stress) due to seismic excitations was noticed at the mid span along the crest line of the pipe in all cases compared

to the pipe ends, which may be caused by the direction of seismic excitation and the type of boundary conditions assigned to the pipe end.

- 5) Roller support can simulate the infinite-length effect of pipelines whereas Hinge and fixed support can simulate the finite-length effect of pipelines.
- 6) The maximum displacement, stress and strain developed in the pipe decreased by up to 59.2%, 84% and 100% respectively, due to an increase in soil density (from 1700 to 2160 kg/m³ by 1.27 times), the modulus of elasticity (from 19 to 96 MPa by ~5 times) of soil, the Poisson's ratio (from 0.2 to 0.45 by 2.25 times) of soil and the friction angle (from 30° to 45° by 1.5 times) of the soil.
- 7) The maximum displacement and stress magnitude generated in the pipe increases by up to 2.87 % and 34.9 % respectively for hinge support; also, it increases by up to 2.83 % and 34.9 % respectively for fixed support with respect to roller support. The observed plastic strain in the pipe was 90.1% lower (roller); 53.1 % higher (hinge); 45.9 % higher (fixed) than the minimum elongation (10%) of DI pipe.
- 8) The greatest displacement and stress values occurred in the pipe considering the traffic load (1100 kPa) on the soil significantly increased by 135.7% and dramatically increased by (1326 %) respectively compared to the no traffic load case. The observed plastic strain in the pipe due to traffic load was 90 % lower than the minimum elongation (10%) of DI pipe.
- 9) The maximum displacement and stress magnitude developed in the pipe decreases by 1.2 % and 0.29 % respectively for full water flow condition (flow through full circular cross-section); also, it increases by 0.22 % and decreases by 0.28 % respectively for half water flow condition (flow through lower half of circular cross-section) with respect to no water flow in the pipe. The observed plastic strain in the pipe was 89.9 % lower (full flow); 89.8% lower (half flow); 88.4 % higher (no flow) than the minimum elongation (10%) of pipe.
- 10) When considering the soil-pipe interaction, the magnitude of maximum displacement, stress, and strain on the pipe increases by 0.03%, 0.11%, and 5.9 %, respectively, as interface friction between the soil and the pipe increases via an interface friction co-efficient or ratio from 0.5 to 0.9 by up to 1.8 times.
- 11) The increase in embedment ratio (h/D) from 1 to 5 by up to 5 times, decreases pipe displacement, stress and strain by 28.7 %, 1.3 % and 23.2 % respectively.

- 12) The increase in pipe diameter to wall thickness ratio (D/t) from 65 to 74 by up to 1.14 times, reduces pipe displacement, stress and strain by 3.23 %, 0.62 % and 25 % respectively.
- 13) The maximum response of pipe at the burial depth of 1D to 2D of the pipelines was discovered. So, it might be more beneficial from the design point of view to prevent the burial depth of pipe equal to 1D to 2D.
- 14) Soil property, seismic excitations, traffic load, buried depth, pipe end restraints are the sensitive parameters than others.
- 15) Higher density, modulus of elasticity, friction angle, Poisson's ratio of soil; higher diameter, wall thickness of pipe; higher buried depth of pipe is recommended for the structural safety of pipe.
- 16) Soil-pipe interaction, seismic excitations, traffic load, and pipe end restraints should be considered carefully for the response analysis of pipes.

5.3 Mitigation Measures Against Seismic Actions

There are several strategies that can be used to reduce seismic damage to pipelines. The simplest and most apparent measure is to modify pipeline alignment (pipeline re-routing) to preclude geo-hazardous zones. This may not be achievable in certain circumstances, however; other mitigating steps should thus be taken (Karamanos et al., 2014). More specifically:

- The increasing diameter and wall thickness of the pipeline enhances the robustness of the pipeline against seismic actions.
- The usage of a superior grade of pipe material with optimized ductility of high-strength steel enhances the strength of the pipeline.
- The designer may consider isolating the pipeline from ground movements in regions where considerable permanent ground-induced activity is predicted.
- Higher density, modulus of elasticity, friction angle, Poisson's ratio of soil; higher diameter, wall thickness of pipe; higher buried depth of pipe may be recommended for the structural safety of pipe.
- Soil-pipe interaction, seismic excitations, traffic load, and pipe end restraints should be considered carefully for the response analysis of pipes.

- In regions of landslides, ground conditions can be improved before the pipe installation and the quantity of soil movement is reduced.
- The application of flexible joints, which may be adaptable at suitable places for expansion/contraction or rotation, can be helpful for the pipeline, therefore minimizing the stress or strains caused, particularly axial tension.
- Avoid the short depth of burial when installing pipeline to decrease the vulnerability of geometric failure of the pipes due to the PGD produced by a strong earthquake.
- The effect of earthquake induced PGD may also be reduced by installing very strong containment around pipes and taking into consideration the flexible kind of pipe material rather than rigid one.
- Pipeline positioning should be away from active faults, steep slopes, and soft ground.
- Improve the pipe flexibility using more ductile and flexible joints.
- Ensuring "fail-safe approach" systems at the areas where the seismic damages may be predicted.

5.4 Limitations of the Current Study

For this research work, the following limitations were identified:

- There are no investigations into soil material parameters and how they are determined; the material parameters are already known.
- Other soils besides sand are not considered
- Only a finite element approach and solid elements are considered in the modeling of the soil as a continuum.
- Only El Centro seismic record was considered. The Parametric study was done by the vertical component of El Centro earthquake only.
- Only dry sandy soil and Ductile iron pipe was used in the simulation.
- Mohr-Coulomb model, a simple and straightforward model was used for modelling the soil.

5.5 Scope for Further Research

While a certain number of issues were identified in this investigation, several concerns arise. For future study, it may be interesting to identify new advance analysis techniques to demonstrate the pipe failure. The failure mechanisms derived from the results of the

finite element analysis reported in this thesis could be indicative of future study. Furthermore, it might be another burning issue for future research to address this influence of seismic load on saturated or partially saturated sandy soil, clay soil and silty soil on pipeline capacity. The effects of different types of pipe material and fluids (gas, oil, sewage etc.) inside the pipe should be considered in the buried pipe seismic analysis. Advanced soil models that are currently available should be used to efficiently model the soil. Also, multidirectional seismic excitations with more prescribed earthquakes should be considered in the analysis to replicate the real scenario.

However, in these specific lifeline systems, a lot of work still must be done. A substantial shortage of field data appears to be one of the greatest obstacles in characterizing the input signal. The formation of a dense strong motion network might probably solve this critical deficit. A minimal number of experimental and field studies for underground pipelines in seismic events is another important shortcoming in this domain. In this regard, the sensitivity of the potential parameters derived from the results of the finite element analysis reported in this thesis could be indicative of future study.

REFERENCES

- Abaqus. (2014). Documentation, Abaqus 6.14. Software Manual, Dassault Systèmes.
- Abuhajar, O., El Naggar, H., Newson, T. (2015a). Experimental and numerical investigations of the effect of buried box culverts on earthquake excitation. *Soil Dyn. Earthquake Eng.*, 79, 130–148.
- Abuhajar, O., El Naggar, H., Newson, T. (2015b). Seismic soil–culvert interaction. *Can. Geotech. J.*, 52(11), 1649–1667.
- Alamatian, E., Ghadamkheir, M., & Karimpour, B. (2013). Stress Estimation on Pipeline and Effect of Burying Depth, *International Research Journal of Applied and Basic Sciences*, Vol, 6 (2): 228-235.
- Ariman, T., & Muleski, G. E. (1981). A review of the response of buried pipelines under seismic excitations. *Earthquake Engineering & Structural Dynamics*, 9(2), 133-152.
- Argyrou, C., O'Rourke, T.D., Stewart, H.E., & Wham, B. P. (2019). Large-scale fault rupture tests on pipelines reinforced with cured-in-place linings. *J. Geotech. Geoenviron. Eng.*, 145(3). [https://doi.org/10.1061/\(ASCE\)GT.1943-5606.0002018](https://doi.org/10.1061/(ASCE)GT.1943-5606.0002018).
- Bardet, J. P. and Davis, C. A. (1997). Seismic analysis of flexible buried structures. IN Pedro, S. S. (Ed.) *Seismic Behaviour of Ground and Geotechnical Structures*. Rotterdam, A.A. Balkema.
- Bolvardi, V. and Bakhshi, A. (2010). A study on seismic behavior of buried steel pipelines crossing active faults. *Proceedings of Pipelines 2010: Climbing New Peaks to Infrastructure Reliability: Renew, Rehab, and Reinvest*, 1–12.
- Boorboor, A., & Hosseini, M. (2015). Sensitivity Analysis of Buried Jointed Pipelines Subjected to Earthquake Waves. *Open Journal of Earthquake Research*, 4(02), 74–84.
- Bower, A. F. (2010). *Applied Mechanics of Solids*. Portland, Oregon, United States.
- BSI. (2010). Guide to the structural design of buried pipelines. In CEN (Ed. BS 9295:2010. London, BSI).
- BSI. (2006). Steel, concrete and composite bridges - Part 2: Specification for loads. In IN CEN (Ed. BS 5400-2:2006. London, BSI.
- Chaudhuri, C. H. & Choudhury, D. (2019). Behaviour of buried pipelines subjected to seismic excitations: a state- of-the-art review. 7th Indian Young Geotechnical Engineers Conference – 7IYGEC 2019, March, 1–6.
- Chaudhari, V., Kumar Pasupuleti, V. D., & Ramancharla P. K. (2013). Finite element

- analysis of buried continuous pipeline subjected to fault motion. *International Journal of Structural Engineering*, 4(4), 314–331.
- Cheong, T. P., Soga, K., & Robert, D. J. (2011). 3D FE analyses of buried pipeline with elbows subjected to lateral loading. *Journal of geotechnical and geoenvironmental engineering*, 137(10), 939-948.
- Chi, W. C., Dreger, D., & Kaverina, A. (2001). Finite-source modeling of the 1999 Taiwan (Chi-Chi) earthquake derived from a dense strong-motion network. *Bulletin of the Seismological Society of America*, 91(5), 1144-1157.
- Chowdhury, I., & Dasgupta, S. P. (2003). Computation of Rayleigh damping coefficients for large systems. *The Electronic Journal of Geotechnical Engineering*, 8(0), 1-11.
- Corrado, V., D'Acunto, B., Fontana, N., & Giugni, M. (2009). Estimation of dynamic strains in finite end-constrained pipes in seismic areas. *Mathematical and Computer Modelling*, 49(3-4), 789-797.
- Dama E., Karamanos, S. A., and Gresnigt, A. M. (2007). Failure of Locally Buckled Pipelines. *J. Pressure Vessel Technology*, ASME, 129(2), 272–279.
- Datta, T. K. (1999). Seismic response of buried pipelines: a state-of-the-art review. *Nuclear engineering and design*, 192(2-3), 271-284.
- Davies, J. P., Clarke, B. A., Whiter, J. T., & Cunningham, R. J. (2001). Factors influencing the structural deterioration and collapse of rigid sewer pipes. *Urban water*, 3(1-2), 73-89.
- Dowding, C.H., Rozen, A. (1978). Damage to rock tunnels from earthquake shaking. *J. Geotech. Eng. Div., ASCE* 104 GT2, 175–191.
- Dwivedi J. P., Singh V. P. and Lal R. K. (2010). Dynamic Analysis of Buried Pipelines under Linear Viscoelastic Soil Condition. *Advances in Theoretical and Applied Mechanics*, 3(12), 551–558.
- EERI, (1995). The Northridge, California Earthquake of 17 January, 1994. EERI Special Earthquake Report.
- EERI. (1999). The Chi Chi, Taiwan Earthquake of September 21, 1999. (EERI), Earthquake Engineering Research Institute. EERI Special Earthquake Report.
- EERI, S. Maule (2010). The Mw 8.8 Chile Earthquake of February 27, 2010. Special Earthquake Report. Earthquake Engineering Research Institute (EERI), Oakland, California.
- Fabozzi, S., Bilotta, E. (2016). Behaviour of a segmental tunnel lining under seismic

- actions. *Procedia Eng.*, 158, 230–235.
- Gautam S. Nair; Suresh R. Dash; and Goutam Mondal (2018). Review of Pipeline Performance during Earthquakes since 1906. *Journal of Performance of Constructed Facilities*, 32(6), (1-18). DOI: 10.1061/(ASCE)CF.1943-5509.0001214.
- Georges, M.K. and Shephard, M. S. (1990). Automatic mesh generator for use in two dimensional h-p analysis. *The Journal of Computing in Civil Engineering*, J. (Ed.) *Advances' In Underground Pipeline Engineering*. New York, American Society of Civil Engineer, 4(3), 199–220.
- Gresnigt, A. M. and Karamanos, S. A. (2009). Local Buckling Strength and Deformation Capacity of Pipes. 19th International Offshore and Polar Engineering Conference, Osaka, Japan, 212–223.
- Gresnigt, A. M. (1986). Plastic Design of Buried Steel Pipes in Settlement Areas. *Heron*, 31(4), 11–13.
- Guo, P., and Stolle, D. F. (2005). Lateral pipe–soil interaction in sand with reference to scale effect. *Journal of Geotechnical and Geoenvironmental Engineering*, 131(3), 338–349. [https://doi.org/10.1061/\(ASCE\)1090-0241\(2005\)131:3\(338\)](https://doi.org/10.1061/(ASCE)1090-0241(2005)131:3(338)).
- Hashash, Y. M. A., Hook, J. J., Schmidt, B., and I-Chiang Yao, J. (2001). Seismic design and analysis of underground structures. *Tunnelling and Underground Space Technology*, 16(4), 247–293. [https://doi.org/10.1016/S0886-7798\(01\)00051-7](https://doi.org/10.1016/S0886-7798(01)00051-7).
- Hassani, R., and Basirat, R. (2019). A 3D numerical modeling of polyethylene buried pipes affected by fault movement. *Engineering Science and Technology, an International Journal*, 22(2), 482–488. <https://doi.org/10.1016/j.jestch.2018.12.004>.
- Hellgren, J. and Lundberg, L. (2011). Finite Element Modelling of Local Interlaminar Slip in Stress-Laminated-Timber Bridges. Chalmers University of Technology, Göteborg.
- Hongjing L., Liu J. and Baohua Y. (2008). Response analysis of buried pipelines due to Large ground movements. In 13th World Conference on Earthquake Engineering, (WCEE), Beijing China. October, 12-17.
- Hosseini, S. and Tafreshi, S. M. (2002). Soil-structure interaction of buried pipes under cyclic loading conditions. *International Journal of Engineering (Transaction B: Applications)*, 15(2), 114–124.
- Hosseiny, S. O., M. M. J. and M. Vaghefi (2014). Soil Structure Interaction Effects on the Seismic Behavior of Buried Pipeline. *International Journal of Current Life*

- Sciences, 4(8), 4535–4543.
- JSCE. (1999). The 1999 Kocaeli Earthquake, Turkey- Investigation into the damage to civil engineering structures. Japan Society of Civil Engineers (JSCE); JSCE Earthquake Engineering Committee.
- Karamanos, S. A., Keil, B., and Card, R. J. (2014). Seismic design of buried steel water pipelines. *Pipelines 2014: From Underground to the Forefront of Innovation and Sustainability - Proceedings of the Pipelines 2014 Conference*, 2006, 1005–1019. <https://doi.org/10.1061/9780784413692.091>.
- Karamitros, D. K., Bouckovalas, G. D., & Kouretzis, G. P. (2007). Stress analysis of buried steel pipelines at strike-slip fault crossings. *Soil Dynamics and Earthquake Engineering*, 27(3), 200-211.
- Katona, M. G., & Center, N. C. B. (1976). CANDE: A modern approach for the structural design and analysis of buried culverts.
- Kazemi, Parham and Saffari, Hamid, (2015), The effect of major parameters changes on seismic behavior of buried pipelines, the third international conference on civil engineering, architecture and urban planning, <https://civilica.com/doc/611196>.
- Kennedy, R. P., Williamson, R. A., & Chow, A. M. (1977). Fault movement effects on buried oil pipeline. *Transportation Engineering Journal of ASCE*, 103(5), 617-633.
- Kim DS, Kim HW, Kim. WC. (2002). Parametric study on the impact-echo method using mock-up shafts. *NDTandE Int*, 35(8), 595–608.
- Kouretzis, G.P., Bouckovalas, G.D. and Gantes, C. J. (2006). 3-D shell analysis of cylindrical underground structures under seismic shear (S) wave action. *Soil Dynamics and Earthquake Engineering*, 26(10), 909–921. <https://doi.org/10.1016/j.soildyn.2006.02.002>.
- Kubo, K. (1974). Behaviour of underground waterpipes during an earthquake. *Proc. 5th Wd Conf. Earthq. Engg* 1, 569 Rome.
- Kuhlemeyer, R.L., & Lysmer, J. (1973). Finite element method accuracy for wave propagation problems. *Journal of Soil Mechanics and Foundations Division*, 99(5), 421–427.
- Lanzano, G., De Magistris, F. S., Fabbrocino, G., and Salzano, E. (2014). Numerical modeling of natural gas buried pipelines under seismic shaking. *Numerical Methods in Geotechnical Engineering - Proceedings of the 8th European Conference on Numerical Methods in Geotechnical Engineering, NUMGE 2014*, 2, 1129–1134. <https://doi.org/10.1201/b17017-200>.

- Lee, L. N. H., Ariman, T. and Chen, C. C. (1984) 'Elastic-plastic buckling of buried pipelines by seismic excitation', *International Journal of Soil Dynamics and Earthquake Engineering*, 3(4), pp. 168173. doi: 10.1016/0261-7277(84)90032-9.
- Lee, D. H., Kim, B. H., Lee, H., & Kong, J. S. (2009). Seismic behavior of a buried gas pipeline under earthquake excitation. *Engineering Structures*, 31(5), 1011–1023.
- Lee, H. (2010). Finite element analysis of a buried pipeline 2010. University of Manchester.
- Leon, R. L. and Wang, M. (1978). Performance of underground pipelines in earthquake. In Division, A. G. E. (Ed.) *Earthquake Engineering and Soil Dynamics*. New York, American Society of Civil Engineers.
- Leeuw, L. W. D., Diambra, A., Kwon, O-S., & Sextos, A. (2022). Modulating pipe-soil interface friction to influence HPHT offshore pipeline buckling. *Ocean Engineering*, 266(2). <https://doi.org/10.1016/j.oceaneng.2022.112713>.
- Liang, J., and Sun, S. (2000). "Site Effects on Seismic Behavior of Pipelines: A Review ."ASME. J. Pressure Vessel Technol. 122(4): 469–475. <https://doi.org/10.1115/1.1285974>
- Liu, W., Miao, H., Wang, C., & Li, J. (2017). Experimental validation of a model for seismic simulation and interaction analysis of buried pipe networks. *Soil Dyn. Earthquake Eng.*, 100, 113–130.
- Liu, P. F., Zheng, J. Y., Zhang, B. J., and Shi, P. (2010). Failure analysis of natural gas buried X65 steel pipeline under deflection load using finite element method. *Materials and Design*, 31(3), 1384–1391. <https://doi.org/10.1016/j.matdes.2009.08.045>.
- Mavridis, G., & Pitilakis, K. (1996). Axial and Transverse Seismic analysis of buried Pipelines. 11th World Conferences on Earthquake Engineering (WCEE), Acapulco Mexico, 1605, 81-88.
- Meesawasdt, N., Boonyasirawat, C., Kongnuan, S., & Chamchod, F. (2016). Finite element modeling for stress analysis of a buried pipeline under soil and traffic loads. 2016 IEEE International Conference on Industrial Engineering and Engineering Management (IEEM), 385-390.
- Miyajima, N. (1976). An example of seismic design and earthquake response measurement of a buried pipeline. U.S.-Japan Seminar.
- Mukherjee, P., Nath, R. R., Khan, N. U., and Prasad, B. B. (2013). A Comparative Study of Lateral Pipe Bending Moment with Fixed Supporting Condition for

- Different Soil Types in India. *Electronic Journal of Geotechnical Engineering*, 18(G), 1279–1291.
- Narita, K. (1976). Study on Pipeline Failure due to Earthquake. In *Proceedings of the US-Japan Seminar on Earthquake Engineering* (pp. 157-176).
- Nath, P. (1994). The effect of traffic loading on buried pipes. In John, W. B. (Ed.) *Soil-Structure Interaction: Numerical Analysis and Modelling*. London, E and FN Spon.
- Newmark, N. M. (1967). Problems in wave propagation in soil and rock. *Civil Engineering Classics*, ASCE, 703–722.
- Newmark, N. M., & Hall, W. J. (1975). Pipeline design to resist large fault displacement. In *Proceedings of US national conference on earthquake engineering* (Vol. 1975, pp. 416-425).
- Ni, P., Moore, I. D., & Take, W. A. (2018). Distributed fibre optic sensing of strains on buried full-scale PVC pipelines crossing a normal fault. *Géotechnique*, 68(1), 1-17.
- Nixon, I. K. and Child, G. H. (1989). Site investigation. In BLAKE, L. S. (Ed.) *Civil Engineer's Reference Book*. 4 Ed. Oxford, Elsevier.
- Ogawa, Y., & Koike, T. (2001). Structural design of buried pipelines for severe earthquakes. *Soil Dynamics and Earthquake Engineering*, 21(3), 199-209.
- O'Rourke, M. J., & Liu, X. (1999). Response of Buried Pipelines Subject to Earthquake Effects. *Monograph Series, Multidisciplinary Center for Earthquake Engineering Research. A National Center of Excellence in Advanced Technology Applications, University at Buffalo*.
- O'Rourke, M.J. and Hmadi, K. E. (1988). Analysis of continuous buried pipelines for seismic wave effects. *Earthquake Engineering and Structural Dynamics*, 16(6), 917–929.
- O'Rourke, T., Wang, Y., Shi, P. and Jones, S. (2004). Seismic wave effects on water trunk and transmission lines. In *Proceedings of the 11th International Conference on Soil Dynamics and Earthquake Engineering and 3rd International Conference on Earthquake Geotechnical Engineering*. Berkeley, CA., 2, 420–428.
- O'Rourke, T. D., Gowdy, T. E., Stewart, H. E., Pease, J. W. (1991). Lifeline and geotechnical aspects of the 1989 Loma Prieta Earthquake. *Proc. of the Second International Conference on Recent Advances in Geotechnical Earthquake Engineering and Soil Dynamics*; Univ. of Missouri-Rolla, 1601–1612.
- O'Rourke, T.D., and McCaffrey, M. A. (1984). Buried pipeline response to permanent earthquake ground movements. In *Proceedings of the 8th World Conference on*

- Earthquake Engineering; Earthquake Engineering Research Institute (EERI), San Francisco California, U.S., 7, 215–222.
- O'Rourke, T. D., & Palmer, M. C. (1996). Earthquake performance of gas transmission pipelines. *Earthquake Spectra*, 12(3), 493-527.
- O'Rourke, M. J. (2003). Buried Pipelines. In C. S. and W.-F. Chen (Ed.), Chapter 23, *Earthquake Engineering Handbook*. CRC Press.
- O'Rourke, T. D., Jezerski, J. M., Olson, N. A., Bonneau, A. L., Palmer, M. C., Stewart, H. E., & Abdoun, T. (2008). Geotechnics of pipeline system response to earthquakes. In *Geotechnical earthquake engineering and soil dynamics IV*, 1-38.
- O'Rourke, T.D., Jung, J.K., & Argyrou, C. (2016). Underground pipeline response to earthquake-induced ground de-formation. *Soil Dynamics and Earthquake Engineering*, 91, pp.272-283.
- Oka, S. (1996). Damage of Gas Facilities by Great Hanshin Earthquake and Restoration Process. In *Proceedings of the 6th Japan-U.S. Workshop on Earthquake Resistant Design of Lifeline Facilities and Countermeasures against Soil Liquefaction*, National Center for Earthquake Engineering Research, Buffalo, NY, U.S., 111–126.
- Paolucci, R., Griffini, S., and Mariani, S. (2010). Simplified modelling of continuous buried pipelines subject to earthquake fault rupture. *Earthquakes and Structures*, 1(3), 253–267.
- Pires, Ana C. G. ; Palmeira, Ennio M. (2021). The influence of geosynthetic reinforcement on the mechanical behavior of soil-pipe systems, *Geotextiles and Geomembranes*, Volume 49, Issue 5, 2021, Pages 1117-1128, ISSN 0266-1144, <https://doi.org/10.1016/j.geotexmem.2021.03.006>.
- Popescu, R., Phillips, R., Konuk, I., Guo, P., and Nobahar, A. (2002). Pipe–soil interaction: large–scale tests and numerical modeling. In *Proceedings of the International Conference on Physical Modelling in Geotechnics (ICPMG'02)*, St. John's, N.L., A.A. Balkema Publishers, Rotterdam, the Netherlands., 917–922.
- Psyras, N. K., and Sextos, A. G. (2018). Safety of buried steel natural gas pipelines under earthquake-induced ground shaking: A review. *Soil Dynamics and Earthquake Engineering*, 106 (February 2017), 254–277. <https://doi.org/10.1016/j.soildyn.2017.12.020>.
- Rao, S. S. (1999). *The finite element method in engineering*. Boston, Butterworth-Heinemann.

- Saadeldin, R., Hu, Y., & Henni, A. (2015). Numerical analysis of buried pipes under field geo-environmental conditions. *International Journal of Geo-Engineering*, 6(1), 1-22.
- Seed, R. B., & Duncan, J. M. (1985). Earth Pressure and Surface Load Effects on Buried Pipelines. In *Advances in Underground Pipeline Engineering* (pp. 320-329). ASCE.
- Sahoo, S., Biswas, S., Manna, B. and Sharma, K. G. (2013). Dynamic Behaviour of Buried Pipelines under Seismic Condition - Finite Element Approach. *Indian Geotechnical Conference (IGC)*, Roorkee.
- Sahoo, S., Manna, B., and Sharma, K. G. (2014a). Seismic Behaviour of Buried Pipelines: 3D Finite Element Approach. *Journal of Earthquakes*, 2014(1), 1–9. <https://doi.org/10.1155/2014/818923>.
- Sahoo, S., Manna, B., and Sharma, K. G. (2014b). Seismic Behaviour of Buried Pipelines: 3D Finite Element Approach. *Journal of Earthquakes*, 2014(August), 1–9. <https://doi.org/10.1155/2014/818923>.
- Sakurai, A. and Takahashi, T. (1969). Dynamic Stresses of Underground Pipelines During Earthquakes. In *Proceedings of the Fourth World Conference on Earthquake Engineering*, Santiago, Chile, 81.
- Sarker J. K., Ansary M. A., Islam M. R., & Safiullah A.M.M. (2010). Potential losses for Sylhet, Bangladesh in a repeat of the 1918 Sri- mangal earthquake. *Environmental Economics*. 1. 12-31.
- Shaan, O. A., Salem, T. N., Eman, A., Shamy, E. I., & Mansour, R. M. (2014). Dynamic analysis of two adjacent tunnels. *International Journal of Engineering and Innovative Technology (IJEIT)*, 4(4), 145–152.
- Shi, P., O'Rourke, T. D., Wang, Y., & Fan, K. (2008). Seismic response of buried pipelines to surface wave propagation effects. *14th World Conference on Earthquake Engineering*. Beijing, China.
- Shinozuka, M., Ballantyne, D., Borchardt, R., Buckle, I., O'Rourke, T., Schiff, A. (1995). The Hanshin–Awaji earthquake of January 17, 1995: Performance of lifelines. Technical Report No. NCEER-95-0015. Buffalo, NY: State Univ. of New York at Buffalo.
- Smith, I.M. and Griffith, D.V. (1982). *Programming the Finite Element Method-Second Edition*. J. Wiley & Sons.
- Somboonyanon, P., and Halmen, C. (2018). FEM Analysis of Pipes Embedded in

- CLSM Under Seismic Wave Propagation. *ACI Structural Journal*, 115(6), 1–29.
<https://doi.org/10.14359/51706890>.
- Somboonyanon, P., & Halmen, C. (2016). 3D Finite Element Seismic Simulation of Steel Pipelines Embedded in Different Backfills. In *Pipelines 2016* (pp. 1875–1886).
- St. John, C.M., Zahrah, T. F. (1987). A seismic design of underground structures. *Tunneling Underground Space Technol.*, 2(2), 165–197.
- Sumer, B. M., Truelsen, C., & Fredsøe, J. (2006). Liquefaction around pipelines under waves. *Journal of waterway, port, coastal, and ocean engineering*, 132(4), 266–275.
- Takada, S., Katagiri, S. and Shinmi, T. (1995). Shell model response analysis of buried pipelines. American Society of Civil Engineers, New York, (United States).
- Trickey, S. A., Moore, I. D., & Balkaya, M. (2016). Parametric study of frost-induced bending moments in buried cast iron water pipes. *Tunnelling and Underground Space Technology*, 51, 291–300.
- Trott, J. J. (1984). *Buried Rigid Pipes: Structural Design of Pipelines*. Taylor & Francis.
- Tsinidis, G., Pitilakis, K., Madabhushi, G. (2016). On the dynamic response of square tunnels in sand. *Eng. Struct.*, 125, 419–437.
- Vasilikis, D., Karamanos, S. A., Van Es, S. and Gresnigt, A. M. (2014). Bending deformation capacity of large-diameter spiral-welded tubes. *Proceedings of the 10th International Pipeline Conference*, Calgary, Alberta, Canada.
- Vazouras, P., Karamanos, S.A. and Dakoulas, P. (2010). Finite element analysis of buried steel pipelines under strike-slip fault displacements. *Soil Dynamics and Earthquake Engineering*, 30(11), 1361–1376;
<https://doi.org/10.1016/j.soildyn.2010.06.011>.
- Wang, Y., O'Rourke, T. and Shi, P. (1906). Seismic wave effects on the longitudinal forces and pullout of underground lifelines. In *Proceedings of The100th Anniversary Earthquake Conference: Commemorating*, 18–22.
- Wang, L. R. L. & Raymond, C. Y. F. (1979) seismic design criteria for buried pipelines. In *Conference, A. P. D. S. (Ed.) Pipelines in adverse environments - a state of the art*. New York, American Society of Civil Engineers.
- Wang, L. R. L., & Yeh, Y. H. (1985). A refined seismic analysis and design of buried pipeline for fault movement. *Earthquake engineering & structural dynamics*, 13(1), 75–96.
- Wang Y, Shi J, N. C. (2011). Numerical modeling of tunneling effect on buried

- pipelines. *Can Geotech J*, 48(7), 1125–1137.
- Wenshui, G., & ZhongHang, H. (1988). Analysis of pipeline responses to seismic wave propagation. *Earthquake Engineering and Engineering Vibration*, 79–85.
- Wood, J. H. (2015). Earthquake design of rectangular underground structures. *NZSEE Conference 2005*, 39.
- Yang, R. and Zhang, S. (2011). Study on mechanical behaviors of buried pipelines subjected to three-dimensional earthquake input motions. *Proceedings of International Conference on Pipelines and Trenchless Technology 2011: Sustainable Solutions for Water, Sewer, Gas, and Oil Pipelines*, 1802–1809. [https://doi.org/10.1061/41202\(423\)190](https://doi.org/10.1061/41202(423)190).
- Ye, Y.X., Wei, L., Chen, D. (1982) Vibration behavior of shallowly buried pipeline. *A. Earthquake Engineering Papers. C.*, 12.
- Yimsiri, S., Soga, K., Yoshizaki, K., Dasari, G.R., and O'Rourke, T. D. (2004). Lateral and upward soil–pipeline interactions in sand for deep embedment conditions. *Journal of Geotechnical and Geoenvironmental Engineering*, 130(8), 830–842. [https://doi.org/10.1061/\(ASCE\)1090-0241\(2004\)130:8\(830\)](https://doi.org/10.1061/(ASCE)1090-0241(2004)130:8(830)).
- Yun, H., & Kyriakides, S. (1990). On the beam and shell modes of buckling of buried pipelines. *Soil Dynamics and Earthquake Engineering*, 9(4), 179-193.

Appendix A: Modal Analysis

Modal Analysis

Modal analysis of the soil-pipe system was carried out in Abaqus, a FEM Program to obtain damping coefficients to use in further simulations. Rayleigh damping is generally used to model the damping in the soil-pipe system. Rayleigh damping consists of mass and stiffness components and can mathematically be presented as (Equation A.1),

$$C = \alpha M + \beta K \quad A.1$$

where α and β are coefficients for mass and stiffness proportional damping, M is the mass matrix and K is the stiffness matrix. The coefficients α and β were evaluated from the natural frequencies of the soil-pipe system obtained separately through modal analyses in Abaqus Program.

Computation of Rayleigh Damping Coefficients

In dynamic analysis of structures and foundations damping plays an important role. The most effective way to treat damping within modal analysis framework is to treat the damping value as an equivalent Rayleigh Damping in the form of

$$[C] = \alpha [M] + \beta [K] \quad A.2$$

where, $[C]$ = damping matrix of the physical system; $[M]$ = mass matrix of the physical system; $[K]$ = stiffness matrix of the system; α and β are pre-defined constants. Figure A-1 represents the variation of natural frequency with damping ratio of a large system.

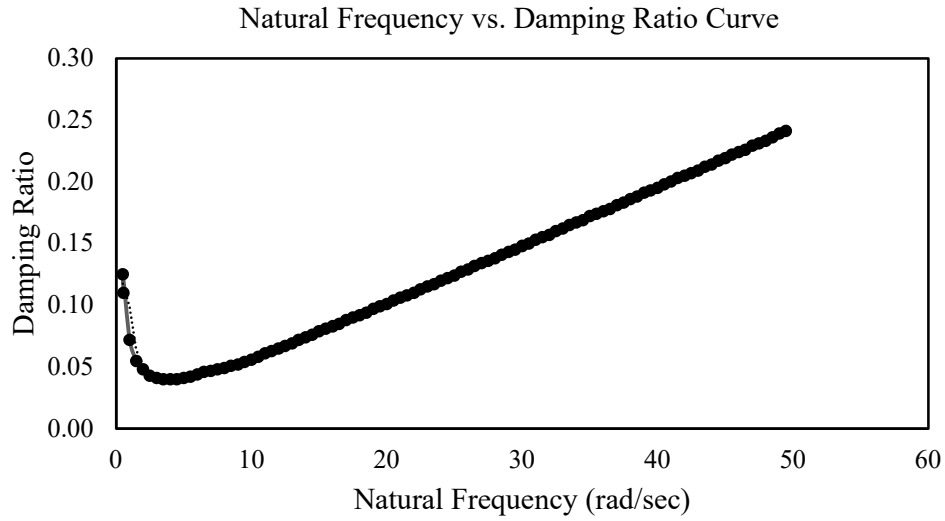


Figure A-1: Variation of damping ratio with natural frequency of a system. (Chowdhury & Dasgupta, 2003)

A method, proposed by Chowdhury & Dasgupta (2003) is described in the following through which one can arrive at the unique values of Rayleigh coefficients. These outputs are valid for systems having large degrees of freedom as well.

1. Select ζ_1 , the damping ratio for the first mode of the system.
2. Select ζ_m , the damping ratio for the m^{th} significant mode.
3. For intermediate modes i , where $1 < i < m$, obtain ζ_i from the following equation based on linear interpolation.

$$\xi_i = \frac{(\xi_m - \xi_1)}{(\omega_m - \omega_1)}(\omega_i - \omega_1) + \xi_1 \quad \text{A.3}$$

in which, ζ_i = damping ratio for the i^{th} mode (for all $i \leq m$); ω_i = natural frequency for the i^{th} mode; ω_1 = natural frequency for the first mode; ω_m = natural frequency for the m^{th} significant mode considered for the analysis.

4. For modes greater than m extrapolate the values based on the following expression

$$\xi_i = \frac{(\xi_m - \xi_1)}{(\omega_m - \omega_1)}(\omega_{m+i} - \omega_m) + \xi_1 \quad , \quad \text{where } m < i \leq km \quad \text{A.4}$$

5. Select first set of data consisting of $\zeta_1, \zeta_m, \omega_1, \omega_m$.
6. Based on the above sets of data obtain β from the equation

$$\beta = \frac{(2\zeta_1\omega_1 - 2\zeta_m\omega_m)}{(\omega_1^2 - \omega_m^2)} \quad \text{A.5}$$

7. Back substituting the value of β in the following expression

$$2\zeta_1\omega_1 = \alpha + \beta\omega_1^2$$

A.6

8. Obtain the value of α .
9. Next select a second set of data consisting of $\zeta_1, \zeta_{km}, \omega_1, \omega_{km}$.
10. Find out α and β based on Equations (A.5) and (A.6).
11. Now one has the three sets of data:
 - (a) Based on linear interpolation
 - (b) Based on data set $\zeta_1, \zeta_m, \omega_1, \omega_m$
 - (c) Based on $\zeta_1, \zeta_{km}, \omega_1, \omega_{km}$
 - (d) Obtain a fourth set of data based on the averages of a, b and c as mentioned above.

Finally, average all values of α and β from (a) to (d), to obtain the desired value of α and β . Table A-1 shows the value of α and β for soil continuum and pipeline considered in this study.

Table A-1: Chart of α and β for soil and pipe

		α	β
Soil	Solid section	0.148	0.011
	With hollow section	0.144	0.012
Pipe	Pipe end roller	0.160	0.010
	Pipe end hinge	0.182	0.010
	Pipe end fixed	0.186	0.010